

ELECTROCHEMICAL IMMUNOSENSOR FOR CANCER BIOMARKER DETECTION

A Thesis Submitted
in Partial Fulfillment of the Requirements
for the Degree of

DOCTOR OF PHILOSOPHY

by

Sweety
(2K20/PHDAC/04)

Under the supervision of

Prof. D. Kumar



Department of Applied Chemistry
DELHI TECHNOLOGICAL UNIVERSITY
(Formerly Delhi College of Engineering)
Shahbad Daultapur, Main Bawana Road, Delhi-110042, India

March, 2025

Dedicated
To My
Parents
&
Husband

ACKNOWLEDGEMENT

God's kindness and grace, which continue to care for me in spite of my imperfections, are the only reasons that make this work possible. It took a lot of struggles and obstacles to finish this thesis. Luckily, a lot of people helped to this endeavour. I would like to thank everyone who helped me to finish the thesis successfully for their advice, support, and unwavering encouragement.

First and foremost, I would like to express my sincere gratitude and respect to my supervisor, **Prof. D. Kumar**, Department of Applied Chemistry, Delhi Technological University, Delhi, for his invaluable advice, continual inspiration, and support throughout my Ph.D. tenure. It had been an honor to work under a polite, motivated, and well-respected supervisor. He helped me to achieve another academic milestone with his constant support, regular help, and careful observation throughout the research investigations.

I owe my heartfelt gratitude to Prof. Parteek Sharma, Honourable Vice Chancellor, Delhi Technological University for his dynamic leadership. I would like to express my sincere gratitude to **Prof. Anil Kumar**, Head of the Department of Applied Chemistry, Delhi Technological University, for providing necessary research facilities in the department. I wish to express my sincere thanks to the whole **faculty members** of Department of Applied Chemistry, DTU for their cooperation and prompt assistance during this research work.

I would like to convey a special thank to **Dr. C.M. Pandey**, assistant professor at SGT university, Gurgaon, for his guidance in the field of biosensors during entire duration of my Ph.D. I was fortunate that the lab had a fantastic work environment that supported my mission effectively. I am thankful to my dear former and current labmates **Owais jalil, Saroj Paneru, Sakshi Verma, Deeksha, Divya, Tanushee, Manu, Ritu, Vaishali, Tanvi** and **Nistha** for their constant support to carry forward my research work.

I appreciate **Mr. Anurag Kaushik** and **Ramesh Kumar**, research scholars at DTU, Department of Applied Physics, for helping to arrange the characterization. I would especially like to thank the Department of Applied Physics for giving us limitless access to XRD and FTIR equipment.

I am grateful to **Dr. Shilpi Agarwal**, Histopathologist, Dr. Lal Path Lab, for her continuous motivation throughout my work. I would especially like to express my appreciation to the **reviewers**, who unwittingly helped me to become a better scholar.

Most significantly, I would want to thank my family for their support and encouragement during my Ph.D. tenure. I am grateful to my parents, **Mr. Krishan Jain & Mrs. Sujata Jain**, who always had faith in me and encouraged me to think outside the box throughout my life. I am grateful to my caring brother, **Mr. Arpit Jain** for being my strength and motivation.

I'm thankful to my spouse, **Mr. Jonny Garg** for being my constant critic, my go-to solution, and most importantly, for keeping my confidence high through all of my highs and lows. Words would never say how grateful I am to my son **Siddham Garg** for bringing joy and happiness in my life. I am grateful to my in-laws, **Mr. Mahavir garg** and **Mrs. Santosh Garg** for their support. I'm also grateful to my loving nieces **Harshi, Somil and Sejal** for their unconditional love.

Finally, I would like to recognize everyone whose contribution make the successful completion of the thesis.

Sweety



DELHI TECHNOLOGICAL UNIVERSITY

(Formerly Delhi College of Engineering)

Shahbad Daultapur, Bawana Road, Delhi- 110042

CANDIDATE'S DECLARATION

I Sweety, hereby certify that the work which is being presented in the thesis entitled “**Electrochemical Immunosensor for Cancer Biomarker Detection**” in partial fulfillment of the requirements for the award of the Degree of Doctor of Philosophy, submitted in the Department of Applied Chemistry, Delhi Technological University is an authentic record of my own work carried out during the period from 10/02/2020 to 28/02/2025 under the supervision of **Prof. D. Kumar**, Department of Applied Chemistry, Delhi Technological University, Delhi.

The matter presented in the thesis has not been submitted by me for the award of any other degree of this or any other institute.

Ms. Sweety

Delhi Technological University



DELHI TECHNOLOGICAL UNIVERSITY

(Formerly Delhi College of Engineering)

Shahbad Daulatpur, Bawana Road, Delhi- 110042

CERTIFICATE BY THE SUPERVISOR

Certified that **Sweety** (Roll No 2K20/PHDAC/04), has carried out her research work presented in this thesis entitled “**Electrochemical Immunosensor for Cancer Biomarker Detection**” for the award of **Doctor of Philosophy** from Department of Applied Chemistry, Delhi Technological University, Delhi under my supervision. The thesis embodies the results of original work, and studies are carried out by the student herself and the contents of the thesis do not form the basis for the award of any other degree to the candidate or to anybody else from this or any other University/Institution.

Prof. Anil Kumar

Head

Department of Applied Chemistry

Delhi Technological University

Delhi- 110042

Prof. D. Kumar

Supervisor

Department of Applied Chemistry

Delhi Technological University

Delhi- 110042

ABSTRACT

The research work presented in this thesis discusses the fabrication of an immunosensor that uses a biological recognition element in direct contact with a transducer to deliver quantitative information. The biological sensing element and the bio-receptor are the two primary components that make up a biosensor. A specific analyte can be detected by using an enzyme, antibody, DNA, or other bio-element. In contrast, the transducer part converts the biological signal into a measurable electrical signal. A new generation of biosensors has recently been developed to assist the combination of biomolecules with biocompatible conducting frameworks. Many interdisciplinary areas of science and technology can be employed to innovate biosensors used in clinical diagnostic and therapeutic applications.

Cancer, which has long been considered the world's top cause of death, is more likely to occur as a result of the enormous population growth and changing lifestyles. Every day, there are an increasing number of new cases of cancer. In a healthy adult, the mechanism of cell formation is a constant and consistent process that maintains the proper number of cells in different tissues. The formation of cancer, which typically manifests as a swollen mass called a malignant tumor, is caused by inappropriate cell division and uncontrollable cell growth. Moles and warts are examples of benign tumors that are usually not dangerous or damaging. Additionally, when a tumor is malignant, the cells spread to surrounding organs by invading neighboring tissue through blood vessels. In this area, they split and grow once more, eventually forming a new tumor in the afflicted organ. The process by which cancer spreads to several body organs is known as metastasis. The highest rates of cancer-related deaths in developing countries are probably caused by delayed diagnosis and limited access to early, standard treatment. It has been noted that traditional detection methods can take several hours or, in certain cases, a few weeks to yield results. These conventional methods, however, are less sensitive, time-consuming, costly, and require specialist equipment. Therefore, the development of trustworthy, sensitive, specific, quick, and user-friendly tools for identifying cancer biomarkers is urgently needed. As a result, efforts have been made to increase the sensitivity and specificity of portable biosensors.

In the last decade, 2D-Mxenes have delivered an excellent performance due to their outstanding metal-like conductivity, layered morphology, superior hydrophilicity and strong ability for incorporation of functional groups.

Furthermore, MXene possesses excellent ion-intercalation behavior, high specific surface area and superior electron transfer ability. $Ti_3C_2T_x$ has been considered as one of the most studied MXene in different fields such as supercapacitors, energy conversions and biosensing fields. The inclusion of nanomaterials like metal particles, metal oxides and metal sulfides has sparked potential to customize the unique characteristics of each component into a single material. The biosensor's performance has been improved by further synergistic effects of these materials, leading to increased sensitivity and selectivity. The present study focuses on the synthesis and characterization of $Ti_3C_2T_x$ and its hybrid materials, for the development of highly sensitive electrochemical immunosensors having application in the detection of EpCAM antigen (a cancer biomarker). The transducer surface has been prepared by two methods viz. electrophoretic deposition and simple dip coating method. The anti-EpCAM has been coupled to the transducer material covalently by using EDC:NHS. Further, electrochemical detection has been performed by DPV and chronoamperometry techniques. Moreover, the clinical validation of the fabricated platforms has been confirmed by analyzing artificial spiked serum samples, thereby proving its efficiency.

CONTENTS

Acknowledgement	iii
Declaration	v
Certificate	vi
Abstract	vii
Contents	ix
List of Tables	xvi
List of Figures	xvii
Abbreviations	xxii
Chapter 1: Introduction & Literature Review	1-34
1.1 Introduction to cancer	1
1.2 Classification of cancer	2
1.2.1 Carcinomas	3
1.2.2 Sarcomas	3
1.2.3 Myelomas	3
1.2.4 Leukemias	3
1.2.5 Lymphomas	4
1.2.6 Mixed types	4
1.3 Diagnosis of cancer	4
1.3.1 Biomarkers based early identification of cancer	5
1.3.2 Cancer biomarkers	6
1.4 Techniques for the cancer biomarker detection	7
1.4.1 Enzyme-linked immunosorbent assay (ELISA)	7
1.4.2 Surface enhanced Raman spectroscopy (SERS)	8
1.4.3 Electrochemiluminescence immunoassay (ECLIA)	8
1.4.4 Radioimmunoassay (RIA)	8
1.5 Advanced detection techniques	9
1.6 Biosensors: A new approach to detect biomarkers	10
1.6.1 Components of a biosensor	11

1.6.1.1 Bio-receptor	11
1.6.1.2 Immobilization matrix	11
1.6.1.3 Transducer	11
1.6.2 Electrochemical biosensors	11
1.6.2.1 Electrochemical enzymatic biosensor	12
1.6.2.2 Electrochemical aptasensor	12
1.6.2.3 Electrochemical geno-biosensor	13
1.6.2.4 Electrochemical Immunosensor	13
1.6.3 Electrochemical immunosensors for cancer biomarkers detection	13
1.7 Two dimensional (2D) materials	14
1.7.1 MXene	17
1.7.2 Properties of MXenes	18
1.7.2.1 Mechanical properties	18
1.7.2.2 Electrical and thermal properties	19
1.7.2.3 Optical properties	19
1.7.2.4 Chemical properties	19
1.7.3 MXene-based hybrid materials	19
1.8 Synthesis of MXene	20
1.8.1 Top-down approach	20
1.8.1.1 HF etching	20
1.8.1.2 Bifluoride salt etching	21
1.8.1.3 Molten salt-based etching	22
1.8.1.4 Electrochemical etching	22
1.8.1.5 Hydrothermal etching	22
1.8.1.6 Ionic liquid-based etching	23
1.8.2 Bottom-up approach	23
1.8.2.1 Chemical vapour deposition (CVD)	23
1.9 Applications of MXenes and MXene-based hybrids for cancer biomarker detection	24
1.10 Objective	24
1.11 Thesis organization	25

References	28
Chapter 2: Materials and Experimental Techniques	35-49
2.1 Introduction	35
2.2 Materials	35
2.2.1 Chemicals	35
2.2.2 Buffers	36
2.3 Structural and morphological characterization techniques	36
2.3.1 X-ray diffraction (XRD)	36
2.3.2 Fourier transform infrared (FTIR) spectroscopy	37
2.3.3 Scanning electron microscopy	39
2.3.4 Transmission electron microscopy	40
2.3.5 Energy dispersive X-ray analysis (EDX)	41
2.4 Electrochemical techniques	41
2.4.1 Cyclic voltammetry (CV)	43
2.4.2 Differential pulse voltammetry (DPV)	44
2.4.3 Chronoamperometry	44
2.5 Antibody immobilization to MXene-based matrix	44
2.5.1 Site oriented antibody binding technique	45
2.5.2 Random immobilization	45
2.5.2.1 Non-covalent immobilization	45
2.5.2.2 Covalent immobilization	46
2.6 Protocols used for estimation of various performance-related metrics for MXene and its hybrids-based immunosensors	46
2.6.1 Linear detection range, detection limit and sensitivity	46
2.6.2 Reproducibility and shelf-life of the immunosensors	47
References	48

Chapter 3: MXene-based Electrochemical Immunosensor for Cancer Biomarker Detection	50-61
3.1 Introduction	50
3.2 Experimental section	51
3.2.1 Synthesis of $Ti_3C_2T_x$	51
3.2.2 Electrophoretic deposition (EPD) of $Ti_3C_2T_x$ onto ITO electrode	51
3.2.3 Fabrication of immunosensor	51
3.3 Results and discussion	52
3.3.1 Structural characterization of $Ti_3C_2T_x$	52
3.3.2 Morphological study of $Ti_3C_2T_x$	53
3.3.3 Electrochemical characterization	55
3.3.4 Optimization studies	57
3.3.5 Electrochemical immunosensing studies	57
3.3.6 Interference, reproducibility, repeatability and stability studies	58
3.3.7 Human serum analysis	59
3.4 Conclusion	60
References	61
Chapter 4: Titanium Dioxide grafted on MXene-based Immunosensor for Cancer Biomarker Detection	62-71
4.1 Introduction	62
4.2 Experimental work	63
4.2.1 Synthesis of $Ti_3C_2T_x$ & $TiO_2/Ti_3C_2T_x$	63
4.2.2 Electrophoretic deposition of $TiO_2/Ti_3C_2T_x$ hybrid	63
4.2.3 Fabrication of $TiO_2/Ti_3C_2T_x$ hybrid based immunosensing platform	63
4.3 Results & discussion	63
4.3.1 Structural analysis	63
4.3.2 Morphological Characterization	64
4.3.3. Electrochemical characterization	65
4.3.4 Optimization studies	66
4.3.5 Electrochemical immunosensing studies	67

4.3.6 Interference, reproducibility and stability studies	68
4.3.7 Human serum analysis	69
4.4 Conclusion	70
References	71
Chapter 5: CuS-Doped Ti₃C₂T_x-based Electrochemical Immunosensor for EpCAM Antigen Detection	72-81
5.1 Introduction	72
5.2 Experimental section	73
5.2.1 Synthesis of CuS and CuS/Ti ₃ C ₂ T _x	73
5.2.2 Electrophoretic deposition of CuS/Ti ₃ C ₂ T _x hybrid	73
5.2.3 Fabrication of biosensing platform	73
5.3 Results & discussion	74
5.3.1 Structural analysis	74
5.3.2 Morphological characterization	75
5.3.3 Electrochemical characterization of fabricated electrodes	75
5.3.4 Electrochemical immunosensing study for EpCAM antigen detection	77
5.3.5 Selectivity, reproducibility and shelf life studies	78
5.3.6 Human serum analysis	79
5.4 Conclusion	80
References	81
Chapter 6: Electrochemical Paper-based Immunosensor Grafted by using CuS@PEDOT:PSS for EpCAM Antigen Detection	82-92
6.1 Introduction	82
6.2 Experimental Section	83
6.2.1 Synthesis of CuS	83
6.2.2 Fabrication of PEDOT:PSS/WP and CuS@PEDOT:PSS/WP electrodes	83
6.2.3 Fabrication of immunosensor	83
6.3 Results & discussion	83
6.3.1 Morphological study	83

6.3.2 Structural characterization	84
6.3.3 Flexibility study	86
6.3.4 Electrical conductivity study	86
6.3.5 Electrochemical characterization	87
6.3.6 Optimization studies	87
6.3.7 Electrochemical immunosensing studies	88
6.3.8 Interference, reproducibility and stability analysis	89
6.3.9 Human serum analysis	90
6.4 Conclusion	91
References	92
Chapter 7: Ag@Ti₃C₂T_x-modified Conducting Paper-based Electrochemical Immunosensor for EpCAM Detection	93-103
7.1 Introduction	93
7.2 Experimental section	94
7.2.1 Synthesis of Ti ₃ C ₂ T _x & Ag/Ti ₃ C ₂ T _x hybrid	94
7.2.2 Fabrication of PEDOT:PSS/WP (CP), Ti ₃ C ₂ T _x /CP and Ag/Ti ₃ C ₂ T _x /CP electrodes	94
7.2.3 Biofunctionalization of DMSO treated Ag/Ti ₃ C ₂ T _x /CP electrode	94
7.3 Results and discussion	95
7.3.1 Morphological characterization	95
7.3.2 Structural characterization	96
7.3.3 Electrical conductivity and flexibility study	97
7.3.4 Electrochemical characterization	98
7.3.5 Electrochemical response studies	99
7.3.6 Real sample studies	100
7.3.7 Specificity, repeatability and stability studies	100
7.4 Conclusion	102
References	103

Chapter 8: Conclusion and Future Scope and Social Impact	104-106
8.1 Conclusion	104
8.2 Future scope	105
8.3 Social impact	106

LIST OF TABLES

Table 1.1:	Summary of numerous techniques used for cancer biomarkers detection	9
Table 3.1:	Detection of biomarker in spiked serum using BSA/anti-EpCAM/Ti ₃ C ₂ T _x @ITO	60
Table 4.1:	Detection of EpCAM in spiked serum sample with BSA/anti-EpCAM/TiO ₂ /Ti ₃ C ₂ T _x @ITO electrode	70
Table 5.1:	Detection of EpCAM in spiked serum sample with BSA/anti-EpCAM/CuS/Ti ₃ C ₂ T _x @ITO electrode	80
Table 6.1	Electrical Conductivity of all the Modified Electrodes	86
Table 6.2:	Detection of biomarker in the spiked serum using BSA/anti-EpCAM/EP electrode	91
Table 7.1:	Electrical conductivity data of different modified electrodes	97
Table 7.2:	EpCAM detection in serum sample by anti-EpCAM/Ag@Ti ₃ C ₂ T _x /CP electrode	100

LIST OF FIGURES

Fig. 1.1:	Various Stages of the Cancer Development	2
Fig. 1.2:	Clinical Applications of Cancer Biomarkers	5
Fig. 1.3:	Schematic view of a biosensing device	10
Fig. 1.4:	Classification of a Biosensor	12
Fig. 1.5:	Schematic representation of 2D-materials along with their structures	15
Fig. 1.6:	Diagrammatic representation of synthesis methods and characteristics of 2D-materials	16
Fig. 1.7:	Structure of $Ti_3C_2T_x$	18
Fig. 1.8:	General synthesis of MXene	20
Fig. 2.1:	(A) Schematic view of XRD; (B) XRD diffraction pattern of $Ti_3C_2T_x$	37
Fig. 2.2:	(A) Schematic view of Michelson interferometer; (B) FTIR spectra of $Ti_3C_2T_x$	38
Fig. 2.3:	(A) Pictorial illustration of SEM instrumentation; (B) SEM image of $Ti_3C_2T_x$	39
Fig. 2.4:	(A) Pictorial view of TEM instrumentation; (B) TEM image of $Ti_3C_2T_x$	40
Fig. 2.5:	Schematic view of Potentiostat workstation with three electrode set-up	42
Fig. 3.1:	Diagrammatic illustration of the immunosensor based on $Ti_3C_2T_x$	50
Fig. 3.2:	(A) XRD diffraction pattern of (a) Ti_3AlC_2 , (b) $Ti_3C_2T_x$ (co-precipitation) and (c) $Ti_3C_2T_x$ (hydrothermal); (B) FTIR spectra of (a) $Ti_3C_2T_x$ /ITO and (b) anti-EpCAM/ $Ti_3C_2T_x$ /ITO; (C) TEM image; and (D) Cross-sectional image of $Ti_3C_2T_x$ (hydrothermal)	53
Fig. 3.3:	SEM micrographs of (A) $Ti_3C_2T_x$ (co-precipitation); (B) $Ti_3C_2T_x$ (hydrothermal); (C) $Ti_3C_2T_x$ /ITO electrode; and (D) anti-EpCAM/ $Ti_3C_2T_x$ /ITO electrode	54

Fig. 3.4:	EDX analysis of $\text{Ti}_3\text{C}_2\text{T}_x$ (hydrothermal)	55
Fig. 3.5:	(A) DPV plot for different electrodes; (B) Scan rate study of $\text{Ti}_3\text{C}_2\text{T}_x@$ ITO; (C) Peak potential against $\log(v)$ for $\text{Ti}_3\text{C}_2\text{T}_x@$ ITO electrode; and (D) anodic and cathodic peak current against $v^{1/2}$ for $\text{Ti}_3\text{C}_2\text{T}_x@$ ITO in PBS (200 mM, pH =7.4) having $[\text{Fe}(\text{CN})_6]^{3-/4-}$ (5 mM)	56
Fig. 3.6:	Optimization of (A) pH; and (B) Time of incubation for EpCAM antigen	57
Fig. 3.7:	(A) DPV response of BSA/anti-EpCAM/ $\text{Ti}_3\text{C}_2\text{T}_x@$ ITO electrode for the detection of EpCAM antigen (from top to bottom, 0.1 fg/mL to 100 ng/mL) in 6.5 pH PBS containing 5 mM $[\text{Fe}(\text{CN})_6]^{3-/4-}$; (B) Plot depicting the linear relationship between $\log(C_{\text{EpCAM}})$ and peak current; (C) Selectivity study of immunosensor in different analytes (100 pg/mL) with respect to EpCAM antigen; and (D) Reproducibility of immunosensor	58
Fig. 3.8:	(A) Stability study of BSA/anti-EpCAM/ $\text{Ti}_3\text{C}_2\text{T}_x@$ ITO electrode and (B) DPV response for serum sample spiked with EpCAM	59
Fig. 4.1:	Schematic representation for the fabrication of BSA/anti-EpCAM/ $\text{TiO}_2/\text{Ti}_3\text{C}_2\text{T}_x@$ ITO immunosensor	62
Fig. 4.2:	(A) XRD spectra of (a) Ti_3AlC_2 , (b) $\text{Ti}_3\text{C}_2\text{T}_x$ and (c) $\text{TiO}_2/\text{Ti}_3\text{C}_2\text{T}_x$; (B) FT-IR peaks of (a) $\text{Ti}_3\text{C}_2\text{T}_x$ and (b) $\text{TiO}_2/\text{Ti}_3\text{C}_2\text{T}_x$; (C) SEM analysis of $\text{Ti}_3\text{C}_2\text{T}_x$; and (D) SEM analysis of $\text{TiO}_2/\text{Ti}_3\text{C}_2\text{T}_x$	64
Fig. 4.3:	(A) CV analysis of (a) bare ITO, (b) $\text{Ti}_3\text{C}_2\text{T}_x@$ ITO, (c) $\text{TiO}_2/\text{Ti}_3\text{C}_2\text{T}_x@$ ITO and (d) BSA/anti-EpCAM/ $\text{TiO}_2/\text{Ti}_3\text{C}_2\text{T}_x@$ ITO; (B) Scan rate analysis of $\text{TiO}_2/\text{Ti}_3\text{C}_2\text{T}_x@$ ITO; (C) Peak potential against $\log(v)$ for $\text{TiO}_2/\text{Ti}_3\text{C}_2\text{T}_x@$ ITO electrode and (D) anodic and cathodic peak current against $v^{1/2}$ for $\text{TiO}_2/\text{Ti}_3\text{C}_2\text{T}_x@$ ITO in PBS (200 mM, pH =7.4) having $[\text{Fe}(\text{CN})_6]^{3-/4-}$ (5 mM)	65
Fig. 4.4:	Optimization of (A) pH and (B) Time of incubation for EpCAM antigen	67

- Fig. 4.5:** (A) DPV response of BSA/anti-EpCAM/TiO₂/Ti₃C₂T_x@ITO electrode for the detection of EpCAM antigen (from top to bottom, 1 ag/mL to 10 ng/mL) in 6.5 pH PBS containing 5 mM [Fe(CN)₆]^{3-/4-} (inset- magnified view of peak currents); (B) Plot depicting linearity between inhibition of peak current and log (C_{EpCAM}); (C) Selectivity study of different analytes (10 fg/mL) w.r.t EpCAM antigen; and (D) Reproducibility of immunosensor 68
- Fig. 4.6:** (A) Stability study of immunosensor; and (B) Peak current of immunosensor in (a) buffer and (b) serum sample 69
- Fig. 5.1:** Schematic representation for the fabrication of BSA/anti-EpCAM/CuS/Ti₃C₂T_x@ITO platform for EpCAM antigen detection 72
- Fig. 5.2:** (A) XRD spectra of Ti₃C₂T_x (a), CuS (b) and CuS/Ti₃C₂T_x (c); (B) FTIR spectra of CuS (a), Ti₃C₂T_x (b), and CuS/Ti₃C₂T_x (c) 74
- Fig. 5.3:** (A) SEM image of Ti₃C₂T_x; (B) and (C) SEM image of CuS/Ti₃C₂T_x; (D) and (E) TEM image of CuS/Ti₃C₂T_x 75
- Fig. 5.4:** (A) CV plots of bare ITO (a), Ti₃C₂T_x@ITO (b), CuS/Ti₃C₂T_x@ITO (c), and BSA/anti-EpCAM/CuS/Ti₃C₂T_x@ITO (d); (B) Scan rate study (10 – 400 mV/s) of CuS/Ti₃C₂T_x@ITO; (C) Plot of the potential with log of scan rate for CuS/Ti₃C₂T_x@ITO; and (D) The plot of I_{pa}, I_{pc} vs. square root of scan rate for CuS/Ti₃C₂T_x@ITO 76
- Fig. 5.5:** (A) DPV study showing the response of BSA/anti-EpCAM/CuS/Ti₃C₂T_x@ITO electrode with increasing concentration of EpCAM antigen (0.01 fg/mL to 100 ng/mL); (B) Linearity plot between peak current change and log of EpCAM antigen concentration; (C) Interference study of immunosensor with multiple analytes (100 pg/mL); (D) Reproducibility study of immunosensor 78
- Fig. 5.6:** (A) Shelf life study of BSA/anti-EpCAM/CuS/Ti₃C₂T_x@ITO; (B) Comparison of DPV response (a) in buffer sample, and (b) in spiked serum sample (0.1 – 10000 fg/mL) 79
- Fig. 6.1:** Scheme of the fabrication and mechanism of EP-based immunosensor 82

- Fig. 6.2:** SEM micrographs of (A) WP; (B) PEDOT:PSS/WP; (C) magnified image of PEDOT:PSS adsorption; (D) CuS powder; (E) CuS@PEDOT:PSS/WP and (F) magnified view of CuS structure incorporated onto a paper 84
- Fig. 6.3:** (A) XRD pattern and (B) FTIR spectra of PEDOT:PSS/WP (a), CuS@PEDOT:PSS/WP (b) and CuS powder (c); (C) Diagrammatic view of EP foldings and (D) Plot of relative conductivity vs. angle of bending 85
- Fig. 6.4:** (A) Chronoamperometry curves of (a) PEDOT:PSS/WP, (b) CuS@PEDOT:PSS/WP, (c) EP and (d) BSA/anti-EpCAM/EP; (B) Optimization of the effect of pH; (C) Optimization of time of incubation of EpCAM antigen; (D) Electrochemical response study of BSA/anti-EpCAM/EP electrode after incubation of different EpCAM antigen concentrations (0.01 pg/mL to 1000 ng/mL) and (E) Linearity plot of current vs. $\log C_{\text{EpCAM}}$ 88
- Fig. 6.5:** Energy dispersive X-ray (EDX) analysis of ash 89
- Fig. 6.6:** (A) Interference data of BSA/anti-EpCAM/EP electrode in the presence of different analytes (10 pg/mL); (B) Reproducibility data of the immunosensor; (C) Stability study of BSA/anti-EpCAM/EP electrode; and (D) Saturated current data of immunosensor in buffer (a) and spiked serum sample 90
- Fig. 7.1:** Scheme depicting the fabrication of Ag@Ti₃C₂T_x/CP-based immunosensor 93
- Fig. 7.2:** SEM micrographs of (A) PEDOT:PSS/WP (B) Ti₃C₂T_x/CP (C) Ag/Ti₃C₂T_x powder and (D) Ag/Ti₃C₂T_x/CP 95
- Fig. 7.3:** SEM micrographs of (A) PEDOT:PSS/WP (B) Ti₃C₂T_x/CP (C) Ag/Ti₃C₂T_x powder and (D) Ag/Ti₃C₂T_x/CP 96
- Fig. 7.4:** (A) Schematic view of conducting paper folding at different angles and (B) Plot of conductivity change (final/initial) vs. angle of bending 98
- Fig. 7.5:** (A) Chronoamperometric plot of CP (a), Ti₃C₂T_x/CP (b), Ag/Ti₃C₂T_x/CP (c), and DMSO treated Ag/Ti₃C₂T_x/CP (d); (B) Optimization for incubation time of EpCAM antigen; (C) 99

Electrochemical response of anti-EpCAM/Ag/Ti₃C₂T_x/CP against different EpCAM antigen concentrations (1 fg/mL – 10000 pg/mL) and **(D)** Calibration plot of current against log (EpCAM antigen, fg/mL)

Fig. 7.6: **(A)** Chronoamperometric saturated current comparison of anti-EpCAM/Ag/Ti₃C₂T_x/CP electrode for EpCAM antigen in buffer and serum sample; **(B)** Interference study of anti-EpCAM/Ag/Ti₃C₂T_x/CP electrode with various analytes (glucose, NaCl, urea and ascorbic acid); **(C)** Repeatability study of three different anti-EpCAM/Ag/Ti₃C₂T_x/CP electrodes; **(D)** Shelf life study of immunosensor

101

ABBREVIATIONS

CB	Cancer Biomarker
EpCAM	Epithelial Cell Adhesion Molecule
Anti-EpCAM	Epithelial Cell Adhesion Molecule Antibody
Ti ₃ AlC ₂	Titanium aluminium carbide
CV	Cyclic Voltammetry
DPV	Differential Pulse Voltammetry
EDC	N-(3-dimethyl aminopropyl)-N'-ethyl carbodiimide hydrochloride
NHS	N-hydroxysuccinimide
BSA	Bovine Serum Albumin
ITO	Indium Tin Oxide
PBS	Phosphate Buffer Saline
EPD	Electrophoretic Deposition
XRD	X-ray Diffraction
FTIR	Fourier Transform Infrared
TEM	Transmission Electron Microscopy
SEM	Scanning Electron Microscopy
EDX	Energy Dispersive X-ray
RSD	Relative Standard Deviation
LOD	Limit of Detection
PEDOT:PSS	Poly(3,4-ethylenedioxythiophene):polystyrene sulfonate
CP	Conducting Paper
WP	Whatman Paper
DMSO	Dimethyl Sulfoxide
DMF	N,N-dimethyl formamide
EG	Ethylene Glycol
DMA	N,N-dimethyl acetamide

CHAPTER 1

INTRODUCTION & LITERATURE REVIEW

1.1 Introduction

Cancer, a complicated illness, is becoming more common cause of death worldwide. As human body is composed of trillions of cells, that normally divide to form the new cells. When old cells die due to the aging, new ones take their positions. This process is known as growth and proliferation. Sometimes, this controlled mechanism breaks down leading to the proliferation and growth of these damaged cells which should not occur. The lumps of tissue formed by such damaged cells may be benign or malignant tumors. Cancerous tumors possess the capacity to metastasize, or spread into adjacent tissues, or organs. This process is known as metastasis.

Uncontrolled cell division is the hallmark of cancer and the essential component of its advancement. The majorities of cancer grow gradually from normal cell structure and function over time. The continual accumulation of novel mutations is the driving force behind the process. It is important to note that in the cancerous cells, mitosis is not faster than that in the normal cell. Cell division completes in around 4 h in both kinds of cells. Single cell transformation from almost each organ in the body give rise to cancer, which spread widely and divide somewhat uncontrollably [1]. It is believed that the incidence of prevalent diseases like cancer increases exponentially with age. As the cancer cells are not very different from their original organ-specific cells, efforts to discover a “magic bullet” to accurately identify, classify and eventually treat cancer have mostly been fruitless [2]. The multi-hit hypothesis of carcinogenesis, which holds that multi-hit accumulation is necessary for full cancer emergence, has been mentioned to clarify ideas like cancer latency, time gap between cancer beginning and identification, and a connection between the cancer and aging. According to the traditional view of carcinogenesis, initiators and promoters affect cells in many stages, initiating the processes of invasion, metastasis, transformation, and tumorigenicity. Basic stages of the cancer have been represented in the following **Fig. 1.1**.

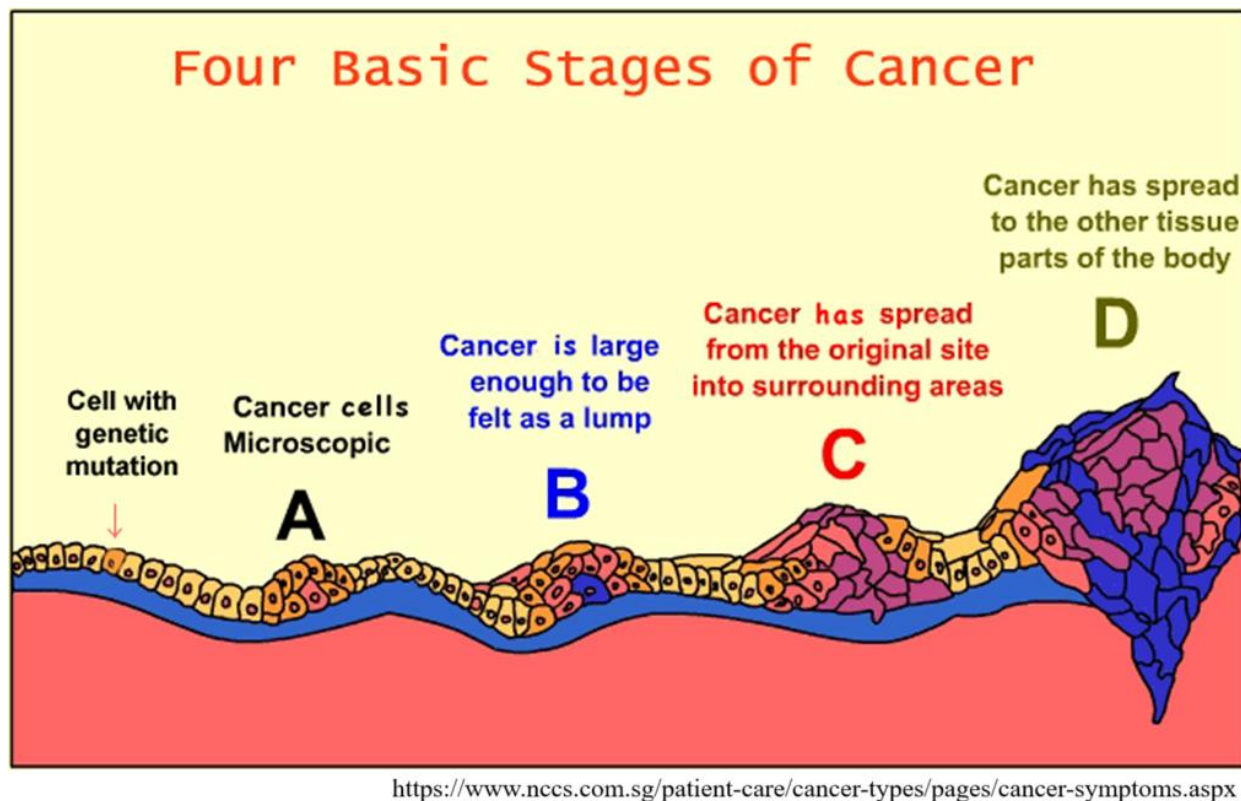


Fig. 1.1: Various Stages of the Cancer Development

According to World Health Organization (WHO), cancer poses a serious risk to human survival [3]. International Agency for Research on Cancer approximates the cancer incidence and death rate by using GLOBOCAN 2020. According to its report, cancer is the world's leading cause of death recorded 19.3 million cases including 10 million deaths from this disease in 2020 alone. Also, it is reported that lung cancer (11.4%), the most often diagnosed cancer has been surpassed by female breast cancer (11.7%). The most frequent cancer is still lung cancer, followed by colorectal, prostate and stomach cancer. In 2040, there will likely be 28.4 million cancer cases worldwide [4]. There are numerous factors contributing to the high death rate from the disease, such as tumor resistance to current treatments and delayed detection brought on by ineffective screening and diagnostic programs.

1.2 Classification of cancer

There are around 200 distinct forms of cancer. Cancer can be classified on the basis of type of cells, or tissues and body part, in which the cancer begins. Some other types are characterized on the basis of tumor grade, genetic profile and cancer stage. The nomenclature employed to

categorize diverse forms of cancer is predicated on the basis of organ of origin, for example lung, prostate, breast, etc. and a specific tissue of genesis within that particular organ. There are mainly four tissues viz., muscle, connective tissue, nerves and epithelium. Epithelium is main tissue that covers each body surface- internal and exterior. The malignant tumors arising from the epithelium are called carcinomas [5]. Depending on the kind of cell, there are six main forms of the cancer which have been discussed in the following sections.

1.2.1 Carcinomas

Eighty to ninety percent of cancers are carcinomas, the most prevalent kind of cancer cell. This type of tumor mainly arises in epithelial cells, which are found in the skin, body cavities and organs. Normal epithelial cells are tightly bonded to the beneath basement membrane as well as to one another. They never come into contact with blood vessels or lymphatic vessels, nor leave their avascular epithelial compartment above the basement membrane. Upon maturing into a carcinoma, these essential characteristics disappear. Based on their distinctive characteristics, carcinomas are further divided into subtypes. In general, carcinomas fall into just three fundamental groups, namely, neuroendo-crine carcinoma, adenocarcinoma and squamous cell carcinoma and the last two accounts for the great majority of carcinomas.

1.2.2 Sarcomas

Sarcomas are the malignancies of the bones and soft tissues in the body composed of mesenchymal cells. Bones, muscles, nerves, tendons, ligaments, cartilage, blood vessels, nerves, and fatty tissues are all affected by this type of cancer.

1.2.3 Myelomas

Multiple myeloma, commonly known as myeloma, is a malignancy of the immune system's plasma cells. The type of cells which produce antibodies are called plasma cells.

1.2.4 Leukemias

Leukemias is blood cells cancer which starts in the bone marrow. Compared to the myelomas and lymphomas, leukemias are referred to as "liquid cancers" among blood-related cancers. These malignancies are generally treated like solid cancers that have spread because they involve blood-circulating cells.

1.2.5 Lymphomas

A kind of cancer which develops from immune system cells is called a lymphoma. Such type of tumors can originate from extranodal locations like testicles, stomach, or they might originate in lymph nodes.

1.2.6 Mixed types

It is not unusual for a malignancy to exhibit traits from multiple tissue types. Certain malignancies can have striking similarities to the healthy cells from which they developed. These are referred as well-differentiated tumors. Some might not resemble with normal cells at all. Their description as undifferentiated can appear on a pathology report. Furthermore, the majority of the cancers exhibit heterogeneity. This implies that the appearance of cells in a tumor's distinct section can differ greatly. For instance, certain cells in a lung cancer may resemble adenocarcinomas, while other cells may resemble squamous cell carcinomas. It is mentioned to have adenosquamous characteristics in pathology report. One form that is sometimes differentiated from the rest is blastomas. These are the malignancies that develop in embryonic cells, which are the cells that have not yet decided to develop into mesenchymal or epithelial cells [6].

1.3 Diagnosis of cancer

One of the most common symptoms experienced by cancer patients is pain. In order to provide cancer patients with appropriate and comprehensive pain treatment tailored to their specific needs, a patient's medical history, clinical examination, cause of pain diagnosis and adherence to the WHO analgesic ladder principles must be taken into account.

The incidence and mortality of cancer can be considerably decreased by an efficient early detection and treatment. Magnetic resonance imaging (MRI), computed tomography (CT), X-rays, endoscopy, biopsy, thermography, and sonography are a few of the sophisticated clinical techniques being utilized to diagnose the malignancies [7-10]. Most commonly, there is an imaging technique employed as well, positron emission tomography (PET) [11]. These techniques take a lot of time since they need sample processing and they can only detect malignancies that are at different stages [12].

1.3.1 Biomarkers based early identification of cancer

According to WHO, a biomarker is a substance which can be evaluated in the body and measure the incidence of disease [13]. Potential biomarkers include peptides, proteins (enzymes or receptors), nucleic acids (DNA or RNA), antibodies, proteomic signatures, metabolic signatures and cell mutations. Cancer biomarkers (CB) are the biological substances produced by the cancer cells or that are present in bodily fluids and tissues [14]. They provide genetic information about the formation of cancerous cells. They can help to determine whether a disease is biologically normal or abnormal. The utilization of CB can serve as a vital component in the diagnosis of patients's overall cancer status. Numerous circulating, oxidative stress, protein and cytogenic biomarkers have been found via an extensive research. These biomarkers can be measured precisely in a clinical setting and may help to ensure the early diagnosis of a number of cancers including head, brain, neck, prostate, lung, oral, colorectal, small intestine, endocrine, osteosarcoma, renal and pancreatic cancer [15]. It is possible to verify the existence of these biomarkers by examining bodily fluids from humans, including blood, urine, serum, plasma and tumor cells. Because of their pertinent capabilities with point of care (POC) applications, CB can be utilized for an early cancer detection, risk assessment and therapy evaluation [16]. **Fig. 1.2** below illustrates the uses and clinical applications of CB.

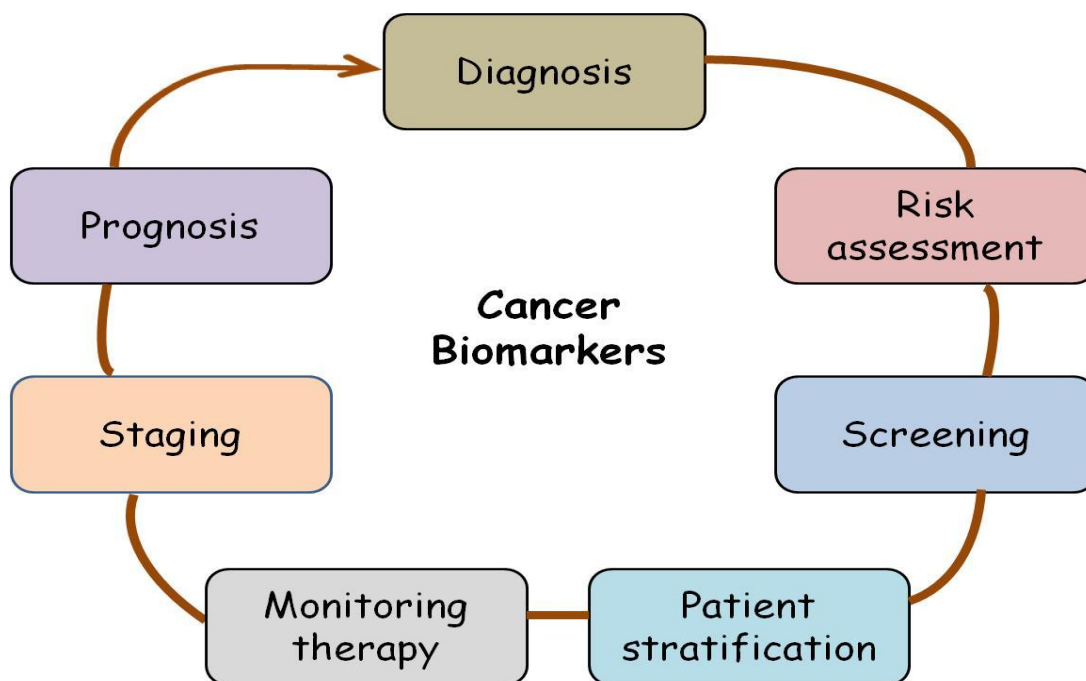


Fig. 1.2: Clinical Applications of Cancer Biomarkers

1.3.2 Cancer biomarkers

To mention a few, Prostate-specific antigen (PSA) is a biomarker for prostate cancer that may be found in both semen and blood, and it is extensively utilized in the diagnosis and treatment of prostate cancer [17].

Comparably, P53 is another promising cancer biomarker that causes unchecked cell development in the body. Hence, it can be used to diagnose a variety of malignancies, like leukemia, lung, ovarian, breast and bone cancers [18].

Furthermore, it has recently been shown that cancer antigen 15-3 is a potential blood biomarker for the identification of breast cancer. CD44 is an additional surface biomarker that may be useful for the detection of breast cancer in stem cells (BCSCs) [19].

A well-known novel biomarker for the early detection of bladder cancer is apolipoprotein-A1 (Apo-A1) [20].

Additionally, other biomarkers- AFP, CEA and CA125, that are present in the blood or urine of patients represent the features of four distinct types of lung cancer [21].

Another possible CB is Y-box 2 (SOX2), which can be used to detect cancer early in the course of skin, breast, lung, prostate and other cancers [22].

Cell adhesion molecules (CAMs) are the receptors on the cell surface that facilitate cell attachment in the extracellular matrix (ECM), also enabling intercellular communication and interaction. EpCAM, epithelial cell adhesion molecule is a distinct type I membrane protein found in CAMs. EpCAM overexpression is highly correlated in most cancer cells with poorer survival rates and worse prognosis for cancer patients. For instance, the expression levels of EpCAM have been linked to a decline in the overall survival rate of patients with gallbladder cancer and are substantially connected with tumor recurrence in colon. Moreover, it has been demonstrated that EpCAM gene silencing reduces lymph node metastasis in both primary and metastatic breast cancer, migration and cell proliferation. Conversely, EpCAM creates functional antagonistic effects on E-cadherin-mediated adhesions and encourages homophilic cell-cell interactions.

1.4 Techniques for the cancer biomarker detection

Numerous immunoassays are employed to identify biomarkers in biological fluids and serum. Immunoassays are based on the characteristic of particular biorecognition of antigens by antibodies [23]. There are weak non-covalent interactions of secondary forces like van der Waals forces and hydrogen bonds etc., between the antibodies and antigen epitopes. The strength with which antibodies attach to antigens is influenced by these reversible interactions. Primary antibodies (pABs) are defined as antibodies in immunoassays that bind directly to a target antigen. The secondary antibodies (sABs) have the ability to attach antigen epitopes apart from those that are bound by the pABs. The sABs are helpful, since they are typically conjugated or labeled with enzymes, they can be used to measure the amount of antigen binding to pAB. The immunoassays can be very sensitive and specific, as long as the pABs and sABs have a high degree of binding specificity to the antigens that are used as biomarkers. Consequently, an active conformation of pAB and sAB determines the specificity and sensitivity of any immunoassay. The most widely explored methods in molecular diagnostics are immunoassays. Most commonly used techniques including Enzyme-linked immunosorbent assay (ELISA) [24], surface enhanced Raman spectroscopy (SERS), electrochemiluminescence immunoassay [25] and radioimmunoassay (RIA) [26] have been discussed and summarized also in the **Table 1.1**.

1.4.1 Enzyme-linked immunosorbent assay (ELISA)

The antibodies which are produced in animals directed against a particular biomarker are commonly used in ELISA. A particular antigen epitope binds to the immobilized pABs on the solid surface. On the other hand, there is bonding between other epitopes and the enzyme-linked sABs, creating a sandwich type complex. The enzyme activity which converts a substrate into the colorful product is helpful to detect the binding of the antigen with pAB. In biological fluids and serum, ELISAs are helpful tools for identifying and measuring biomarker proteins [27]. The immobilization chemistry employed to attach the pABs on the surface has an impact on the assay's specificity, which makes the specificity of ELISA-based assays a significant cause for worry. pABs can be immobilized by hydrophobic, ionic and covalent interactions. The gradual loss of pABs activity leading to non-specific interactions is the main problem with direct protein immobilization on the surface.

1.4.2 Surface enhanced Raman spectroscopy (SERS)

Using the ultrasensitive vibrational spectroscopy, the biomarker proteins present on, or near the surface of plasmonic nanostructures can be found. The scattering cross-sections of molecules immobilized on the metallic nanostructure in SERS are critical to the technology's usefulness in the environmental monitoring, clinical diagnosis and biochemical research. As a result, the metallic nanostructures and the immobilization of antibodies on them are essential to the success of SERS. New nanoprobe known as SERS tags have been designed as a result of recent developments in SERS. By generating robust and distinctive Raman signals, the SERS-active nanoprobe can be employed in laser Raman spectrometry or SERS microscopy to identify the biomarkers [28].

1.4.3 Electrochemiluminescence immunoassay (ECLIA)

ECLIA works on the same principle as ELISA, antigen-antibody interaction is investigated by the fluorescence produced by the chemical reaction. The ECLIA employs specialized reagents, such as a captured antibody to neutralize the antigen and a tagged antibody to detect contact. On a sturdy support, such as microplate or magnetic bead, the capture antibody is rendered immobile [29]. On the other hand, the labeled antibody has an electrochemically active molecule and a luminous marker coupled to it.

1.4.4 Radioimmunoassay (RIA)

The radioimmunoassay relies on labeled and unlabeled antigens competing with one another for a particular antibody sites to generate antigen-antibody complexes. The binded radioactive complex gets separated from a free radioactive antigen upon reaching equilibrium. The amount of non-radioactive antigen determines the ratio of bound to free forms. A ratio of bound to free forms, which is derived by incubating different amounts of known non-radioactive antigen with an equal quantity of the antibody, determines the concentration of analytes in blood samples. An antibody with a high affinity constant and a highly specific, tagged antigen are needed for this procedure. The antibody's specificity depends on its capacity to identify minute structural details of the analytes. They can be quantitatively measured using the radioimmunoassay approach because of its many advantages, including high precision, high sensitivity, signal detection without optimization, ease of isotope conjugation, and the stability against environmental

interference. However, the limited reagent shelf life and requirement for radiation safety precautions are the drawbacks of radioimmunoassay.

Table 1.1: Summary of numerous techniques used for cancer biomarkers detection

Technique	Advantages	Limitations
Enzyme-linked immunosorbent assay (ELISA)	<ul style="list-style-type: none"> • Well known method • Absorbance is proportional to the antigen concentration 	<ul style="list-style-type: none"> • Lower detection limit • Non-specific interactions • pH and buffer solution affect the result
Surface enhanced Raman spectroscopy (SERS)	<ul style="list-style-type: none"> • Ultrasensitive technique • No photo-bleaching 	<ul style="list-style-type: none"> • Lack of deeper understanding of mechanism and principles • Expensive instrument • Need of advance microscopic techniques for better detection
Electrochemiluminescence immunoassay (ECLIA)	<ul style="list-style-type: none"> • Highly sensitive • No requirement of radioisotope 	<ul style="list-style-type: none"> • Require specific equipment • Suitable for larger analytes
Radioimmunoassay (RIA)	<ul style="list-style-type: none"> • High sensitivity • Ease of isotope conjugation • Signal detection without optimization 	<ul style="list-style-type: none"> • Short shelf-life • Need for protection against hazardous radiation

1.5 Advanced detection techniques

The aforementioned techniques typically require laborious separations and complex label processing, and thus are unable to satisfy the growing clinical needs for the quick detection of cancer biomarkers. Furthermore, the identification of tumor markers with low biogenic concentrations is not effectively served by the current methods. Therefore, novel and commercially viable techniques that can identify biomarkers quickly and sensitively are the need of time.

In last ten years, several biosensors have been developed for the early and efficient detection of the biomarkers [7, 30, 31]. These biosensors are remarkable because of their high sensitivity, low detection limit, great specificity, multiplexing capability and ease of use.

1.6 Biosensors: A new approach to detect biomarkers

An analytical tool called a biosensor is used to find any chemical substance or a particular target molecule. It is made up of a transducer that generates an electronic signal and a biological sensing device. It recognizes the overall physiological shift in the process, which is followed by the information transfer that generates the signal. The man known as the father of biosensors is Prof. Leland C. Clark. In 1962, he created the first enzyme electrode for glucose analysis using glucose oxidase, thus introducing the term “biosensor”. The first biosensor for quick glucose detection in the blood samples was introduced to the market commercially in 1975 [32]. Currently, numerous research groups are investigating a range of biosensing approaches that are utilized in diverse industries. Biosensors are rapid, portable, highly selective and sensitive analytical tools. Over the last ten years, biosensors have emerged as the most dependable, efficient and precise analytical methods for the biomarker detection globally. The schematic representation of biosensor is shown below in **Fig. 1.3**.

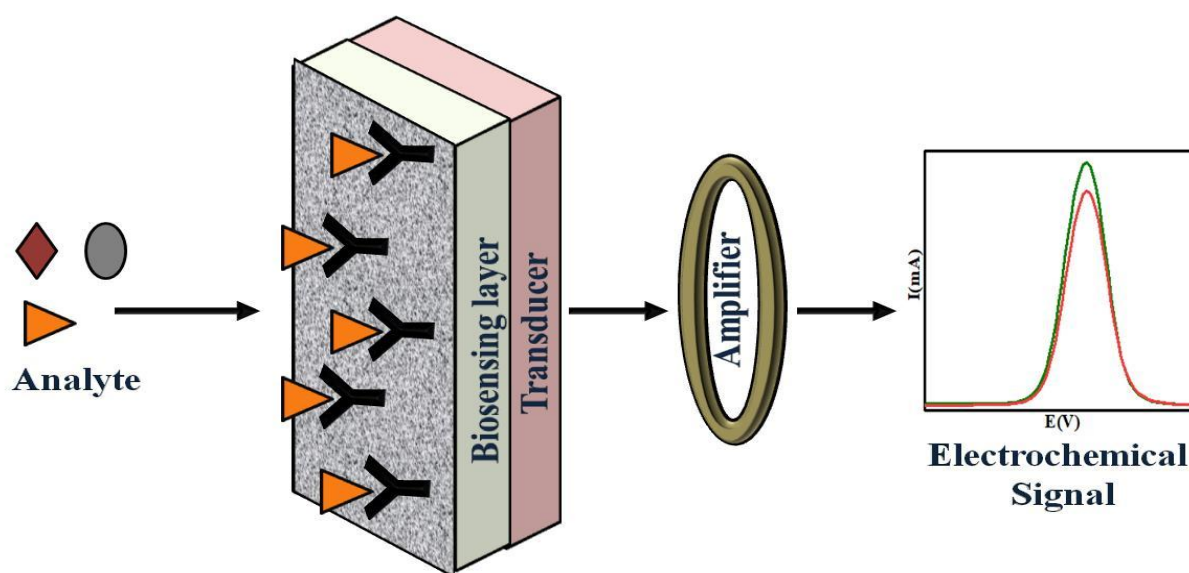


Fig. 1.3: Schematic View of Biosensing Device

1.6.1 Components of a biosensor

1.6.1.1 Bio-receptor

Bio-receptors, also known as bio recognition elements are the molecules that particularly interact with the analyte, such as an enzyme, antibody, cell, DNA, etc. Bio-receptors require a high degree of selectivity towards the particular analyte molecules.

Antibodies are the most often employed bio-receptor in biosensors; they are categorized as polyclonal, monoclonal, or recombinant depending on their production technique and selective characteristics. The optimal method for the interaction between an antigen and its specific antibody is like a lock and key fit model.

1.6.1.2 Immobilization matrix

Bio-recognition components are integrated onto the transducer's surface using a matrix. It can support the preservation of the biomolecule's functionality and increase the analyte molecule's accessibility. The optimal solid support should possess characteristics, which can improve the electron kinetics and biosensor performance. Furthermore, it should be inert, having strong bioaffinity, being hydrophilic and readily available at a low cost [33]. The immobilization process- covalent bonding, adsorption, trapping, cross-linking, etc., is entirely determined by the solid surface that are the chemical characteristics of the bio-receptors. To date, a number of immobilization matrices have been proposed by the researchers.

1.6.1.3 Transducer

An interaction between the biological sensing element and the analyte turns into a measurable electrical signal by transducer. In other words, it has the ability to transform energy from one form to another. This procedure is referred as signalization.

Biosensors can be classified as optical, calorimetric, piezoelectric and electrochemical based on the nature of transducing element [34]. Mainly, we are focusing on the electrochemical biosensors.

1.6.2 Electrochemical biosensors

Electrochemical biosensors are becoming more and more popular, Because of their excellent sensitivity, high selectivity, ease of instrumentation and high reproducibility. They are comprised of three electrodes in which Ag/AgCl behaves like reference electrode, Pt works as counter

electrode and the prepared electrode functions as a working electrode. On the basis of bio-receptor such as enzyme, aptamer, nucleic acid and antibody; electrochemical biosensors are divided in to four categories. A complete classification of a biosensor is presented in the following **Fig. 1.4**.

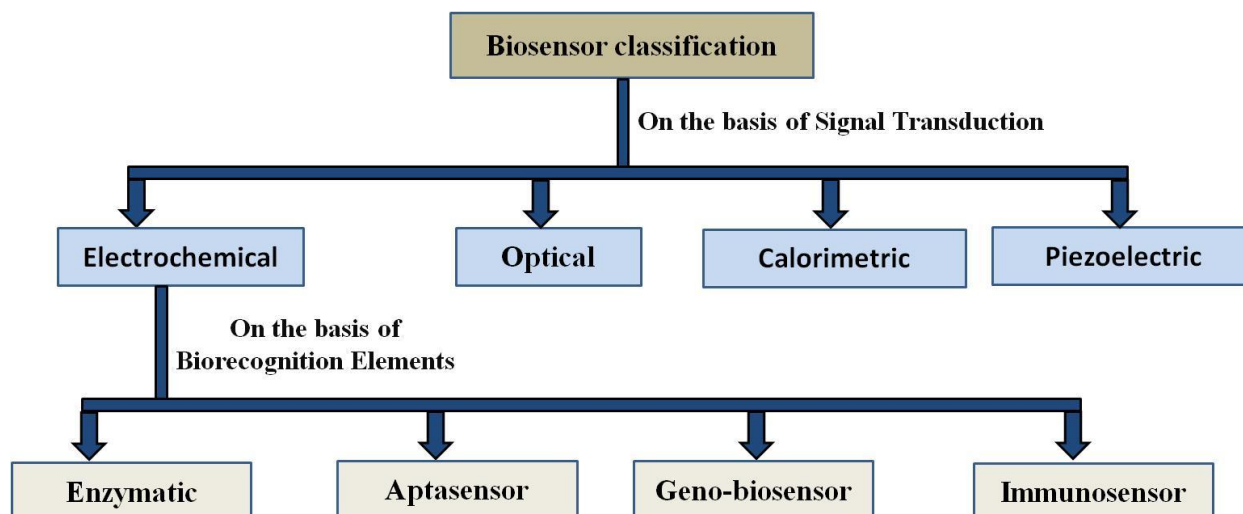


Fig. 1.4: Classification of a Biosensor

1.6.2.1 Electrochemical enzymatic biosensor

The fundamental idea of electrochemical enzyme biosensors is the detection of an electroactive entity following a redox reaction occurring either on electrode or through the use of a mediator. There are various advantages to enzyme biosensors. A variety of commercially available enzymes have the ability to improve the catalytic properties of an enzyme or its substrate specificity. A steady supply of material can be used to catalyze the amplification of a biosensor's response [35].

1.6.2.2 Electrochemical aptasensor

Utilizing aptamer biorecognition elements along with other pseudo-natural modalities opens up a vast array of biosensor applications that can target different bioanalytes such as proteins, metal ions, tiny compounds and even more complicated targets like entire cells. A combinatorial selection method namely systemic evolution of ligands by exponential enrichment (SELEX) was used to create the single-stranded oligonucleotides known as aptamers. Finding significant binding affinities between the target analyte and oligonucleotide sequences is the iterative process of SELEX, which ensures the strong and selective interaction pair.

1.6.2.3 Electrochemical geno-biosensor

Nucleic acid (NA) biosensors also known as genosensors are often made up of single-stranded (ss) DNA; that hybridizes with the complimentary strand with a very high efficiency and strong specificity, making it simple to identify a complementary strand DNA or RNA. In general, the use of NA sensors makes it possible to detect various analytes by using functional nucleic acids (FNAs) as their probe molecules, many of which go beyond the inherent function of NAs [36].

1.6.2.4 Electrochemical immunosensor

Electrochemical immunosensors are a great biosensing platform for precise measurement of protein biomarkers. The biological recognition element, which usually comprises of antibodies or antibody fragments, is the essential part of an immunosensor. Electrochemical biosensor that monitor the interaction between antibody and antigen is known as electrochemical immunosensor. This technique offers high selectivity, sensitivity and low detection cost through the process of antibody-antigen interaction. Additionally, immunosensors enhance their analytical performance, particularly the sensitivity, in order to meet the demand for a precise assessment of the ultra-low quantities of the protein biomarkers. Then, a growing number of signal amplification approaches will be widely used in the immunosensing field, such as molecular biological techniques and nanosignal amplification strategies. In conclusion, immunosensors will become more and more crucial for precise protein biomarker identification in the realm of clinical diagnosis due to their rapid development.

1.6.3 Electrochemical immunosensors for cancer biomarkers detection

The development of electrochemical immunosensors holds up the possibility of an intriguing solution to the problems in the field of cancer diagnostics [37, 38]. Through the straightforward transmission of electrical signals originating from the particular antibody-antigen interaction, which produces a direct readout, these immunosensing approaches can quickly detect the tumor markers. However, the need for intricate setups, labeled antibodies, or tagged antigens frequently prevents these techniques from being widely used. Label-free analysis and detection is therefore the better option [39]. Label-free detection helps with shrinking and the development of extremely portable equipment in addition to saving laborious and time-consuming operations. The label-free immunosensors can immediately analyse the electrochemical signals produced as a result of immunochemical reaction on electrode's surface by using a redox probe. The redox

probe will experience a decreased electrochemical signal as a result of the non-conductive immunocomplex that was produced as a result of the particular immunological reaction. This is because the immunocomplex will increase in impedance and prevent the direct electron transfer through the redox probe. Real-time and in-situ detection is made possible by the redox probe's electrochemical signal's direct reliance on biomolecular interactions. Though there have been some recent advancements [40, 41], these methods are still in their early stages and additional research is undoubtedly needed. A modification is still required for further improvement in the sensitivity and selectivity of immunosensor. The most important factor to improve the sensitivity of electrochemical immunosensors is based on the highly active transducer material having a large specific surface area and numerous active sites.

1.7 Two dimensional (2D) materials

Crystalline solids with one or more atomic layers make up 2D materials. On the basis of chemical composition and structural arrangement, the 2D materials are classified as insulators, superconductors, metallic and semiconductors. Specifically, 2D materials are the best choice for enhancing their physicochemical characteristics and creating their functionalities at the atomic level through element doping, bandgap engineering, surface functionalization or chemical modification and thickness control, all of which are challenging to accomplish in bulk materials [42]. Recently, there is a significant interest in 2D ultrathin materials, such as graphene and transition metal dichalcogenide (TMDs), as well as other 2D materials, such as hexagonal boron nitride (h-BN), MXenes, transition metal oxides (TMOs), graphitic carbon nitride (g-C₃N₄), layered double hydroxide (LDH) with modified physicochemical and electrical characteristics. The schematic representation of various 2D-materials along with their structures is shown in **Fig. 1.5**.

The most studied material, graphene possesses extraordinary properties such as 2D planar structure, high surface area, excellent thermal conductivity and fast carrier mobility.

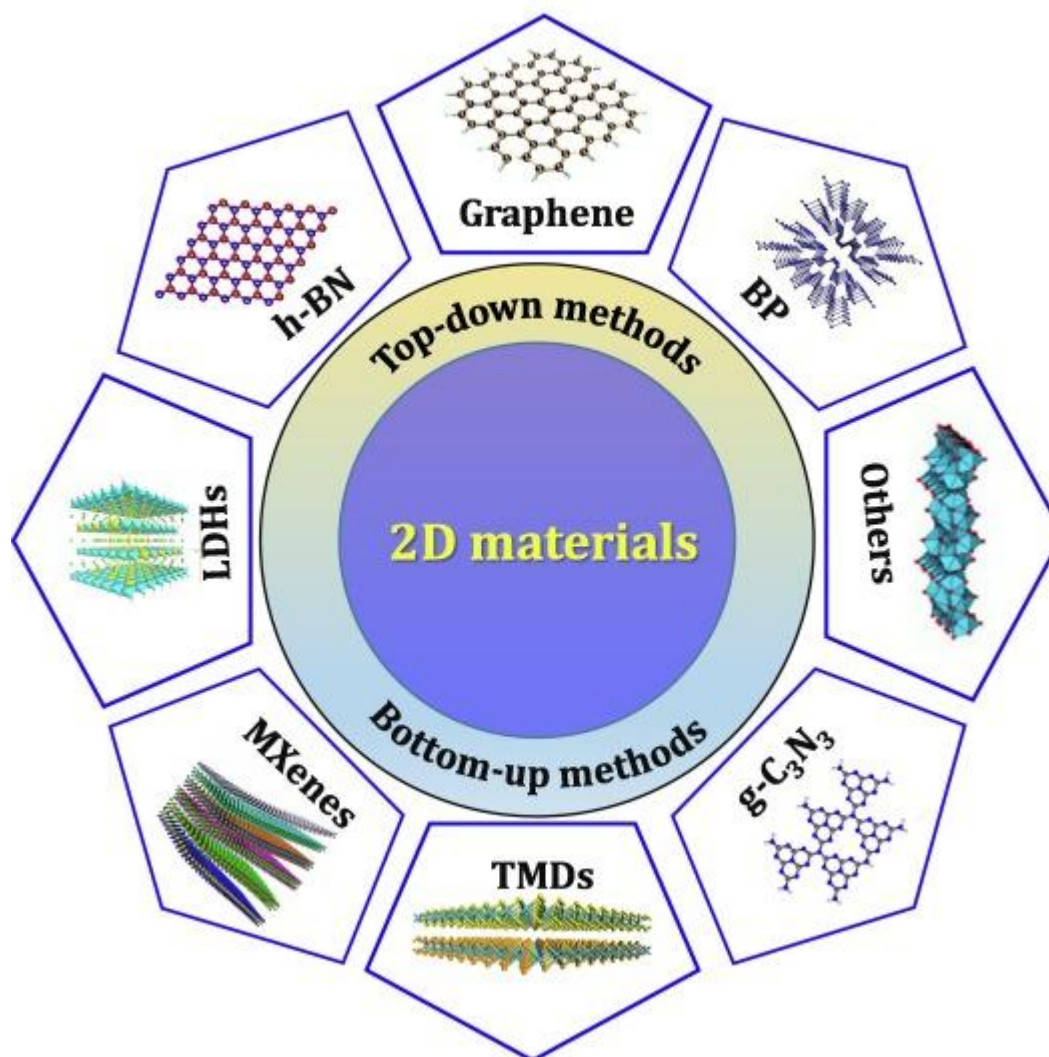


Fig. 1.5: Schematic representation of 2D-materials along with their structures, Adapted with the permission from [43]. Copyright © 2022 Elsevier

The development of 2D heterostructures is driven by their potential applications and areas of crucial interest. Generally, the creation of a heterointerface through the stacking of two distinct materials is referred as a heterostructure [44]. Based on the various functions, a variety of heterostructures have been described, including inorganic–semiconductor, semiconductor–metal, and semiconductor–carbon. On the other hand, the design and consumption of 2D/2D heterostructures have gained attention in electrochemical applications [45]. 2D heterostructures are fabricated by both ex-situ and in-situ techniques. The ex-situ synthetic approach involves the preparation of each 2D material component individually, after which the 2D heterostructure

composite is formed via liquid-phase exfoliation, chemical vapor deposition (CVD), or epitaxial growth [46]. In terms of cost-effectiveness and scalability production, the ex-situ synthetic approach offers a number of benefits. However, it takes a long time to get the component ingredients and involves multiple intricate synthesis techniques and expensive instruments. The hydrothermal, solvothermal and sol–gel techniques are the part of in-situ synthesis strategy and can manufacture 2D heterostructure at the nanolevel with uniform distribution [47]. The diagrammatic representation of synthesis methods and properties of 2D heterostructures is shown in Fig. 1.6.

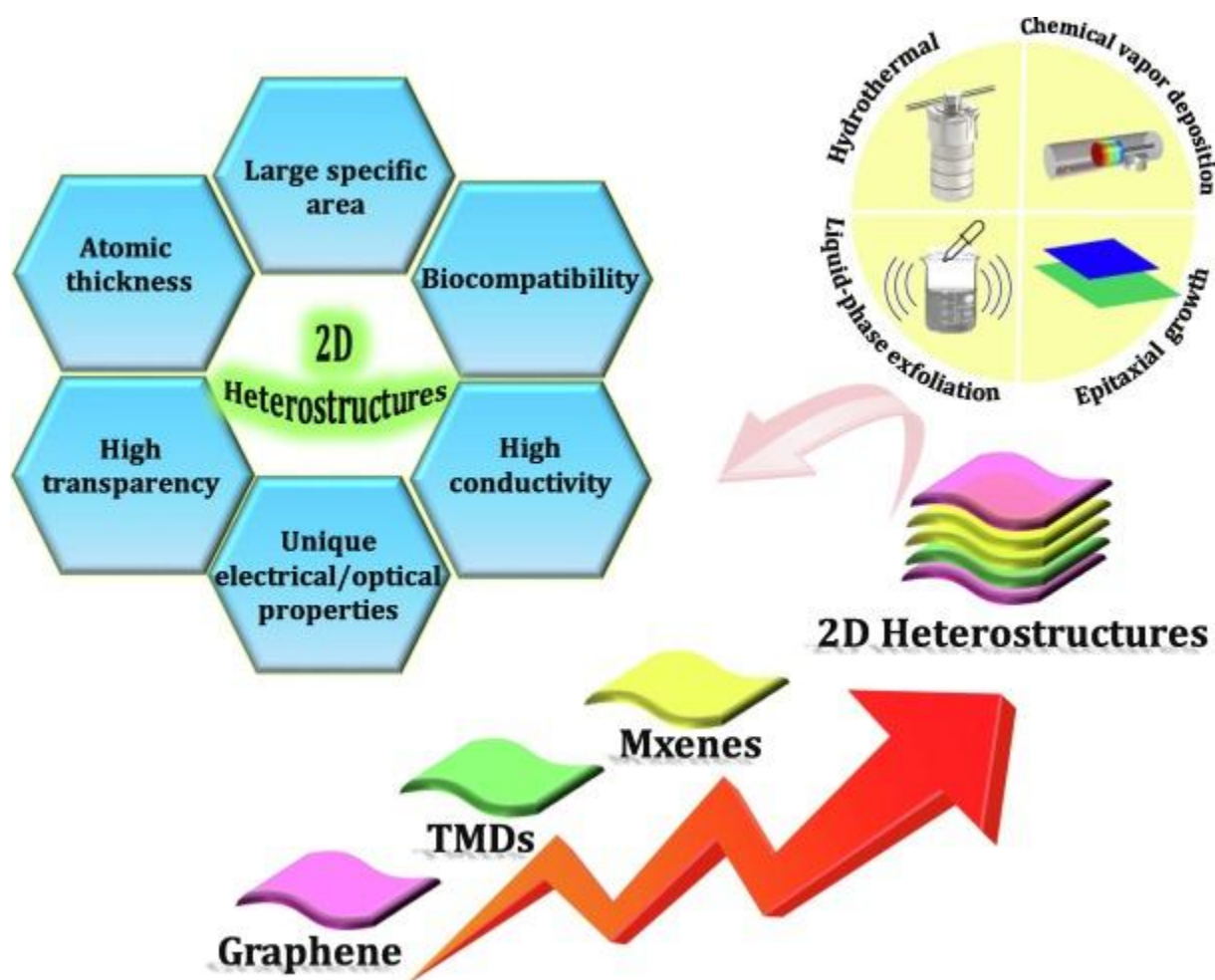


Fig. 1.6: Diagrammatic representation of synthesis methods and characteristics of 2D-materials, Adapted with the permission from [43]. Copyright © 2022 Elsevier

The 2D heterostructures exhibit remarkable characteristics, such as good electric conductivity, reasonably high electrocatalytic activity, and high concentrations of the electroactive sites. These improved characteristics enable the redox properties of the various electroactive molecules or ions, thereby improving peak-to-peak separation, selectivity, and sensitivity in complex samples.

On the other hand, 2D material surfaces functionalized with biomolecules and/or linkers offer mechanical stability, conductivity, and affix sites to enhance direct electron transport [48]. Because of this, 2D materials have been used to develop the biosensors. Additionally, by simply functionalizing their surfaces, 2D materials can work as extremely effective probes for the detection of biomolecules and cancer biomarkers. Recently, MXene has been extensively studied as a novel material. MXene possess distinct electronic characteristics, high surface area, excellent biocompatibility as well as terminated with multiple active groups, including hydroxyl groups, oxygen ions and fluorine ions, which make it a suitable candidate for the cancer biomarker detection [49].

1.7.1 MXene

In 2011, researchers at Drexel University made the discovery of a brand-new class of 2D-materials called MXenes [50]. The MXenes group consists of carbonitrides, carbides and nitrides of transition metals having the general formula $M_{n+1}X_n$, where X is carbon and/or nitrogen, M is early transition metals (Sc, Ti, Zr, Hf, V, Nb, Ta, Cr, Mo etc.) and n is 1, 2 or 3 [51]. The name “MXene” is chosen to detect the parent carbonitride, nitrides and carbide, or MAX phases, that are the main precursors for MXenes synthesis, as well as to highlight the similarities between the 2D-materials family and graphene. The general formula for MAX phases, which are stacked ternary carbides and nitrides, is $M_{n+1}AX_n$, where A represents group 13 or 14 elements [52].

The first step in the synthesis of MXene is to etch the A-element atomic layers of the MAX phase. Generally, ‘A’ layers etching from the MAX phase results in the surface modified with various functional groups ($-OH$, $-F$, $-O$), which further provide a favorable microenvironment for the bioreceptor (DNA, enzymes, proteins, etc.) immobilization and help to retain their bioactivity and stability. After etching, multilayered MXene sheets are produced having hydrogen bonds and van der Waals forces among the 2D-layers. Since, all the A-element layers have been removed, therefore washing is necessary to eliminate the remaining acid and the reaction products and bring the pH down to a safe level (about 6). Typically, washing involves

decanting the acidic supernatant and repeatedly centrifuging the multilayered MXene to separate it from the acidic solution. The multilayered flakes can be collected, either by vacuum-assisted filtering or vacuum-dried. It is well known that the $\text{Ti}_3\text{C}_2\text{T}_x$ is one of the most studied MXene having a large specific surface area, good biocompatibility, and the excellent electrical properties. Such features enable $\text{Ti}_3\text{C}_2\text{T}_x$ for its better applications in supercapacitors, sodium and lithium ion batteries, biosensing and energy conversion fields. The 2D-structure of $\text{Ti}_3\text{C}_2\text{T}_x$ has been shown in **Fig. 1.7**.

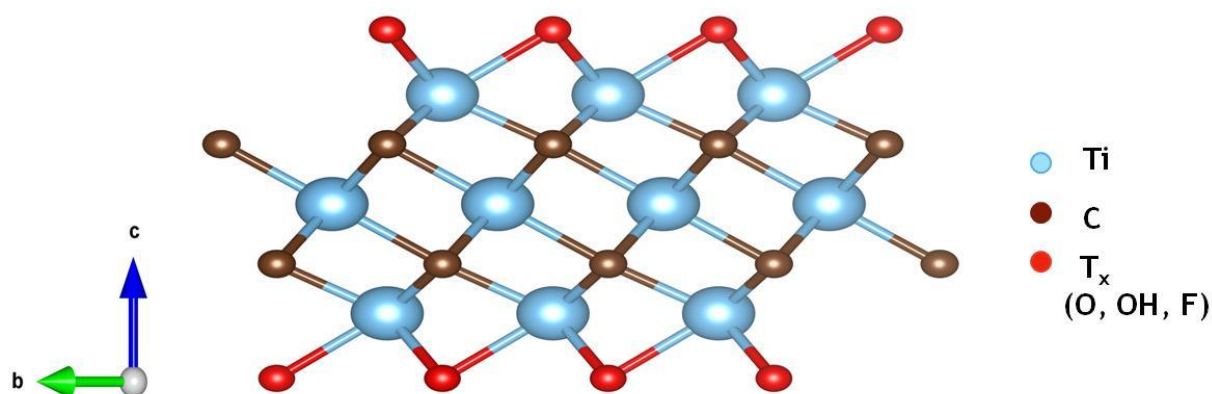


Fig. 1.7: Structure of $\text{Ti}_3\text{C}_2\text{T}_x$

1.7.2 Properties of MXenes

MXene's notable characteristics are its tunable bandwidth, high electric and thermal conductivities, and maximum range of Young's modulus, all of which are acknowledged as special and advantageous. Especially, the enhanced thermal conductivities and hydrophilic nature of MXenes distinguish them from other two-dimensional materials [53]. Finally, morphology/geometric structure correlations, surface functionality and composition can all be used to modify the related features and explosive performances. MXene's tunable bandwidth, widest Young's modulus range, and enhanced thermal and electrical conductivities are considered as unique and most beneficial attributes.

1.7.2.1 Mechanical properties

Using atomic force microscopy measurements, the Young's modulus and breaking strength of $\text{Ti}_3\text{C}_2\text{T}_x$ (MXene) flakes were found to be 333 GPa and 17.3 GPa, respectively. The value of Young's modulus was found to be highest, when compared to the other similar 2D-materials,

such as graphene oxide etc. In comparison to graphene membranes, the synthesized $Ti_3C_2T_x$ monolayer via HF etching giving a flexible layer which exhibits much more localized punctures. MXenes have better interaction with polymeric matrix because of the surface functionalities than graphene in composite applications [54]. Some theoretical research indicates that functional groups improve the mechanical characteristics of MXene. MXene's -F, -O and -OH terminals have the ability to relieve both monoaxial and biaxial stresses. Once comparing the MXene to graphene compounds, it is far better for further use. The functional groups increase the mechanical flexibility by preventing the atomic layer disintegration. The MXene planes exhibit stronger bonding than other planes. Therefore, it is feasible to mechanically exfoliate MAX phase as opposed to chemically exfoliate them.

1.7.2.2 Electrical and thermal properties

Ti_3AlC_2 exhibits high thermal oxidation and thermal conductivity. Thermal conductivity for $Ti_3C_2T_x$ films is discovered experimentally to be approximately 2.84 W/m K. $Ti_3C_2T_x$ films are extremely flexible in nature and have a metallic conductivity of 2400 S/cm [55]. It is reported that the annealing temperature and film thickness have a big impact on the sheet conductivities.

1.7.2.3 Optical properties

Two main optical characteristics of MXene are their high transparency and photothermal effect. Another crucial characteristic of $Ti_3C_2T_x$ films is the strong surface plasmonic effect [56].

1.7.2.4 Chemical properties

MXenes often have a surface that is hydrophilic. High volumetric capacitance is a property of titanium-based MXene due to the redox-active Ti atom. The carbide layer owing to its conductive nature has the ability to increase the flow of electrons toward redox-active spots [57]. Additionally, it can transport ion quickly. As a result, it gained popularity as a candidate for pseudocapacitors, which increase energy density by utilizing the rapid redox reactions.

1.7.3 MXene-based hybrid materials

MXene sheets are bound together by van der Waals forces of attraction. There may be restacking due to weak forces present in between the sheets, which further reduces the exposure of electrochemical active sites. Furthermore, MXene has a serious disadvantage of agglomeration in biological medium [58]. Hence, it becomes necessary to modify the MXene's surface to improve

its stability in biological sensing applications. Consequently, in order to improve the stability and biocompatibility of MXene, numerous metals, metal oxides and metal sulphides are being studied for MXene-based hybrids formation.

1.8 Synthesis of MXene

To synthesize MXene, numerous top-down and bottom-up methods have been devised. These methods include non-etching methods such as chemical vapor deposition as well as etching of MAX phase precursors and other ternary stacked carbides [59].

1.8.1 Top-down approach

Top-down technique is generally used to fragment bulk materials thereby producing nanostructured materials. MXenes are currently being synthesized by various methods via top-down approach. Hydrogen fluoride (HF) etching, electrochemical etching, hydrothermal etching and fluorine-free etching etc are such methods. These preparation techniques not only have a significant impact on MXene's shape, but also determine the properties of the prepared material simultaneously. General synthesis of MXene is represented in **Fig. 1.8**.

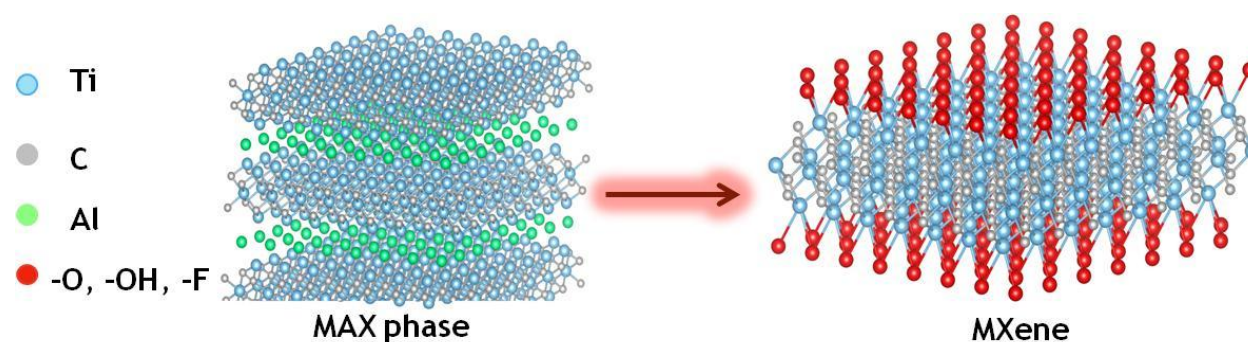


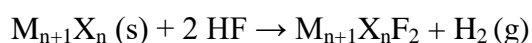
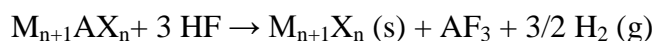
Fig. 1.8: General synthesis of MXene

1.8.1.1 HF etching

Recently, HF etching of MXenes has become more and more popular, with potential global applications. In-situ HF etching and direct HF etching are two most popular techniques used for the preparation of MXenes.

In-situ HF etching is usually produced by HCl and LiF mixture, which are less aggressive etchants. They can produce MXene flakes with greater lateral dimensions, improved electrochemical parameters and lesser flaws [60].

On the other hand, direct HF etching is based on immersing MXene's precursors directly in HF, for example, the Al layer from Ti_3AlC_2 to create multi-layered $Ti_3C_2T_x$, where the 2D layers are held together by hydrogen and van der Waals forces [61]. In the first synthesis method, Naguib et al. used direct HF as an etching reagent to create MXene from the MAX phase (Ti_3AlC_2). They dissolved Ti_3AlC_2 powder in a 50% aqueous dispersion of HF and agitated the mixture for 2 h at 25 °C [62]. This approach is based on the following reaction:



In this process, the "A" layer etching of the MXene precursors results in the multilayered MXene nanosheets [63]. According to the aforementioned equation, hydrogen evolution paves the stage for the probable exfoliation of MXene's adjacent layers. Furthermore, intercalation and delamination of etched MXene are often needed to increase the interlayer spacing between the MXene sheets so that these may be converted into the individual 2D sheets. Polar chemical compounds like tetramethyl ammonium hydroxide (TMAOH) and dimethyl sulfoxide (DMSO) are often used as intercalants [64].

1.8.1.2 Bifluoride salt etching

Bifluoride salts are another alternative to HF, as they are somewhat milder etchants. Etching the "A" layers from MAX phases may require more time and higher temperature when using the milder etchant. Ammonium bifluoride (NH_4HF_2), sodium bifluoride ($NaHF_2$), and potassium bifluoride (KHF_2) are the three types of salt that are being utilized most frequently [65]. $Ti_3C_2T_x$ nanosheets were created by Feng et al. using the etchants NH_4HF_2 and HF [66]. A comparative morphological and electrochemical analysis was then conducted for the purpose of desalination. The results showed that the HF-etched $Ti_3C_2T_x$ interlayer spacing rise by 1.6 Å from 18.4 to 20.0 Å, while the NH_4HF_2 -etched $Ti_3C_2T_x$ interlayer spacing increased by 6.4 Å. Furthermore, it has been reported that the high value of O and F content in NH_4HF_2 -etched $Ti_3C_2T_x$ as compared to the HF-etched $Ti_3C_2T_x$ further improves the conductivity and oxidative stability.

1.8.1.3 Molten salt-based etching

Molten salt etching has proved to be one of the most popular etching techniques as an alternative to HF-etching. Urbankowski et al. created titanium nitride (MXene) using molten salt etching technique [67]. Since HF is not used, this method of etching MAX phase is far safer than previous techniques. A replacement reaction mechanism is employed to etch Max phase by heating them in the presence of molten Lewis acid salt. This method broadens the range of MAX-phase precursors that can be used to create new 2D materials and presents significant chances to adjust the surface chemistry, characteristics of MXenes, and oxidative stability [68].

1.8.1.4 Electrochemical etching

It is an intrinsically electron transfer electrochemical mechanism which is used during the etching process. Although the majority of techniques depend on the etchants, they can modify the etching outcomes to a certain degree, however this can be disregarded in electrochemical etching because it doesn't need an etchant [69]. This method can be applied to carbide-derived-carbon (CDC) by employing salts based on fluoride and chloride as the electrolytic system. Although, this method is frequently criticized for producing low yields due to the concurrent CDC layer over MXenes, it is possible to selectively remove the "A" layer under a specific voltage by using the MAX phase as an electrode, and precise control over the synthesis is made possible by the modulation of the etching voltage window [69]. CFC substrates and diluted HCl electrolytes are two of the most common electrochemical etching materials.

1.8.1.5 Hydrothermal etching

An effective method for isolating HF exposure and etching MXene precursors in a closed environment is the hydrothermal technique. Composites with controlled morphologies and high crystallinity can be made by sealing etchant and MAX phase in a vessel at high temperature and pressure [70]. Guo et al. reported the complete etching of Ga from $\text{Mo}_2\text{Ga}_2\text{C}$ at 140–180 °C in 24 h [71]. $\text{Ti}_3\text{C}_2\text{T}_x$ and Nb_2CT_x were synthesized by Peng et al. in an autoclave by using a mixture of NaBF_4 and HCl, and then compared with their equivalents that were directly HF etched. By using hydrothermal treatment, it takes 16 h to thoroughly etch the Al layer from Ti_3AlC_2 . That was proved by very less shift of (002) diffraction peak than that of its HF-etched counterpart, suggesting a greater interlayer gap. It's noteworthy to understand that, in contrast to the conventional HF etching, strong peaks of TiC impurities are started to appear after etching for

more than 20 h at temperatures of 140–180 °C. This analysis reveals the efficacy of hydrothermal treatment for precursors which are unable to exfoliate easily.

1.8.1.6 Ionic liquid-based etching

During synthesis of MXene, fluorine based etchants generally produce fluoride ions, which are bad for the environment and people. Recently, Husmann et al. reported a novel synthesis technique that uses fluorine-containing ionic liquids (IL) to etch off the Al from Ti_3AlC_2 and Ti_2AlC to generate $Ti_3C_2T_x$ and Ti_2CT_x , respectively, without the need of acid [72]. In an aqueous environment, ILs such as 1-butyl-3-methylimidazolium hexafluorophosphate ($BMIMPF_6$) and 1-ethyl-3-methylimidazolium tetrafluoroborate ($EMIMBF_4$) act as etching and intercalating agents. The IL serves as an etchant and an intercalant, therefore it creates MXenes with more interlayer space in between the sheets. Unlike other fluorine-containing acid methods, this method does not cause fluorine to dissociate as fluoride ions.

1.8.2 Bottom–up approach

The needs of various point-of-care devices are still not met by MXenes synthesized using the aforementioned top-down approaches. The use of MXenes in electrochemical applications may be limited by their weak electrical characteristics, faulty structure and surface entanglement with numerous functional groups, including -Cl, -OH, -F, and -O. Fortunately, bottom-up methods such as CVD offer innovative ways to create high-grade, thermally stable MXenes [73].

1.8.2.1 Chemical vapour deposition (CVD)

CVD is frequently utilized as a fluorine-free etching technique to fabricate 2D-nanosheets. Xu et al. have used this technique to produce ultrathin Mo_2C with a large and clean surface area. The growth of 2D- Mo_2C crystals was characterized by HAADF-STEM and could be regulated by applying a high temperature to achieve thick and lateral size. The remarkable chemical and thermal stability of ultrathin- Mo_2C made their superconductivity exceptionally dependable. Additionally, the MXenes produced by this flexible CVD growth process have rather high transverse dimensions. Even so, a great deal of research has shown that pyrolysis and CVD are effective ways to produce MXenes. However, the shape of the MXenes synthesized using this approach varies, making it challenging to identify the MXene structure.

1.9 Applications of MXenes and MXene-based hybrids for cancer biomarker detection

The review of existing literature reveals that MXenes and their hybrids have been utilized as a sensing platform for cancer biomarkers detection. An electroactive screen-printed electrode (SPE) platform based on MXene has been developed by Selcan et al. [74] for the detection of sarcosine (a prostate cancer biomarker). An efficient SPE based on MXene pre-loaded with methylene blue has been proposed by Sana et al. [75] for selective detection of CD44 proteins. Further, Sue et al. [76] constructed a novel bifunctional electrochemical biosensor for circulating tumor cells (CTCs) detection using prussian blue-MXene composite films. A surface plasmon resonance biosensor has been designed by Anil et al. [77] for CEA detection using graphene, MXene and MoS₂. A gold nanoparticles and MXene composite based electrochemical sensing platform has been developed by Xiongtao et al. [78] for KRAS gene detection. The Ti₃C₂T_x-Au hybrid was further used by Gul et al. [79] to fabricate a novel electrochemical immunosensor for calreticulin detection. An esophageal cancer marker, CA19-9 has been detected by Qifie et al. [80] using MXene based electrochemical immunosensor. Qiong et al. [81] developed a two-dimensional amino-functionalized MXene based SPR biosensor for CEA antigen detection. The aminosilane functionalized MXene nanosheets have been developed by Saurabh et al. [82] for CEA antigen detection. Further, Quan et al. [83] proposed an electrochemical immunoassay based on AuNPs/M-NTTO-PEDOT composite for sensitive detection of prostate specific antigen. Huixin et al. [49] developed an electrochemical biosensor by in-situ hybridization of Prussian blue on the surface of MXene for successful detection of exosomes. Furthermore, a sensitive electrogenerated chemiluminescence (ECL) biosensor was reported by Huixin et al. [84] based on aptamer modified MXene nanosheets for exosomes detection. A novel sandwich type biosensor has been fabricated by Linlin et al. [85] for high performance detection of exosomes. They used amino-functionalized Fe₃O₄ combined with EpCAM aptamer modified MXene nanosheets. Further, exosomes are identified by Qiannan et al. [86] by constructing an electrochemical biosensor using Au-nanoarray modified MXene nanosheets as a transducer.

1.10 Objective

The main objective of this thesis is to develop an immunosensor by using a new class of 2D-materials, MXene and its hybrids with metal, metal oxides and metal sulphides for the detection of cancer biomarker. The fabrication of electrochemical immunosensor has been accomplished by following stages:

- Synthesis and modification of MXene by less hazardous method as well as investigating the parameters, which affect the electrochemical performance.
- Characterization of synthesized materials by structural and morphological techniques.
- Fabrication of transducer matrix by electrophoretic deposition of material on ITO electrode and dip coating method.
- Covalent immobilization of antibody onto the prepared coated electrode.
- Electrochemical response studies of the bioelectrode using different electrochemical techniques for cancer biomarker detection.
- Reproducibility, selectivity and stability studies of immunosensors.
- Clinical validation of the results using spiked artificial serum samples with biomarker.

1.11 Thesis Organization

This thesis focuses on the synthesis, characterization and application of $Ti_3C_2T_x$ and its hybrid with Ag, TiO_2 and CuS, in order to create efficient electrochemical immunosensors for the targeted detection of EpCAM antigen.

This thesis comprises of eight chapters highlighting the research work in the following sections:

Chapter 1 presents a thorough overview of cancer, its classification and various techniques available for the detection. Further, biomarker based early cancer detection has been explained with special emphasis on electrochemical biosensors. In addition, an attempt has been made to provide a descriptive literature review of MXene especially properties and different methods of synthesis.

Chapter 2 outlines the details of experimental methods used for the structural and morphological analysis of all prepared materials and modified electrodes. These methods include scanning electron microscopy (SEM), transmission electron spectroscopy (TEM), X-ray diffraction (XRD) and energy dispersive X-ray spectroscopy (EDX). Further, there have been attempts to explain all the electrochemical techniques such as differential pulse voltammetry (DPV) and chronoamperometry which are being used to characterize all the fabricated electrodes and electrochemical immunosensors.

Chapter 3 describes the fabrication of electrochemical immunosensor by using the $\text{Ti}_3\text{C}_2\text{T}_x$ for cancer biomarker detection. The hydrothermally synthesized- $\text{Ti}_3\text{C}_2\text{T}_x$ has been proved to be an efficient material to fabricate the immunosensor's platform for biosensing studies due to its high metal-like conductivity and hydrophilic nature. The electrochemical response data of the fabricated BSA/anti-EpCAM/ $\text{Ti}_3\text{C}_2\text{T}_x$ immunosensor show a very broad linear range (0.1 fg/ml to 100 ng/ml) for the detection of EpCAM antigen. Additionally, the long stability of this immunosensor provides a benefit for EpCAM antigen detection in serum samples.

Chapter 4 deals with the research findings of novel CuS-anchored 2D- $\text{Ti}_3\text{C}_2\text{T}_x$ hybrid based electrochemical immunosensor. Wherein, a CuS/ $\text{Ti}_3\text{C}_2\text{T}_x$ hybrid has been synthesized by a novel one-pot hydrothermal method. The synthesized material was then deposited onto the ITO electrode by electrophoretic method. It was observed from the investigations that there is an increase in the rate of electron transfer for CuS/ $\text{Ti}_3\text{C}_2\text{T}_x$ @ITO electrode as compared to $\text{Ti}_3\text{C}_2\text{T}_x$ @ITO, thereby making it promising material for anti-EpCAM immobilization. Further, the electrochemical results with anti-EpCAM/CuS/ $\text{Ti}_3\text{C}_2\text{T}_x$ @ITO electrode demonstrated the good reproducibility, selectivity and stability for EpCAM antigen detection.

Chapter 5 reveals the development of an extremely sensitive electrochemical immunosensor for the detection of label-free EpCAM antigen by using 2D/2D TiO_2 / $\text{Ti}_3\text{C}_2\text{T}_x$ hybrid. An in-situ development of 2D- TiO_2 on $\text{Ti}_3\text{C}_2\text{T}_x$ -sheets leads to the enhancement of surface area and biocompatibility of immunosensor. The immunosensor is developed by immobilization of anti-EpCAM onto the electrophoretically deposited ITO electrode. The developed BSA/anti-EpCAM/ TiO_2 / $\text{Ti}_3\text{C}_2\text{T}_x$ @ITO immunosensor is found to possess very low detection limit (0.7 ag/mL) and extremely high sensitivity. This immunosensor has exceptional selectivity, excellent long term stability and specificity.

Chapter 6 elaborates the fabrication of a cost effective, biodegradable and flexible paper-based immunosensor for EpCAM antigen detection. The conducting paper (CP) was fabricated by the dip coating of Whatman paper in aq. suspension of CuS and PEDOT:PSS. Further, electrochemical parameters were enhanced by doping the CP with dimethyl sulfoxide (DMSO). Then, anti-EpCAM was immobilized and the resulted immunosensor was further utilized to detect the EpCAM antigen. It was observed that, the immunosensor shows an excellent

reproducibility, stability and selectivity along with high sensitivity ($104.31 \mu\text{A pg}^{-1} \text{mL}$) for EpCAM detection.

Chapter 7 deals with the fabrication of novel CP immunosensor based on Ag, $\text{Ti}_3\text{C}_2\text{T}_x$ and PEDOT:PSS for EpCAM antigen detection. CP based transducer matrix was prepared by dip coating method. Further, anti-EpCAM was covalently immobilized and kept the same for 8 h at 4°C in a humid chamber. The electrochemical studies suggested that the biodegradable immunosensor shows the good selectivity ($K_{\text{selectivity}} < 1$), and clinical applicability to detect the EpCAM antigen in humans.

Chapter 8 outlines the summary of all the investigations and applications of MXene-based 2D-materials for cancer biomarker detection. Further, the potential avenues for future research based on 2D-materials have also been reported in this chapter.

References:

- [1] S.D. Ferrell Jr, I. Ahmad, C. Nguyen, S.C. Petrova, S.R. Wilhelm, Y. Ye, S.H. Barsky, Why is cancer so common a disease in people yet so rare at a cellular level?, *Medical Hypotheses*, 144 (2020) 110171.
- [2] R.L. Elliott, Combination cancer immunotherapy" Expanding Paul Ehrlich's Magic Bullet Concept", *Surgical oncology*, 21 (2010) 53-55.
- [3] F. Islami, K.D. Miller, R.L. Siegel, Z. Zheng, J. Zhao, X. Han, J. Ma, A. Jemal, K.R. Yabroff, National and state estimates of lost earnings from cancer deaths in the United States, *JAMA oncology*, 5 (2019) e191460-e191460.
- [4] H. Sung, J. Ferlay, R.L. Siegel, M. Laversanne, I. Soerjomataram, A. Jemal, F. Bray, Global cancer statistics 2020: GLOBOCAN estimates of incidence and mortality worldwide for 36 cancers in 185 countries, *CA: a cancer journal for clinicians*, 71 (2021) 209-249.
- [5] Q. Song, S.D. Merajver, J.Z. Li, Cancer classification in the genomic era: five contemporary problems, *Human genomics*, 9 (2015) 1-8.
- [6] K. Lewin, Carcinoid tumors and the mixed (composite) glandular-endocrine cell carcinomas, *The American Journal of Surgical Pathology*, 11 (1987) 71-86.
- [7] M.R.A. Wahab, T. Palaniyandi, M. Ravi, G. Baskar, H. Surendran, S. Gangadharan, B.K. Rajendran, Biomarkers and biosensors for early cancer diagnosis, monitoring and prognosis, *Pathology-Research and Practice*, 250 (2023) 154812.
- [8] S. Ellis, J. Husband, P. Armstrong, D. Hansell, Computed tomography screening for lung cancer: back to basics, *Clinical radiology*, 56 (2001) 691-699.
- [9] I.J. Das, H. Sagreiya, P. Yadav, B.D. Allen, Basics of MR imaging for the radiation oncologist, *Advances in Magnetic Resonance Technology and Applications*, Elsevier, 2023, pp. 5-32.
- [10] A. Safari, F. Falahati, M. Mahdavi, M. Akbarnejad, A. Mohammadzadeh, Evaluation of organ dose, effective dose and cancer risk of head and neck dual-energy computed tomography, *Radiation Physics and Chemistry*, (2024) 111539.
- [11] D. Barba, A. León-Sosa, P. Lugo, D. Suquillo, F. Torres, F. Surre, L. Trojman, A. Caicedo, Breast cancer, screening and diagnostic tools: All you need to know, *Critical reviews in oncology/hematology*, 157 (2021) 103174.
- [12] J. Wang, H. Li, X. Wang, T. Shen, S. Wang, D. Ren, Alisol B-23-acetate, a tetracyclic triterpenoid isolated from *Alisma orientale*, induces apoptosis in human lung cancer cells via the mitochondrial pathway, *Biochemical and Biophysical Research Communications*, 505 (2018) 1015-1021.
- [13] W.H. Organization, Biomarkers in risk assessment: Validity and validation, World Health Organization, 2001.

- [14] T.M. Gorges, K. Pantel, Circulating tumor cells as therapy-related biomarkers in cancer patients, *Cancer Immunology, Immunotherapy*, 62 (2013) 931-939.
- [15] R.L. Siegel, K.D. Miller, A. Jemal, Cancer statistics, 2019, *CA: a cancer journal for clinicians*, 69 (2019) 7-34.
- [16] J.G. Pacheco, M.S. Silva, M. Freitas, H.P. Nouws, C. Delerue-Matos, Molecularly imprinted electrochemical sensor for the point-of-care detection of a breast cancer biomarker (CA 15-3), *Sensors and Actuators B: Chemical*, 256 (2018) 905-912.
- [17] P.F. Pinsky, P.C. Prorok, B.S. Kramer, Prostate Cancer Screening-A Perspective on the Current State of the Evidence, *The New England journal of medicine*, 376 (2017) 1285-1289.
- [18] H. Afsharan, F. Navaeipour, B. Khalilzadeh, H. Tajalli, M. Mollabashi, M.J. Ahar, M.-R. Rashidi, Highly sensitive electrochemiluminescence detection of p53 protein using functionalized Ru-silica nanoporous@ gold nanocomposite, *Biosensors and Bioelectronics*, 80 (2016) 146-153.
- [19] J. Zhao, Y. Tang, Y. Cao, T. Chen, X. Chen, X. Mao, Y. Yin, G. Chen, Amplified electrochemical detection of surface biomarker in breast cancer stem cell using self-assembled supramolecular nanocomposites, *Electrochimica Acta*, 283 (2018) 1072-1078.
- [20] S.-E. Kim, Y.J. Kim, S. Song, K.-N. Lee, W.K. Seong, A simple electrochemical immunosensor platform for detection of apolipoprotein A1 (Apo-A1) as a bladder cancer biomarker in urine, *Sensors and Actuators B: Chemical*, 278 (2019) 103-109.
- [21] D. Tang, R. Yuan, Y. Chai, Magnetic control of an electrochemical microfluidic device with an arrayed immunosensor for simultaneous multiple immunoassays, *Clinical Chemistry*, 53 (2007) 1323-1329.
- [22] E.B. Aydın, M.K. Sezgintürk, A sensitive and disposable electrochemical immunosensor for detection of SOX2, a biomarker of cancer, *Talanta*, 172 (2017) 162-170.
- [23] Y. Chen, L.-P. Mei, J.-J. Feng, P.-X. Yuan, X. Luo, A.-J. Wang, Simple one-pot aqueous synthesis of 3D superstructured PtCoCuPd alloyed tripods with hierarchical branches for ultrasensitive immunoassay of cardiac troponin I, *Biosensors and Bioelectronics*, 145 (2019) 111638.
- [24] H. Li, Q. Wei, J. He, T. Li, Y. Zhao, Y. Cai, B. Du, Z. Qian, M. Yang, Electrochemical immunosensors for cancer biomarker with signal amplification based on ferrocene functionalized iron oxide nanoparticles, *Biosensors and Bioelectronics*, 26 (2011) 3590-3595.
- [25] M.Y. Rubtsova, G.V. Kovba, A.M. Egorov, Chemiluminescent biosensors based on porous supports with immobilized peroxidase, *Biosensors and Bioelectronics*, 13 (1998) 75-85.
- [26] X. Zhang, X. Peng, W. Jin, Scanning electrochemical microscopy with enzyme immunoassay of the cancer-related antigen CA15-3, *Analytica chimica acta*, 558 (2006) 110-114.

- [27] B. Acevedo, Y. Perera, M. Ruiz, G. Rojas, J. Benítez, M. Ayala, J. Gavilondo, Development and validation of a quantitative ELISA for the measurement of PSA concentration, *Clinica chimica acta*, 317 (2002) 55-63.
- [28] Y.C. Cao, R. Jin, C.A. Mirkin, Nanoparticles with Raman spectroscopic fingerprints for DNA and RNA detection, *Science*, 297 (2002) 1536-1540.
- [29] S.M. Premnath, M. Zubair, Electrochemiluminescence Method, in: *StatPearls*, StatPearls Publishing, 2023.
- [30] Q. Wu, Z. Li, Q. Liang, R. Ye, S. Guo, X. Zeng, J. Hu, A. Li, Ultrasensitive electrochemical biosensor for microRNA-377 detection based on MXene-Au nanocomposite and G-quadruplex nano-amplification strategy, *Electrochimica Acta*, 428 (2022) 140945.
- [31] L. Liu, Y. Yao, K. Ma, C. Shangguan, S. Jiao, S. Zhu, X. Xu, Ultrasensitive photoelectrochemical detection of cancer-related miRNA-141 by carrier recombination inhibition in hierarchical $Ti_3C_2@ReS_2$, *Sensors and Actuators B: Chemical*, 331 (2021) 129470.
- [32] V.B. Juska, M.E. Pemble, A critical review of electrochemical glucose sensing: Evolution of biosensor platforms based on advanced nanosystems, *Sensors*, 20 (2020) 6013.
- [33] R.A.M. Sardar, Enzyme immobilization: an overview on nanoparticles as immobilization matrix, *Biochemistry & Analytical Biochemistry*, 4 (2015).
- [34] S.G. Priya, *Biosensor Classification and Principle Operation*, *Biosensors: Developments, Challenges and Perspectives*, Springer, 2024, pp. 1-12.
- [35] N.M. Kilic, S. Singh, G. Keles, S. Cinti, S. Kurbanoglu, D. Odaci, Novel approaches to enzyme-based electrochemical nanobiosensors, *Biosensors*, 13 (2023) 622.
- [36] Y. Du, S. Dong, Nucleic acid biosensors: recent advances and perspectives, *Analytical chemistry*, 89 (2017) 189-215.
- [37] B.S. Munge, A.L. Coffey, J.M. Doucette, B.K. Somba, R. Malhotra, V. Patel, J.S. Gutkind, J.F. Rusling, Nanostructured immunosensor for attomolar detection of cancer biomarker interleukin-8 using massively labeled superparamagnetic particles, *Angewandte Chemie*, 123 (2011) 8061-8064.
- [38] V. Mani, B.V. Chikkaveeraiah, V. Patel, J.S. Gutkind, J.F. Rusling, Ultrasensitive immunosensor for cancer biomarker proteins using gold nanoparticle film electrodes and multienzyme-particle amplification, *ACS nano*, 3 (2009) 585-594.
- [39] Q. Wei, Y. Zhao, C. Xu, D. Wu, Y. Cai, J. He, H. Li, B. Du, M. Yang, Nanoporous gold film based immunosensor for label-free detection of cancer biomarker, *Biosensors and Bioelectronics*, 26 (2011) 3714-3718.

- [40] S. Guo, Y. Du, X. Yang, S. Dong, E. Wang, Solid-state label-free integrated aptasensor based on graphene-mesoporous silica–gold nanoparticle hybrids and silver microspheres, *Analytical chemistry*, 83 (2011) 8035-8040.
- [41] W. Shi, Z. Ma, A novel label-free amperometric immunosensor for carcinoembryonic antigen based on redox membrane, *Biosensors and Bioelectronics*, 26 (2011) 3068-3071.
- [42] A. Di Bartolomeo, Emerging 2D materials and their van der Waals heterostructures, *MDPI*, 2020, pp. 579.
- [43] R. Sakthivel, M. Keerthi, R.-J. Chung, J.-H. He, Heterostructures of 2D materials and their applications in biosensing, *Progress in Materials Science*, 132 (2023) 101024.
- [44] T.A. Shifa, F. Wang, Y. Liu, J. He, Heterostructures based on 2D materials: a versatile platform for efficient catalysis, *Advanced Materials*, 31 (2019) 1804828.
- [45] A.K. Geim, I.V. Grigorieva, Van der Waals heterostructures, *Nature*, 499 (2013) 419-425.
- [46] A. Yan, J. Velasco Jr, S. Kahn, K. Watanabe, T. Taniguchi, F. Wang, M.F. Crommie, A. Zettl, Direct growth of single-and few-layer MoS₂ on h-BN with preferred relative rotation angles, *Nano letters*, 15 (2015) 6324-6331.
- [47] K. Xie, K. Yuan, X. Li, W. Lu, C. Shen, C. Liang, R. Vajtai, P. Ajayan, B. Wei, Superior potassium ion storage via vertical MoS₂ “nano-rose” with expanded interlayers on graphene, *Small*, 13 (2017) 1701471.
- [48] R. Khan, A. Radoi, S. Rashid, A. Hayat, A. Vasilescu, S. Andreescu, Two-dimensional nanostructures for electrochemical biosensor, *Sensors*, 21 (2021) 3369.
- [49] H. Zhang, Z. Wang, F. Wang, Y. Zhang, H. Wang, Y. Liu, Ti₃C₂ MXene mediated Prussian blue in situ hybridization and electrochemical signal amplification for the detection of exosomes, *Talanta*, 224 (2021) 121879.
- [50] M. Naguib, M. Kurtoglu, V. Presser, J. Lu, J. Niu, M. Heon, L. Hultman, Y. Gogotsi, M.W. Barsoum, Two-dimensional nanocrystals produced by exfoliation of Ti₃AlC₂, *Advanced materials*, 23 (2011) 4248-4253.
- [51] M. Naguib, Y. Gogotsi, Synthesis of two-dimensional materials by selective extraction, *Accounts of chemical research*, 48 (2015) 128-135.
- [52] M.W. Barsoum, *MAX phases: properties of machinable ternary carbides and nitrides*, John Wiley & Sons, 2013.
- [53] F. Shahzad, M. Alhabeb, C.B. Hatter, B. Anasori, S. Man Hong, C.M. Koo, Y. Gogotsi, Electromagnetic interference shielding with 2D transition metal carbides (MXenes), *Science*, 353 (2016) 1137-1140.

- [54] M. Khazaei, A. Ranjbar, M. Arai, S. Yunoki, Topological insulators in the ordered double transition metals $M_2M'C_2$ MXenes ($M' = \text{Mo, W}$; $M = \text{Ti, Zr, Hf}$), *Physical Review B*, 94 (2016) 125152.
- [55] Z. Ling, C.E. Ren, M.-Q. Zhao, J. Yang, J.M. Giammarco, J. Qiu, M.W. Barsoum, Y. Gogotsi, Flexible and conductive MXene films and nanocomposites with high capacitance, *Proceedings of the National Academy of Sciences*, 111 (2014) 16676-16681.
- [56] M. Mariano, O. Mashtalir, F.Q. Antonio, W.-H. Ryu, B. Deng, F. Xia, Y. Gogotsi, A.D. Taylor, Solution-processed titanium carbide MXene films examined as highly transparent conductors, *Nanoscale*, 8 (2016) 16371-16378.
- [57] M. Ghidui, J. Halim, S. Kota, D. Bish, Y. Gogotsi, M.W. Barsoum, Ion-exchange and cation solvation reactions in Ti_3C_2 MXene, *Chemistry of Materials*, 28 (2016) 3507-3514.
- [58] Y. Sun, P. Li, Y. Zhu, X. Zhu, Y. Zhang, M. Liu, Y. Liu, In situ growth of TiO_2 nanowires on Ti_3C_2 MXenes nanosheets as highly sensitive luminol electrochemiluminescent nanoplatforM for glucose detection in fruits, sweat and serum samples, *Biosensors and Bioelectronics*, 194 (2021) 113600.
- [59] L. Jiang, D. Zhou, J. Yang, S. Zhou, H. Wang, X. Yuan, J. Liang, X. Li, Y. Chen, H. Li, 2D single- and few-layered MXenes: synthesis, applications and perspectives, *Journal of Materials Chemistry A*, 10 (2022) 13651-13672.
- [60] A.S. Zeraati, S.A. Mirkhani, P. Sun, M. Naguib, P.V. Braun, U. Sundararaj, Improved synthesis of $\text{Ti}_3\text{C}_2\text{T}_x$ MXenes resulting in exceptional electrical conductivity, high synthesis yield, and enhanced capacitance, *Nanoscale*, 13 (2021) 3572-3580.
- [61] M. Alhabeab, K. Maleski, B. Anasori, P. Lelyukh, L. Clark, S. Sin, Y. Gogotsi, Guidelines for synthesis and processing of two-dimensional titanium carbide ($\text{Ti}_3\text{C}_2\text{T}_x$ MXene), *Chemistry of Materials*, 29 (2017) 7633-7644.
- [62] M. Naguib, O. Mashtalir, J. Carle, V. Presser, J. Lu, L. Hultman, Y. Gogotsi, M.W. Barsoum, Two-dimensional transition metal carbides, *ACS nano*, 6 (2012) 1322-1331.
- [63] T. Zhang, L. Pan, H. Tang, F. Du, Y. Guo, T. Qiu, J. Yang, Synthesis of two-dimensional $\text{Ti}_3\text{C}_2\text{T}_x$ MXene using $\text{HCl} + \text{LiF}$ etchant: enhanced exfoliation and delamination, *Journal of Alloys and Compounds*, 695 (2017) 818-826.
- [64] J. Liew, L. Liu, K. Loh, S. Bashir, K. Ramesh, S. Ramesh, How viable are MXenes? Recent developments of MXene synthesis and its application in solid-state electrolytes, *Journal of Energy Storage*, 84 (2024) 110868.
- [65] V. Natu, R. Pai, M. Sokol, M. Carey, V. Kalra, M.W. Barsoum, 2D $\text{Ti}_3\text{C}_2\text{T}_z$ MXene synthesized by water-free etching of Ti_3AlC_2 in polar organic solvents, *Chem*, 6 (2020) 616-630.
- [66] A. Feng, Y. Yu, L. Mi, Y. Yu, L. Song, Comparative study on electrosorptive behavior of NH_4HF_2 -etched Ti_3C_2 and HF-etched Ti_3C_2 for capacitive deionization, *Ionics*, 25 (2019) 727-735.

- [67] P. Urbankowski, B. Anasori, T. Makaryan, D. Er, S. Kota, P.L. Walsh, M. Zhao, V.B. Shenoy, M.W. Barsoum, Y. Gogotsi, Synthesis of two-dimensional titanium nitride Ti_4N_3 (MXene), *Nanoscale*, 8 (2016) 11385-11391.
- [68] Y. Li, H. Shao, Z. Lin, J. Lu, L. Liu, B. Duployer, P.O. Persson, P. Eklund, L. Hultman, M. Li, A general Lewis acidic etching route for preparing MXenes with enhanced electrochemical performance in non-aqueous electrolyte, *Nature Materials*, 19 (2020) 894-899.
- [69] P. Srivastava, A. Mishra, H. Mizuseki, K.-R. Lee, A.K. Singh, Mechanistic insight into the chemical exfoliation and functionalization of Ti_3C_2 MXene, *ACS applied materials & interfaces*, 8 (2016) 24256-24264.
- [70] Q. Zhong, Y. Li, G. Zhang, Two-dimensional MXene-based and MXene-derived photocatalysts: Recent developments and perspectives, *Chemical Engineering Journal*, 409 (2021) 128099.
- [71] Y. Guo, S. Jin, L. Wang, P. He, Q. Hu, L.-Z. Fan, A. Zhou, Synthesis of two-dimensional carbide Mo_2CT_x MXene by hydrothermal etching with fluorides and its thermal stability, *Ceramics International*, 46 (2020) 19550-19556.
- [72] S. Husmann, Ö. Budak, H. Shim, K. Liang, M. Aslan, A. Kruth, A. Quade, M. Naguib, V. Presser, Ionic liquid-based synthesis of MXene, *Chemical Communications*, 56 (2020) 11082-11085.
- [73] J.-C. Gui, L. Han, W.-y. Cao, Lamellar MXene: A novel 2D nanomaterial for electrochemical sensors, *Journal of Applied Electrochemistry*, 51 (2021) 1509-1522.
- [74] S. Karakuş, S.H. Tumrani, İ.M. Kahyaoğlu, R.A. Soomro, R.H. Alshammari, A.A. Al-Kahtani, A. Nafady, Wrinkled MXene-modified screen-printed electrodes for highly efficient sarcosine detection, *Biochemical Engineering Journal*, 202 (2024) 109151.
- [75] S. Jawaid, S. Hussain Tumrani, A. Nafady, Sirajuddin, S. Karakuş, M. Tabish, N. Ahmed, Dye adsorbed few-layer thick $Ti_3C_2T_x$ -MXenes for direct electrochemical detection of CD44 proteins, *Electroanalysis*, 35 (2023) e202300091.
- [76] X. Su, Q. You, L. Zhuang, Z. Chang, M. Ge, L. Yang, W.-F. Dong, Bifunctional electrochemical biosensor based on PB-MXene films for the real-time analysis and detection of living cancer cells, *Journal of Pharmaceutical and Biomedical Analysis*, 234 (2023) 115479.
- [77] A. Kumar, A. Kumar, S. Srivastava, A study on surface plasmon resonance biosensor for the detection of CEA biomarker using 2D materials graphene, Mxene and MoS_2 , *Optik*, 258 (2022) 168885.
- [78] X. Yu, S. Bai, L. Wang, In situ reduction of gold nanoparticles-decorated MXenes-based electrochemical sensing platform for KRAS gene detection, *Frontiers in Bioengineering and Biotechnology*, 11 (2023) 1176046.

- [79] G. Naz, M.A. Salem, B.P. Sharma, S.D. Mekkey, R.A. Soomro, S. Karakuş, Z.M. El-Bahy, $\text{Ti}_3\text{C}_2\text{T}_x$ -Au hybrid composites-based electrochemical biosensors for calreticulin biomarker detection, *Microchemical Journal*, 194 (2023) 109307.
- [80] Q. Wang, F. Chen, L. Qiu, Y. Mu, S. Sun, X. Yuan, P. Shang, B. Ji, Detection of esophageal cancer marker CA19-9 based on MXene electrochemical immunosensor, *International Journal of Electrochemical Science*, 17 (2022) 220712.
- [81] Q. Wu, N. Li, Y. Wang, Y. Xu, J. Wu, G. Jia, F. Ji, X. Fang, F. Chen, X. Cui, Ultrasensitive and selective determination of carcinoembryonic antigen using multifunctional ultrathin amino-functionalized Ti_3C_2 -MXene nanosheets, *Analytical chemistry*, 92 (2020) 3354-3360.
- [82] S. Kumar, Y. Lei, N.H. Alshareef, M. Quevedo-Lopez, K.N. Salama, Biofunctionalized two-dimensional Ti_3C_2 MXenes for ultrasensitive detection of cancer biomarker, *Biosensors and Bioelectronics*, 121 (2018) 243-249.
- [83] Q. Xu, J. Xu, H. Jia, Q. Tian, P. Liu, S. Chen, Y. Cai, X. Lu, X. Duan, L. Lu, Hierarchical Ti_3C_2 MXene-derived sodium titanate nanoribbons/PEDOT for signal amplified electrochemical immunoassay of prostate specific antigen, *Journal of Electroanalytical Chemistry*, 860 (2020) 113869.
- [84] H. Zhang, Z. Wang, Q. Zhang, F. Wang, Y. Liu, Ti_3C_2 MXenes nanosheets catalyzed highly efficient electrogenerated chemiluminescence biosensor for the detection of exosomes, *Biosensors and Bioelectronics*, 124 (2019) 184-190.
- [85] L. Zhuang, Q. You, X. Su, Z. Chang, M. Ge, Q. Mei, L. Yang, W. Dong, L. Li, High-performance detection of exosomes based on synergistic amplification of amino-functionalized Fe_3O_4 nanoparticles and two-dimensional MXene nanosheets, *Sensors*, 23 (2023) 3508.
- [86] Q. You, L. Zhuang, Z. Chang, M. Ge, Q. Mei, L. Yang, W.-F. Dong, Hierarchical Au nanoarrays functionalized 2D Ti_2CT_x MXene membranes for the detection of exosomes isolated from human lung carcinoma cells, *Biosensors and Bioelectronics*, 216 (2022) 114647.

CHAPTER 2

MATERIALS AND EXPERIMENTAL TECHNIQUES

2.1 Introduction

The details of all the materials and experimental techniques used for the fabrication of MXene and its hybrids based electrochemical immunosensor to detect the EpCAM antigen have been reported in this chapter. Further, a range of analytical methods were used to characterize the $\text{Ti}_3\text{C}_2\text{T}_x$, $\text{CuS}/\text{Ti}_3\text{C}_2\text{T}_x$, $\text{TiO}_2/\text{Ti}_3\text{C}_2\text{T}_x$ and $\text{Ag}/\text{Ti}_3\text{C}_2\text{T}_x$ and other modified electrodes. An attempt has been made to provide an explanation of the methods and techniques employed to estimate several factors associated with the effectiveness of synthesized materials for detecting the cancer biomarkers. Moreover, various factors are being discussed for the effective immobilization of antibody onto the fabricated transducer surfaces. This chapter also covers the summary of different protocols used to estimate the performance-related characteristics for the reliability of immunosensors.

2.2 Materials

All the details of materials utilized during different studies are being reported in the following sections.

2.2.1 Chemicals

Titanium aluminium carbide (Ti_3AlC_2), sodium tetrafluoroborate (NaBF_4), copper sulfate pentahydrate ($\text{CuSO}_4 \cdot 5\text{H}_2\text{O}$, ~98.5%), sodium thiosulfate pentahydrate ($\text{Na}_2\text{S}_2\text{O}_3 \cdot 5\text{H}_2\text{O}$), hydrochloric acid (HCl, 36.46%), PEDOT:PSS (1.3 wt% dispersion in H_2O), silver nitrate (AgNO_3 , ~99%), PEDOT:PSS (1.3 wt% dispersion in H_2O), N-(3-dimethyl aminopropyl)-N'-ethyl carbodiimide hydrochloride (EDC), artificial human serum, N-hydroxy succinimide (NHS), epithelial cell adhesion molecule (EpCAM) antigen and bovine serum albumin (BSA) all were procured from the Sigma-Aldrich, USA. Atlas Antibodies provided the epithelial cell adhesion molecule antibody (anti-EpCAM) while Thermo-Fischer Scientific provided the ethylene glycol (EG), potassium phosphate (KH_2PO_4), N,N-dimethyl formamide (DMF), dibasic potassium phosphate (K_2HPO_4), dimethyl sulfoxide (DMSO), sodium chloride (NaCl) and N,N-dimethyl acetamide (DMA). The Whatman filter paper grade 1 (thickness ~ 0.18 mm) was purchased from GE healthcare, UK. Indium tin oxide (ITO) coated glass sheet was procured from Techinstro. All

the solutions including buffers were freshly prepared in distilled water (Milli-Q, 18.2 MΩ cm) prior to their use.

2.2.2 Buffers

- ❖ 0.2 M phosphate buffer saline (PBS) having 0.9% NaCl of pH 7.4
- ❖ PBS (pH= 6 to 8.2) containing 5 mM $[\text{Fe}(\text{CN})_6]^{3-/4-}$

2.3 Structural and morphological characterization techniques

The research work presented in this thesis focuses on the (1) synthesis of MXene ($\text{Ti}_3\text{C}_2\text{T}_x$) and its hybrids ($\text{CuS}/\text{Ti}_3\text{C}_2\text{T}_x$, $\text{TiO}_2/\text{Ti}_3\text{C}_2\text{T}_x$, $\text{Ag}/\text{Ti}_3\text{C}_2\text{T}_x$), followed by fabrication of transducer by using glass substrate coated with ITO and Whatman paper, and then (2) immobilization of anti-EpCAM (antibody) onto the fabricated electrodes for investigating their potential for EpCAM antigen detection. The prepared materials and the modified electrodes were structurally characterized at different stages of fabrication by techniques like Fourier transform infrared (FTIR) spectroscopy and X-ray diffraction (XRD). An elemental characterization was done by energy dispersive X-ray (EDX) spectroscopy, while scanning electron microscopy (SEM) and transmission electron microscopy (TEM) techniques were used for the morphological analysis.

2.3.1 X-ray diffraction (XRD)

It is a structural characterization method explored to detect the crystalline nature, chemical composition of unknown material in depth. The atomic structure of macromolecules can be ascertained with this technique, whereas for extremely small-sized materials, it can determine the material's crystallinity, composition, strain, crystal size and crystal structure. This method is also useful to describe the preferred orientation, crystallite size and crystallographic structure of a polycrystalline sample [1]. This technique's operation is based on Bragg's rule, which describes how an X-ray beam strikes the sample's crystal lattice and reflected at specific angles, revealing the details about the sample's composition and structure. The X-ray diffractometer is being used to capture the XRD patterns. A pictorial representation of X-ray diffractometer is shown in **Fig. 2.1**.

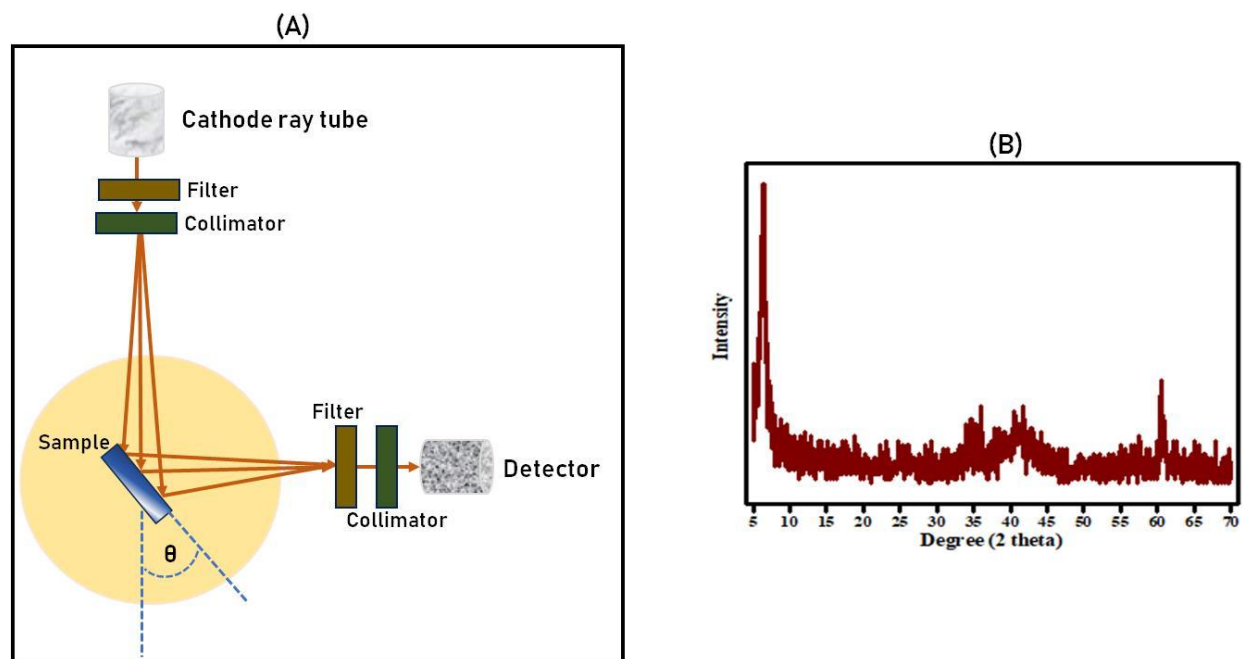


Fig. 2.1: (A) Schematic view of XRD; (B) XRD diffraction pattern of $\text{Ti}_3\text{C}_2\text{T}_x$

Additionally, the data of five highly intense peaks are utilized to determine average peak broadening. Thereafter, the material's structural characteristics can be examined with this data [2]. An average particle size of a material can be calculated by using the Eq. 2.1, namely, Debye-Scherrer equation as given below.

$$D = K\lambda / \beta \cos\theta \quad (2.1)$$

Where, D denotes the crystalline size of particle, λ is the X-ray wavelength, K is the Scherrer's constant (0.98), θ is the Bragg's angle and β is the line broadening at full-width half maxima.

In this thesis, a Bruker D-8 advance X-ray diffractometer having radiation of monochromatic wavelength radiation (1.54 \AA) is used to perform structural characterization of all the synthesized materials and electrodes.

2.3.2 Fourier transform infrared (FTIR) spectroscopy

The foundation of the Fourier transform infrared spectrometer is infrared spectroscopy which is useful to study the interaction of electromagnetic radiation with the material. Due to its excellent accuracy, quick analysis, easy handling and increased sensitivity, it is widely used for the structural characterization. The basic idea behind FTIR is that certain infrared radiation energy or

frequencies are absorbed by molecules due to their atomic vibrations. Once the material absorbs electromagnetic radiation from a light beam at each wavelength, it creates a variety of spectral lines that further reveal the chemical composition of the material [3].

The Michelson interferometer has been found helpful to examine the chemical composition of any material in FTIR spectroscopy. Basically, it is made up of four parts: (a) a filament, (b) a beam splitter, (c) a detector and (d) two mirrors positioned as depicted below in **Fig. 2.2**. The infrared radiation is emitted by the source and splits into two parts via a beam splitter. These two distinct light beams continue travel on two separate paths, and reflecting off by mirrors at the end. Following reflection, these distinct beams merge to produce interference, which is then analyzed by the detector. FTIR is an effective characterization method that has many benefits over other dispersive measurements, like greater spectrum range, increased sensitivity, quicker data acquisition, reduced sample requirements, improved signal to noise ratio etc [4].

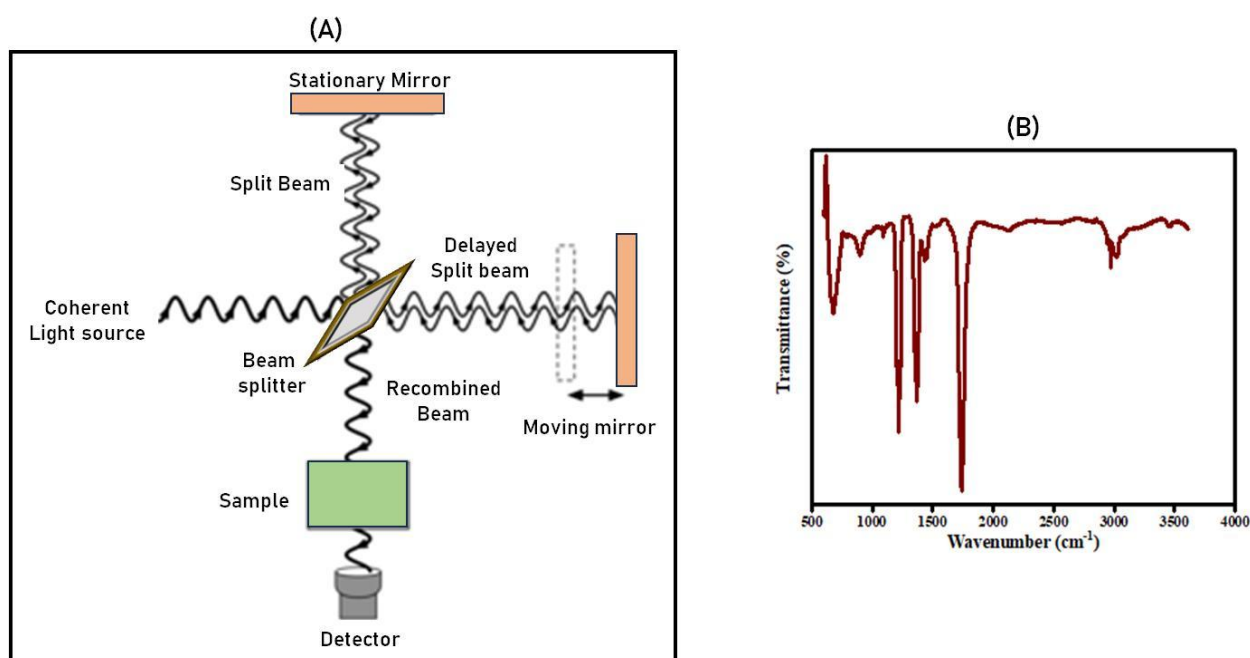


Fig. 2.2: (A) Schematic view of Michelson interferometer; (B) FTIR spectra of $\text{Ti}_3\text{C}_2\text{T}_x$

In this thesis work, the FTIR Perkin Elmer Spectrum 2 in attenuated total reflection (ATR) mode is being used to investigate the functional groups present in all the sample materials (MXene and its hybrids) and modified electrodes from $400\text{--}4000\text{ cm}^{-1}$ frequency range.

2.3.3 Scanning electron microscopy (SEM)

The purpose of this technique here is to examine the sample's surface morphology. An image of a sample is observed by the SEM using electrons instead of light. In comparison to other microscopes, SEM has the advantage of providing a considerably higher depth of field, which allows for the simultaneous access to more specimens.

The primary parts of a SEM are an electron source, a column through which an electron beam travels by using electromagnetic lenses, an electron detector, a specimen chamber, a computer and a display unit that shows the images. As seen in **Fig. 2.3**, the SEM uses a concentrated, high-energy electron beam to produce signals at the surface of the solid objects [5].

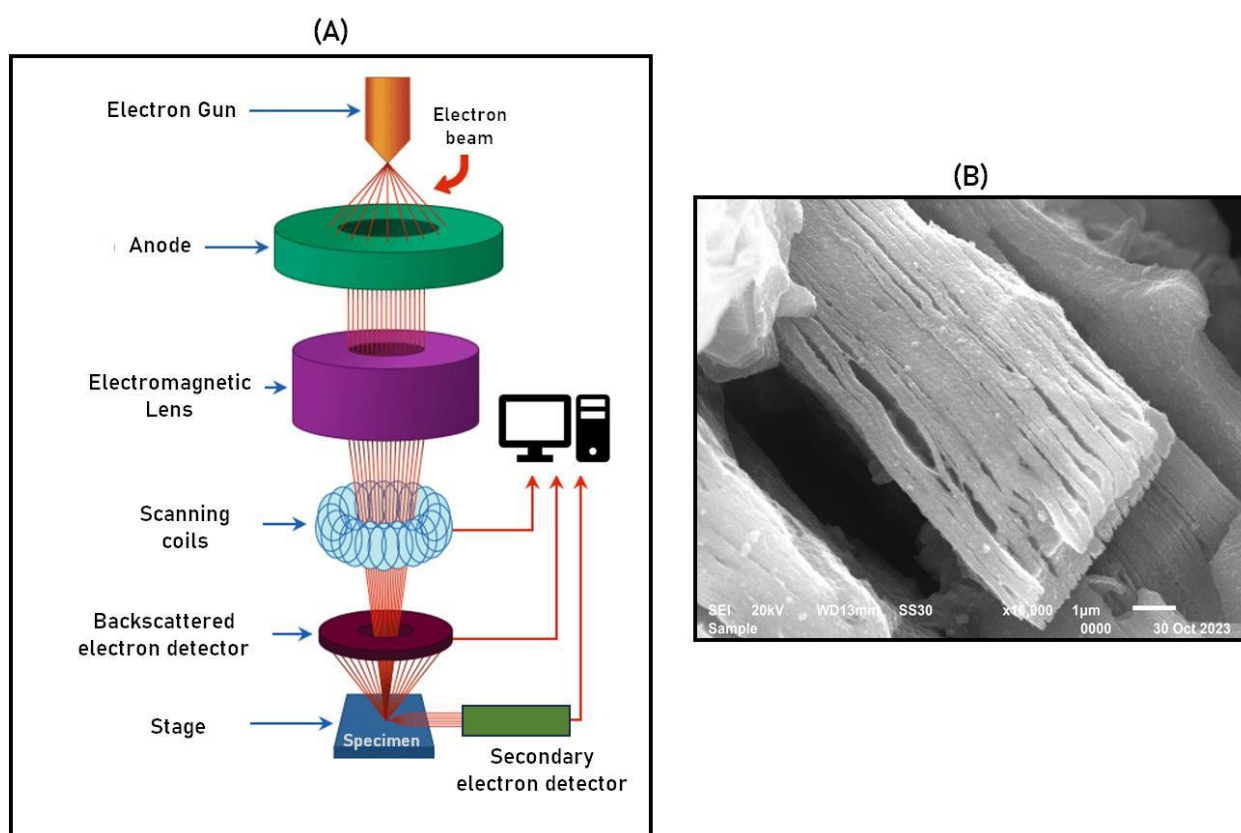


Fig. 2.3: (A) Pictorial illustration of SEM instrumentation; (B) SEM image of $\text{Ti}_3\text{C}_2\text{T}_x$

The principle of this technique is based on the production of high-energy electrons at the top of the column, where they accelerate downward and pass through several lenses to form a concentrated electron beam that strikes the specimen surface [6]. Additionally, SEM uses a variety of pumps to create vacuum conditions in the specimen chamber, which produces

specimen micrographs. As the specimen and electrons interact, resulting in the production of signals which are subsequently detected by the detector. In this work, the morphology of the synthesized 2D-materials and the constructed electrode surface before and after antibody immobilization were examined by using SEM (EVO-18, ZEISS).

2.3.4 Transmission electron microscopy (TEM)

TEM is being used to study the smallest structure of any material or specimen. High-energy electrons are utilized under this microscope to provide information about the sample's morphology, crystallographic data and composition. TEM can both visualize a specimen's nanoscale range in detail and magnify it up to a million times.

In comparison to other microscopes, TEM employs an electron beam that is far shorter in wavelength than visible light, which further increases the resolution of this instrument. This explains TEM's enormous importance in the biological and medicinal domains [7]. The process of image visualization in TEM is quite similar to that of SEM. The mechanism of TEM includes the production of high-energy electron beam by an electron gun, which further travels through the microscope's vacuum tube as shown in **Fig 2.4**.

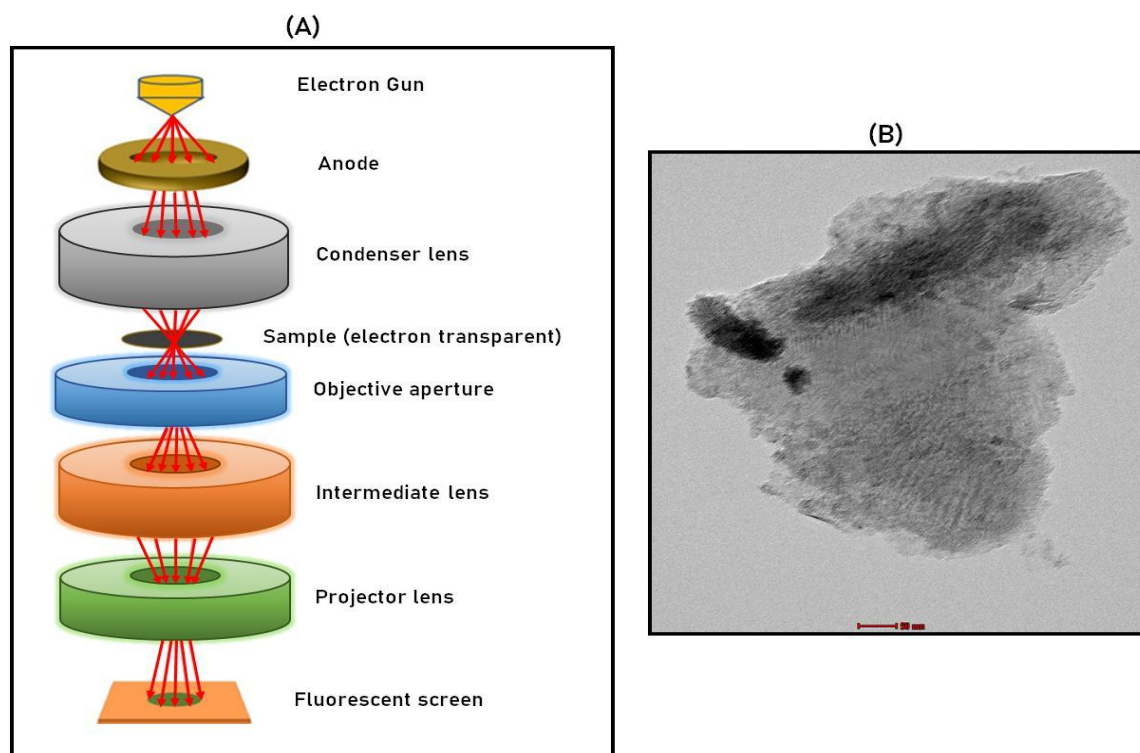


Fig. 2.4: (A) Pictorial view of TEM instrumentation; (B) TEM image of $Ti_3C_2T_x$

The electrons move through the tube in a fine beam that is focused by the electromagnetic lens positioned in between, and then striking the thin specimen. Depending on how this turned out, the electrons may either hit or scatter onto a fluorescent screen that is positioned at the bottom of the microscope. Subsequently, the display device reflects the specimen's image. Basically, the image consists of different shades of the specimen's sections based on how densely the specimen displays on the screen [8].

In this thesis, the layered morphology of MXene was observed by using CRYO-transmission electron microscope (TALOS).

2.3.5 Energy dispersive X-ray (EDX) spectroscopy

It is an excellent method for measuring the chemical compositions in conjunction with TEM. Although EDX is not a quantitative technique, it can identify the contaminants by detecting the small amounts of elemental composition. The mechanism of EDX speaks about the interaction of TEM's electron beam and atoms present in the sample when it strikes on the sample surface. An X-ray radiation is produced by this interaction that is unique to each element. Hence, the chemical elements in the sample are identified and quantified using this characteristic X-ray.

It is simple to quantify the content and amount of heavy metal ions using the EDX, but it is more difficult to identify the elements with atomic numbers lower than 11. When heavy metal ions such as palladium, silver, and gold are present in the material that are close to or at the surface of the sample, the composition of these particles can be analyzed by using the EDX [9]. Here, we have used the TEM-EDX (TALOS) to perform the elemental evaluation of prepared materials.

2.4 Electrochemical techniques

To study the electrochemistry of the samples, we employed an electroanalytical technique, where potential or current responses are measured that occurs within the electrochemical cell. In case of biosensors, this method is very helpful to determine the reactivity of analyte by measuring current or potential changes against the concentration of analyte. In majority of the electrochemical methods, three electrodes set up are employed: the counter electrode (CE), the reference electrode (RE) and a working electrode (WE) [10]. A potentiostat is attached to these three electrodes, a device that measures the current generated by adjusting the working electrode's potential. The electrochemical experiment typically involves an application of

voltage to a working electrode, and measures the resulting current, and plotting that data against time. In a different scenario, the applied potential is varied in a linear manner and resulting current is plotted against the varying potential. Nernst's equation correlates the equilibrium concentrations of redox couple's reduced and oxidized forms in a solution to the potential (E), as depicted by Eq. 2.2.

$$E = E_o + (RT/nF) \ln \{[\text{oxi}]/[\text{red}]\} \quad (2.2)$$

Here, E_o = standard potential, R = universal gas constant, F = Faraday's constant, T = temperature, $[\text{oxi}]$ and $[\text{red}]$ = conc. of oxidized and reduced species, respectively. The redox couple presents at the electrode modify their concentration ratios in accordance with Nernst's equation on the application of potential to WE.

In this thesis work, all the electrochemical characterizations have been performed by using Autolab Potentiostat/Galvanostat (EcoChemie, Netherlands), having Ag/AgCl as a reference electrode and platinum as a counter electrode (CE). Different electrochemical techniques such as cyclic voltammetry (CV), chronoamperometry (CA) and differential pulse voltammetry (DPV) are being used to perform electrochemical studies of various modified electrodes. A potentiostat uses a DC power source to generate a precisely calculated and maintained potential by supplying the system with an even fraction of current at a steady voltage. A pictorial view of the potentiostat work station is shown in **Fig. 2.5** as given below.

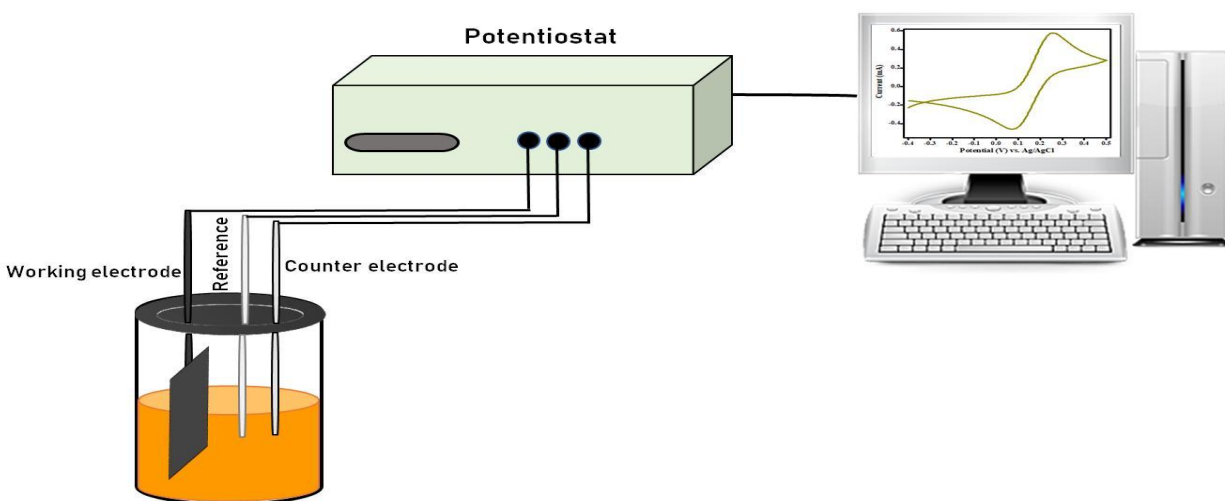


Fig. 2.5: Schematic view of Potentiostat workstation with three electrode set-up

2.4.1 Cyclic voltammetry (CV)

CV is a useful electro-analytical technique for studying the electrochemical characteristics of the electro-active species. In this study, the potential of the working electrode changes over time and returns to the initial point after reaching the fixed point. Such potential cycles may be swept as necessary to create a cyclic voltammogram. Further, to learn more about the electrochemical processes with known redox potentials for electroactive species, cyclic voltammetry is employed. During the potential scans against a constant RE potential, the current is monitored at the WE. Here, the CE conducts electricity from the signal source to WE. During the redox process, the electrolytic solution facilitates the supply of ions to the electrodes [11]. In CV studies, various physical parameters can be calculated on the basis of obtained peak current value, to investigate the efficiency of fabricated electrodes. Laviron's theory is used to calculate the α (electron transfer coefficient) and K_s (charge transfer coefficient) with the help of equations 2.3 to 2.5.

$$E_{pa} = 2.303 RT/(1-\alpha) n F; \text{ and } E_{pc} = -2.303 RT/\alpha n F \quad (2.3)$$

$$\Delta E_p = E_{pa} - E_{pc} \quad (2.4)$$

$$\ln K_s = \alpha \cdot \ln(1 - \alpha) + (1 - \alpha) \cdot \ln(\alpha) - \ln(RT/n F v) - \alpha (1 - \alpha) \cdot n F \cdot \Delta E_p/RT \quad (2.5)$$

Where, E_{pa} & E_{pc} represents the anodic and cathodic peak potentials, respectively. v is the scan rate.

Electrochemical parameter like D (Diffusion coefficient) can be calculated by using Randles-Sevcik equation (Eq. 2.6) and τ (surface coverage) [12] of modified electrodes were evaluated by Eq 2.7 given below:

$$I_p = 2.69 \times 10^5 n^{3/2} A C D^{1/2} v^{1/2} \quad (2.6)$$

$$I_p = n^2 F^2 A \tau v / 4RT \quad (2.7)$$

Here, I_p denotes the anodic peak current, n is the electrons oxidized or reduced, C represents the $[\text{Fe}(\text{CN})_6]^{3-/4-}$ concentration (mole/cm³). This thesis work contains the CV studies at different scan rates (10 mV/s to 400 mV/s) for all different modified electrodes.

2.4.2 Differential pulse voltammetry (DPV)

The DPV study provides an improved detection limit over the CV technique and also allows the resolution of electrode processes that are close together. Here, a ramp that grows linearly is used to subject the electrode to the voltage versus time program. The current between the pulse voltage and ramped baseline voltage is presented after a series of modestly amplitude pulses are superimposed on a ramped voltage. Prior to the application of each pulse, the current has been measured (first point), and after the pulse has ended, the current has been measured (second point) [13]. The locations were also picked to permit the non-faradic (charging) current to fade. The base potential of each pulse is recorded based on variations in current measurements at these points. DPV has a higher detection limit than CV and other voltammetric methods, due to its stronger selectivity between charging current and impurity Faradic currents.

2.4.3 Chronoamperometry

An electrochemical technique called chronoamperometry is the simplest time dependent electrochemical analysis technique. Basically, it is used to record the current response against time in order to investigate the behavior of an electrochemical system. It is especially beneficial for studying processes involving electron transfer reactions, including enzyme reactions, electrode reactions, and chemical reactions involving redox species. The working electrode is here subjected to a constant voltage, and the resulting current is continuously measured. Measurements of low currents with high sensitivity are possible with this approach [14]. Considering that paper electrodes often have poor conductivity and can produce lower currents than other electrodes, this is especially advantageous for paper electrodes. The efficiency of paper-based biosensors is improved overall by the high sensitivity of chronoamperometry, which makes it possible to detect low analyte concentrations. Hence, chronoamperometry has been considered as a highly sensitive method owing to its independency on biological recognition element that is used for immunosensing application [15]. In this research work, paper based immunosensors have been characterized by using this technique and reported in chapter 7 and chapter 8.

2.5 Antibody immobilization to MXene-based matrix

To improve the stability, longevity, efficacy and reusability of fabricated biosensors for cancer biomarker detection, the successful immobilization of antibody onto the appropriate matrices is

crucial. After conjugation, antibodies must maintain their proper shape, particularly at the active region, to produce a fully functioning and efficient antibody. The primary determinant responsible for the performance of an immunosensor depends on the extent of antibody-antigen bonding. It's crucial to remember that immobilized antibodies indirectly boost the signal and improve sensitivity [16]. Mainly, there are two strategies to immobilize antibody discussed in the following sections.

2.5.1 Site oriented antibody binding technique

To increase the sensitivity of the electrochemical immunosensors, the site oriented binding strategies have been used. The primary advantage of site-directed conjugation is its ability to enhance the antigen-binding capacity by up to 8 times, leading to an improved stability and sensitivity in the detection of different biomarkers. Site-directed immobilization of antibodies can be achieved by targeting multiple functional groups on antibodies.

2.5.2 Random immobilization

Random immobilization can be done in two ways as discussed in the following sections:

2.5.2.1 Non-covalent immobilization

Non-covalent immobilization is based on electrostatic interactions between proteins and substrates. Although non-covalent immobilization is an easy and affordable method, it frequently results in weaker, random immobilization and denaturation of antibodies, which ultimately leads to poor reproducibility. Because of the steric hindrance, random immobilization reduces the accessibility of the active sites. Guadalupe et al. have studied the impact of pH on the orientation of antibodies that are physically adsorbed onto gold nanoparticles by electrostatic interactions [17]. It was discovered that the antigen-binding site's accessibility increases with decreasing pH, because of the variation in surface charge distribution on the antibodies.

The physical adsorption technique is frequently ineffective and sensitive to temperature and pH resulting in inadequate operational and storage stability, as well as poor analytical performance. In order to limit nonspecific binding, some blocking agents such as PEG (polyethylene glycol) or BSA (bovine serum albumin) are frequently added.

2.5.2.2 Covalent immobilization

Covalent immobilization is a very robust technique for immobilizing the antibodies. The existence of mutually combining groups on the transducer's surface and antibody is necessary for the covalent antibody conjugation process. Reactive groups on antibodies include primary amines found in lysine amino acid, imidazole found in histidine, carboxylic acid found in aspartic acid, thioether found in methionine, thiol found in cysteine and guanidino found in arginine. In line with this, the substrate needs to be functionalized for the conjugation with different groups such as amino, carboxyl, and sulfhydryl. The covalent connection between the antibody and the carboxylated substrate can be achieved by targeting antibodies with amino groups and -COOH groups using carbodiimide (EDC) in conjunction with N-hydroxy succinimide (NHS). The creation of an amide linkage during random contact between antibodies and substrate is determined by the distribution of amine and carboxyl groups on the antibody. Hence, as compared to physical adsorption, the covalent immobilization approach produces remarkable results with higher repeatability.

EDC/NHS has been used in the present work as a crosslinker for MXene and its hybrids to create a bonding between the amino group of antibody and hydroxyl group present on the substrate's surface.

2.6 Protocols used for estimation of various performance-related metrics for MXene and its hybrids-based immunosensors

2.6.1 Linear detection range, detection limit and sensitivity

The concentration range across which the current response varies proportionately with the analyte concentration is known as the biosensor's linear detection range. In this thesis work, linear range has been determined by DPV as reported in chapter 3 to 5 and chronoamperometry reported in chapters 6 and 7.

The sensitivity (S) of a biosensor is the connection between the variation in analyte concentration and strength of the signal generated by the transducer. In general, an immunosensor should be capable to detect even the slightest variation in the concentration of the target analyte and give a signal. The sensitivity can be calculated by using the following equation 2.8.

$$\text{Sensitivity} = \text{slope}/\text{effective surface area} \quad (2.8)$$

Detection limit (LOD) is expressed as the lowest concentration of analyte which is detectable by the immunosensor reliably. LOD can be calculated by using the following relationship as given in equation 2.9.

$$\text{LOD} = 3\sigma/m \quad (2.9)$$

Here, m = slope of calibration plot and σ = bioelectrode's standard deviation.

2.6.2 Reproducibility and shelf-life of the immunosensors

The biosensor's lifespan has been determined on the basis of its repeatability and shelf life. The term "shelf life" describes how long a sensor is appropriate to store without losing its highest level of activity. This can be accomplished by periodically monitoring the bioelectrode's current response. Reproducibility, on the other hand, is the measurement of the drift or scatter in a series of the observations or conclusions over time. On the other hand, the current response of various bioelectrodes at constant analyte concentration is monitored in order to verify repeatability. The material utilized to produce the sensor, the morphology of the matrices and the method used to immobilize biomolecules are very important factors which influence the stability of bioelectrode.

References:

- [1] R.A. Dunlap, X-ray diffraction techniques, Novel Microstructures for Solids; Morgan & Claypool Publishers: Halifax, NS, Canada, (2018).
- [2] J. Epp, X-ray diffraction (XRD) techniques for materials characterization, Materials characterization using nondestructive evaluation (NDE) methods, Elsevier, 2016, pp. 81-124.
- [3] F. Mangolini, A. Rossi, Attenuated total reflection-Fourier transform infrared spectroscopy: a powerful tool for investigating polymer surfaces and interfaces, Polymer Surface Characterization, 113 (2014).
- [4] P.R. Griffiths, J.M. Chalmers, Handbook of vibrational spectroscopy, Wiley Online Library, 2002.
- [5] J.I. Goldstein, D.E. Newbury, J.R. Michael, N.W. Ritchie, J.H.J. Scott, D.C. Joy, Scanning electron microscopy and X-ray microanalysis, Springer, 2017.
- [6] W. Zhou, R. Apkarian, Z.L. Wang, D. Joy, Fundamentals of scanning electron microscopy (SEM), Scanning microscopy for nanotechnology: techniques and applications, (2007) 1-40.
- [7] D.B. Williams, C.B. Carter, D.B. Williams, C.B. Carter, The transmission electron microscope, Springer, 1996.
- [8] H. Saka, Transmission Electron Microscopy, Carbon Alloys, Elsevier, 2003, pp. 223-238.
- [9] T.R. Shojaei, S. Soltani, M. Derakhshani, Synthesis, properties, and biomedical applications of inorganic bionanomaterials, Fundamentals of bionanomaterials, Elsevier, 2022, pp. 139-174.
- [10] S. Verma, C.M. Pandey, D. Kumar, A highly efficient rGO grafted MoS₂ nanocomposite for dye adsorption and electrochemical detection of hydroquinone in wastewater, New Journal of Chemistry, 46 (2022) 21190-21200.
- [11] N. Elgrishi, K.J. Rountree, B.D. McCarthy, E.S. Rountree, T.T. Eisenhart, J.L. Dempsey, A practical beginner's guide to cyclic voltammetry, Journal of chemical education, 95 (2018) 197-206.
- [12] Sweety, D. Kumar, Development of Ti₃C₂T_x-based novel immunosensor for cancer biomarker detection, Applied Organometallic Chemistry, 38 (2024) e7570.
- [13] A.J. Bard, L.R. Faulkner, Electrochemical methods: fundamentals and applications, Surf. Technol, 20 (1983) 91-92.
- [14] R.J. Mortimer, Spectroelectrochemistry, methods and instrumentation, (1999).
- [15] Sweety, S. Paneru, D. Kumar, CuS modified PEDOT:PSS grafted paper-based electrochemical immunosensor for EpCAM biomarker detection, Materials Chemistry and Physics, 313 (2024) 128687.
- [16] M. Patel, M. Agrawal, A. Srivastava, Signal amplification strategies in electrochemical biosensors via antibody immobilization and nanomaterial-based transducers, Materials Advances, 3 (2022) 8864-8885.

[17] G. Ruiz, K. Tripathi, S. Okyem, J.D. Driskell, pH impacts the orientation of antibody adsorbed onto gold nanoparticles, *Bioconjugate chemistry*, 30 (2019) 1182-1191.

CHAPTER 3

MXENE BASED ELECTROCHEMICAL IMMUNOSENSOR FOR CANCER BIOMARKER DETECTION

3.1 Introduction

Here, we are presenting the novel approach for developing a $\text{Ti}_3\text{C}_2\text{T}_x$ (Mxene) based immunosensor for EpCAM antigen (cancer biomarker) detection. 2D- $\text{Ti}_3\text{C}_2\text{T}_x$ has been selected as a transducer material owing to its exceptional metal-like conductivity, high hydrophilicity, large surface area and superior capacity for incorporation of functional groups [1, 2]. $\text{Ti}_3\text{C}_2\text{T}_x$ has been synthesized by a less hazardous hydrothermal method followed by its deposition on an ITO coated glass substrate electrophoretically. The details for the synthesis, characterization, optimization and electrochemical studies of immunosensor have been described in the following segments.

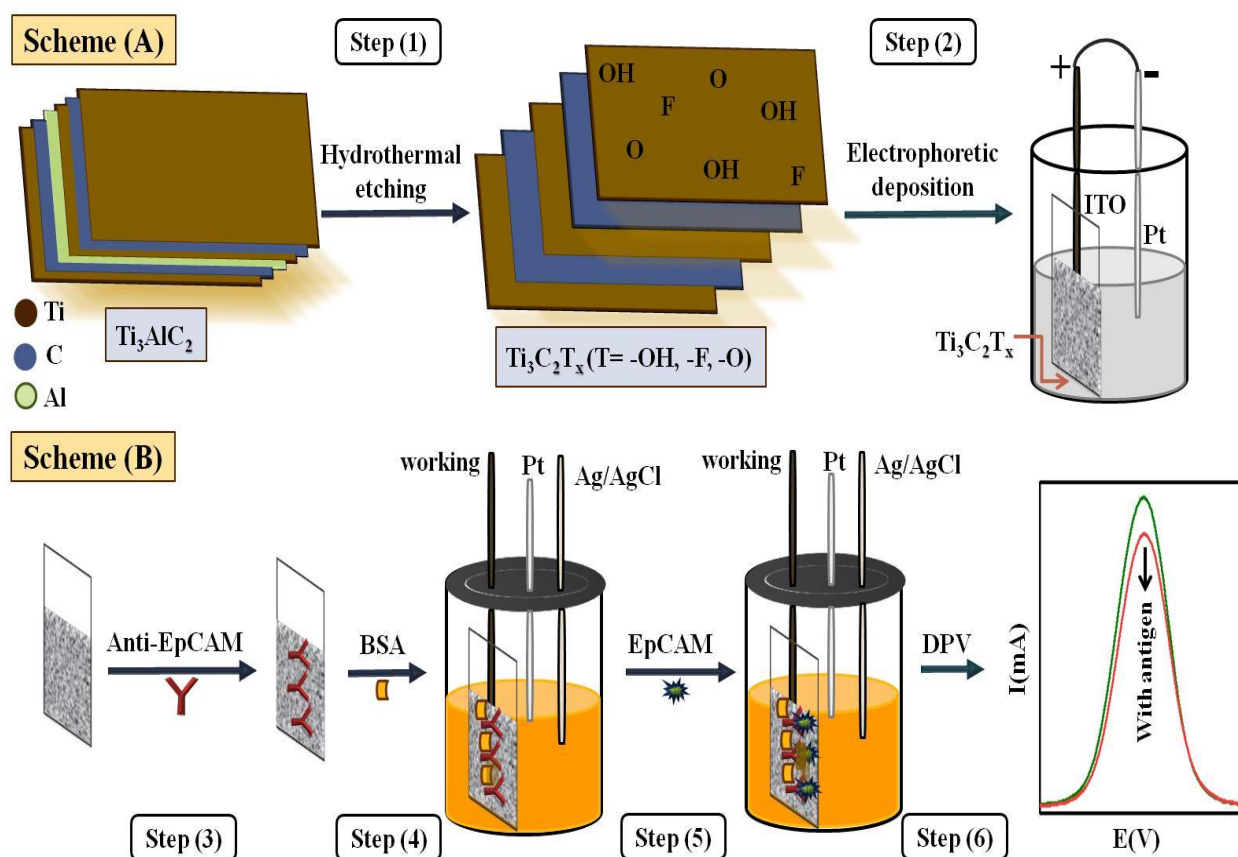


Fig. 3.1: Diagrammatic illustration of the immunosensor based on $\text{Ti}_3\text{C}_2\text{T}_x$

3.2 Experimental section

3.2.1 Synthesis of $Ti_3C_2T_x$

Two distinct techniques, namely, co-precipitation and hydrothermal method, were used to synthesize 2D- $Ti_3C_2T_x$. In case of co-precipitation, 30 mL of 9M HCl solution was stirred with the addition of 1g LiF. To prevent a rapid reaction, 1g of Ti_3AlC_2 (MAX phase) was then added gradually. After stirring this mixture at 35 °C for 24 h, it was washed with deionized water till the pH value of supernatant reaches to 6. Subsequently, the suspension was filtered and vacuum-dried for overnight [3].

On the other hand, hydrothermal method includes the dispersion of 1g $NaBF_4$ in 20 ml HCl (36 wt%) under stirring. Next, 0.35 g of Ti_3AlC_2 was gradually added to the suspension as mentioned above, and stirred constantly until it dissolves. This mixture is placed in an autoclave and heated to 170 °C for 16 h. After cooling down to room temperature, the resultant suspension was centrifuged with deionized water and dried for 12 h at 70 °C in a vacuum oven [4].

After comparing the two techniques, it was determined that the hydrothermally produced $Ti_3C_2T_x$ has a 2D-layered sheet-like structure free of aluminum traces. This was verified by SEM and XRD characterization, which have been further detailed in sections 3.1 and 3.2 of the results and discussion. Therefore, in all subsequent research procedures, $Ti_3C_2T_x$ (hydrothermal) was employed.

3.2.2 Electrophoretic deposition (EPD) of $Ti_3C_2T_x$ onto ITO electrode

Initially, a colloidal suspension of $Ti_3C_2T_x$ (50 $\mu\text{g/mL}$) was prepared by ultrasonically sonicating it in deionized water. The smooth deposition of $Ti_3C_2T_x$ onto the pre-hydrolyzed ITO electrode was optimized by experimenting with a range of potentials. It was observed that a consistent layer of $Ti_3C_2T_x$ was produced on ITO substrate after 8s at DC potential of 10 V. On the other hand, burning of the electrode was noticed at greater potential and no film was visible at lower potential.

3.2.3 Fabrication of immunosensor

The $Ti_3C_2T_x@ITO$ electrode was incubated for 40 min at room temperature with 10 μL of 2mM EDC and 10 μL of 5mM NHS. Next, 20 μL of anti-EpCAM (40 $\mu\text{g/mL}$) was immobilized at 4 °C for 12 h. The -COOH groups that are present in the antibody structure were invertibly activated by the crosslinker EDC:NHS. An ester bond was formed by covalently joining the

accessible hydroxyl groups present on the surface of $\text{Ti}_3\text{C}_2\text{T}_x$ with the activated carboxylic groups [5]. To prevent any non-specific binding with antigen, the anti-EpCAM/ $\text{Ti}_3\text{C}_2\text{T}_x$ /ITO electrodes were also treated with 1% BSA and then washed with PBS.

3.3 Results and discussion

3.3.1 Structural characterization of $\text{Ti}_3\text{C}_2\text{T}_x$

Fig. 3.2A depicts the XRD pattern of the powdered samples- Ti_3AlC_2 , $\text{Ti}_3\text{C}_2\text{T}_x$ (co-precipitation), and $\text{Ti}_3\text{C}_2\text{T}_x$ (hydrothermal), as represented by curves (a), (b), and (c), respectively. Peaks at $2\theta = 9.63^\circ$, 39.14° , 41.90° , and 60.29° are visible in the Ti_3AlC_2 spectra (curve a). A strong diffraction peak of Ti_3AlC_2 at $2\theta = 9.63^\circ$ in curves (b) and (c) migrating towards a lower angle at $2\theta = 6.36^\circ$, indicating that the Ti–Al bond is ruptured. Additionally, there is broadening of peak indicating the decrease in crystallinity in $\text{Ti}_3\text{C}_2\text{T}_x$. This finding is consistent with the literature report [6]. The existence of peaks in curve (b) at 9.63° and 39.14° suggests that the co-precipitation approach has not entirely removed the Al from the Ti_3AlC_2 . On the other hand, the primary peak of aluminum at 39.14° is absent from the $\text{Ti}_3\text{C}_2\text{T}_x$ (hydrothermal) spectra (curve c), indicating that the Ti_3AlC_2 has been successfully exfoliated to $\text{Ti}_3\text{C}_2\text{T}_x$ using the hydrothermal approach. Moreover, the interlayer spacing (d) can be easily determined by applying Bragg's equation, which is $2d \sin\theta = n\lambda$. The etching of Al from Ti_3AlC_2 is further confirmed by the observation that the interlayer spacing of $\text{Ti}_3\text{C}_2\text{T}_x$ (hydrothermal) increases to 13.88 \AA (the d-spacing of Ti_3AlC_2 is 9.18 \AA).

Fig. 3.2B shows the FTIR spectra of $\text{Ti}_3\text{C}_2\text{T}_x$ /ITO (hydrothermal, curve a) and anti-EpCAM/ $\text{Ti}_3\text{C}_2\text{T}_x$ /ITO (curve b). The distinctive band at 1216 cm^{-1} in curve a, is observed due to the stretching vibrations in the C–F bond. The stretching vibrations of the O–H and C=O bonds are responsible for the peaks at 1366 and 1738 cm^{-1} , respectively [7]. Conversely, the distinctive C=O bond stretching vibrations that emerged at 1738 cm^{-1} is displaced to a lower wavenumber at 1638 cm^{-1} for immobilization in the FTIR spectra of anti-EpCAM/ $\text{Ti}_3\text{C}_2\text{T}_x$ /ITO (curve b) due to the formation of ester bond after antibody immobilization. The characteristic peak at 1043 cm^{-1} is ascribed to C–O bond stretching vibrations. The O–H stretching vibrations are responsible for the broad peak seen at 3300 cm^{-1} .

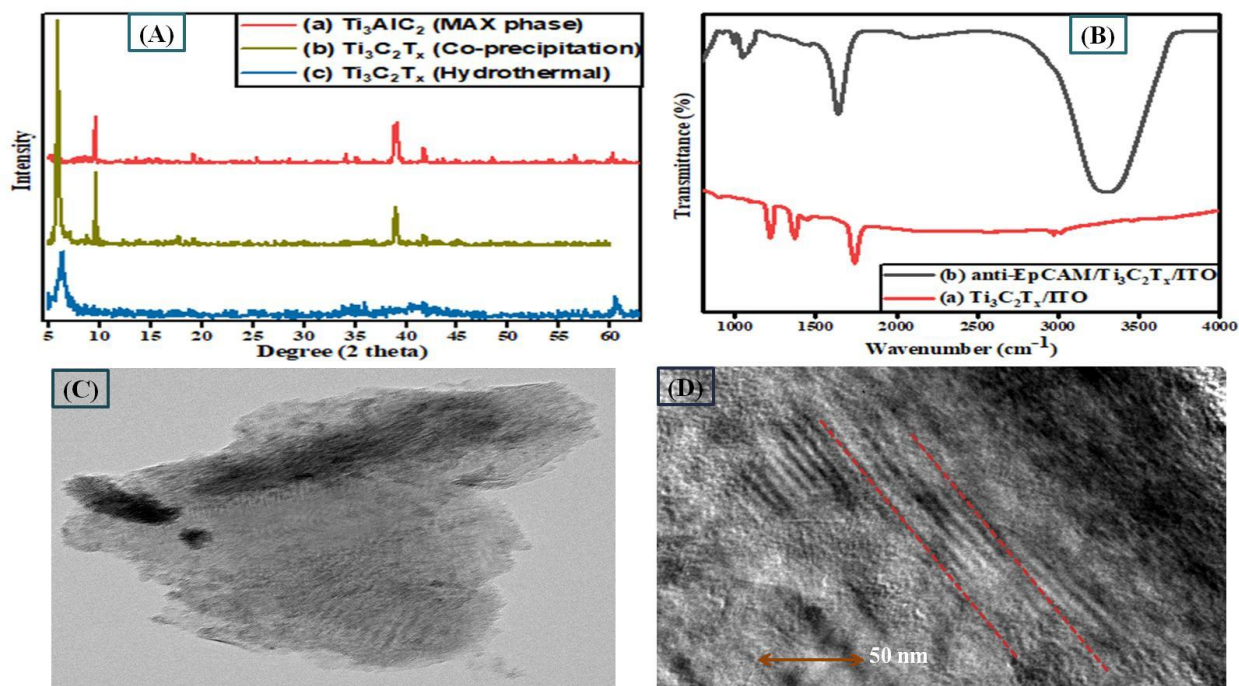


Fig. 3.2: (A) XRD diffraction pattern of (a) Ti_3AlC_2 , (b) $\text{Ti}_3\text{C}_2\text{T}_x$ (co-precipitation) and (c) $\text{Ti}_3\text{C}_2\text{T}_x$ (hydrothermal); (B) FTIR spectra of (a) $\text{Ti}_3\text{C}_2\text{T}_x/\text{ITO}$ and (b) anti-EpCAM/ $\text{Ti}_3\text{C}_2\text{T}_x/\text{ITO}$; (C) and (D) TEM image and Cross-sectional image of $\text{Ti}_3\text{C}_2\text{T}_x$ (hydrothermal)

3.3.2 Morphological study of $\text{Ti}_3\text{C}_2\text{T}_x$

The transmission electron microscope (TEM) is used to examine $\text{Ti}_3\text{C}_2\text{T}_x$ (hydrothermal), as illustrated in **Fig. 3.2C**, where the micrograph depicts the two-dimensional sheet-like structure of $\text{Ti}_3\text{C}_2\text{T}_x$. A cross-sectional picture of multilayered $\text{Ti}_3\text{C}_2\text{T}_x$ is shown in **Fig. 3.2D**. The distinct layers of titanium and carbon atoms that make up the structure of $\text{Ti}_3\text{C}_2\text{T}_x$ are shown by the red dotted lines [8].

Using a scanning electron microscope (SEM), the morphology of $\text{Ti}_3\text{C}_2\text{T}_x$ produced by two distinct techniques was examined. In $\text{Ti}_3\text{C}_2\text{T}_x$ made by the co-precipitation approach, as shown in **Fig. 3.3A**, no layered sheet-like structure is clearly visible. It seems that agglomeration in layers occurred during the synthesis. A distinctive two-dimensional layered structure of $\text{Ti}_3\text{C}_2\text{T}_x$ sheet produced by hydrothermal technique is shown in **Fig. 3.3B**. For the purpose of anti-EpCAM immobilization, the loosely packed multilayered structure provides a large surface area [9]. Since, it has been demonstrated that $\text{Ti}_3\text{C}_2\text{T}_x$ made via hydrothermal process has superior

structural properties, and therefore it is utilized for all the subsequent characterization and electrochemical studies.

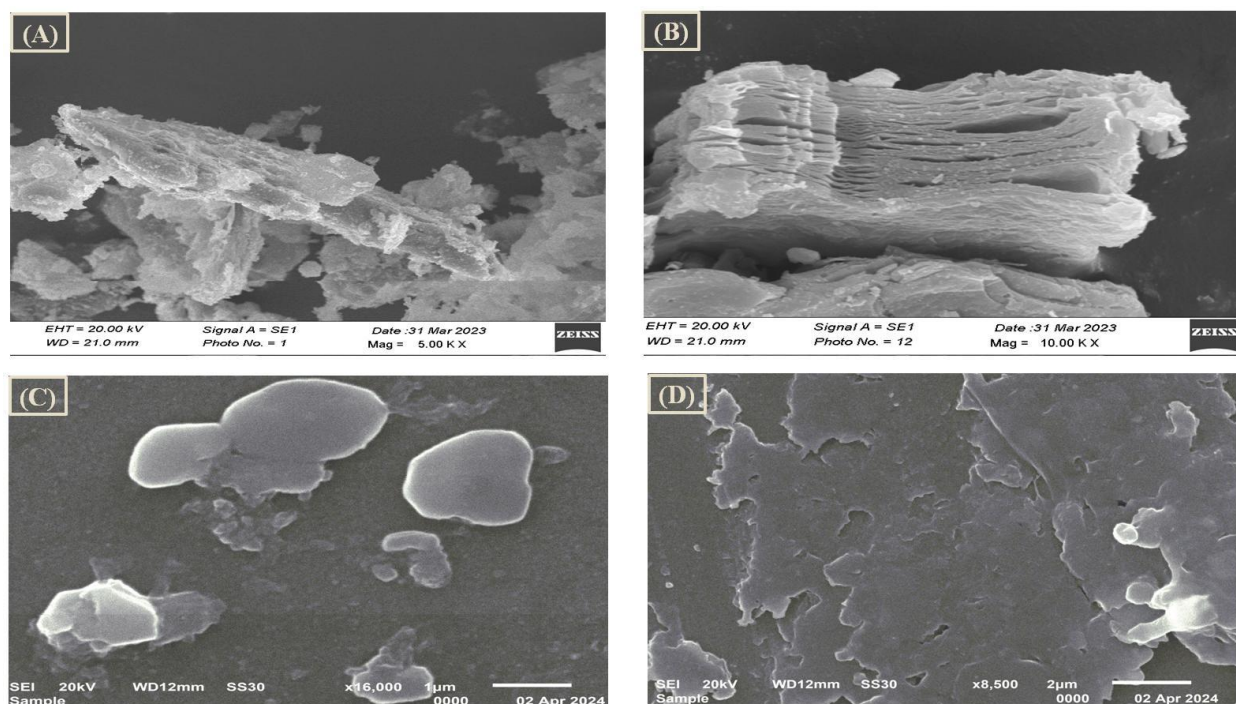


Fig. 3.3: SEM micrographs of (A) Ti₃C₂T_x (co-precipitation); (B) Ti₃C₂T_x (hydrothermal); (C) Ti₃C₂T_x/ITO electrode; and (D) anti-EpCAM/Ti₃C₂T_x/ITO electrode

The Ti₃C₂T_x/ITO electrode SEM image (**Fig. 3.3C**) reveals that 2D-sheets are dispersed across the ITO electrode surface. The covalent interactions alter the layered morphology of Ti₃C₂T_x, when anti-EpCAM is immobilized onto the Ti₃C₂T_x/ITO electrode, further demonstrating that the anti-EpCAM has been coated on the electrode surface, as shown in (**Fig. 3.3D**).

Fig. 3.4 represents the energy-dispersive X-ray (EDX) data of Ti₃C₂T_x. The synthesis of Ti₃C₂T_x is again confirmed by the EDX peaks corresponding to Ti, C, O, F, and Cu. The copper grid utilized for the TEM-EDX investigation is the cause of an extra peak of Cu.

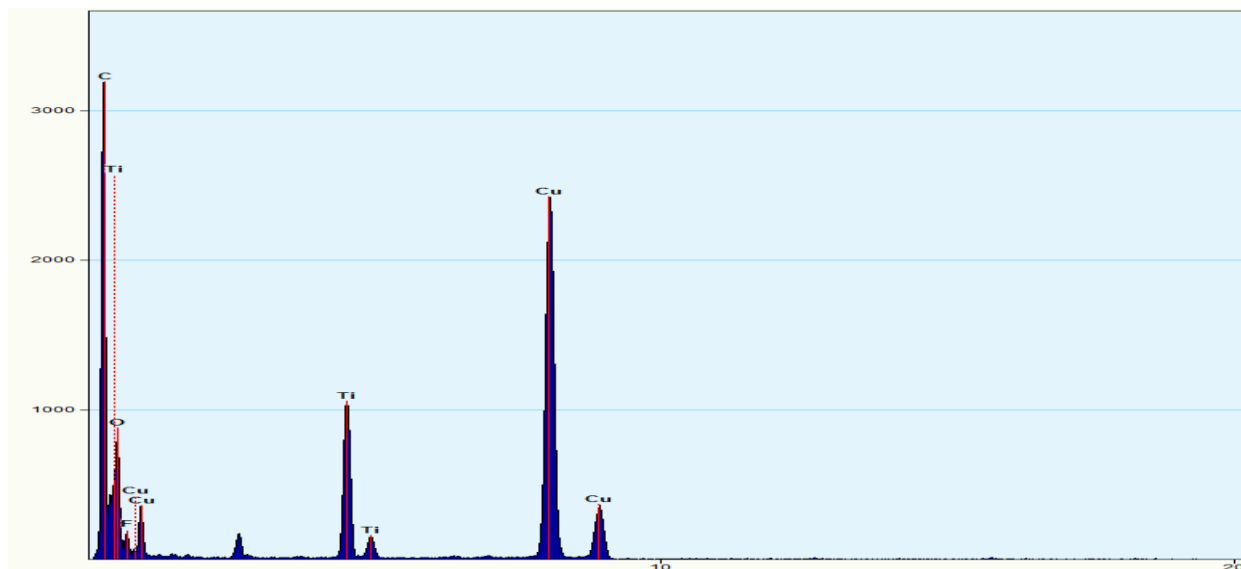


Fig. 3.4 EDX analysis of $\text{Ti}_3\text{C}_2\text{T}_x$ (hydrothermal)

3.3.3 Electrochemical characterization

Using DPV technique, the fabricated electrodes were characterized electrochemically in PBS (7.4 pH) containing $[\text{Fe}(\text{CN})_6]^{3-/4-}$ (5mM). According to **Fig. 3.5A**, the $\text{Ti}_3\text{C}_2\text{T}_x/\text{ITO}$ electrode displays the highest electrochemical current (0.169 mA), while a bare hydrolyzed ITO electrode displays the lowest current (0.074 mA). The addition of $\text{Ti}_3\text{C}_2\text{T}_x$ enhances the electrode's effective surface area, which further speed up the electron transport and considerably raises the redox peak current. The blocking of the electrode's conducting area by the antibody causes the reduction of electrochemical current to 0.136 mA.

The CV scan rate ($v = 10$ to 300 mV/s) analysis of the $\text{Ti}_3\text{C}_2\text{T}_x/\text{ITO}$ electrode is shown in **Fig. 3.5B**. This figure clearly demonstrates that the reduction peak goes towards a more negative value as the scan rate increases, while the oxidation peak shifts towards a more positive value. **Fig. 3.5C** inferred a linear relationship between peak potentials and $\log(\text{scan rate})$ as described by Eqs. (3.1) and (3.2).

$$E_{\text{pa}} (\text{V}) [\text{Ti}_3\text{C}_2\text{T}_x/\text{ITO}] = 0.1313 (\text{V}) + 0.0668 (\text{V}) * \log(v) ; R^2 = 0.97 \quad (3.1)$$

$$E_{\text{pc}} (\text{V}) [\text{Ti}_3\text{C}_2\text{T}_x/\text{ITO}] = 0.1446 (\text{V}) - 0.05937 (\text{V}) * \log(v) ; R^2 = 0.98 \quad (3.2)$$

Using the Laviron's theory (Eqs. 2.3 to 2.5), α and K_s for the $\text{Ti}_3\text{C}_2\text{T}_x/\text{ITO}$ electrode is calculated to be 0.893 and 0.127 s^{-1} , respectively.

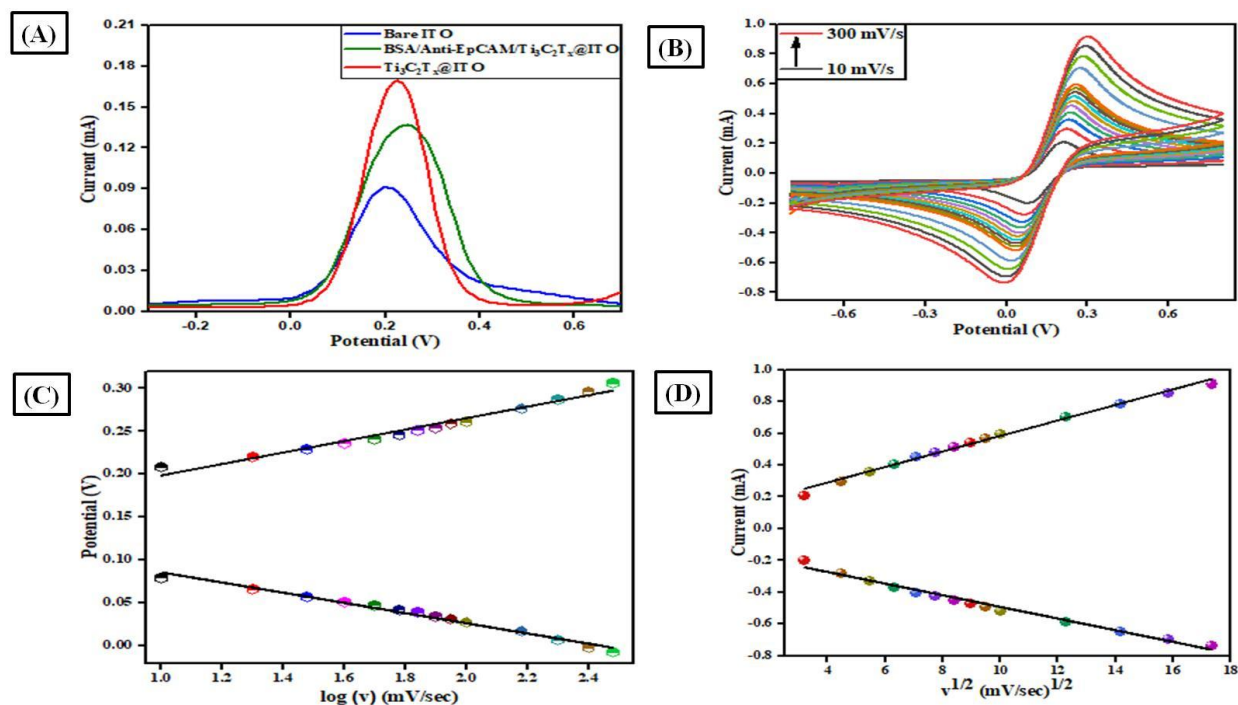


Fig. 3.5 (A) DPV plot for different electrodes; (B) Scan rate study of $\text{Ti}_3\text{C}_2\text{T}_x@/\text{ITO}$; (C) Peak potential against $\log(v)$ for $\text{Ti}_3\text{C}_2\text{T}_x@/\text{ITO}$ electrode; and (D) anodic and cathodic peak current against $v^{1/2}$ for $\text{Ti}_3\text{C}_2\text{T}_x@/\text{ITO}$ in PBS (200 mM, pH = 7.4) having $[\text{Fe}(\text{CN})_6]^{3-/4-}$ (5 mM)

In **Fig. 3.5D**, anodic and cathodic peak current densities are shown to have a linear relationship with the square roots of their corresponding scan rates. It is thus verified that the electron transfer from the $\text{Ti}_3\text{C}_2\text{T}_x@/\text{ITO}$ electrode follows the eqs. 3.3 and 3.4, which describe a surface-controlled mechanism.

$$I_{pa} (\mu\text{A}) [\text{Ti}_3\text{C}_2\text{T}_x/\text{ITO}] = 934.48 (\mu\text{A}) + 48.90 (\mu\text{A}) (\text{s/mV}) * v^{1/2}; R^2 = 0.99 \quad (3.3)$$

$$I_{pc} (\mu\text{A}) [\text{Ti}_3\text{C}_2\text{T}_x/\text{ITO}] = -128.24 (\mu\text{A}) - 36.70 (\mu\text{A}) (\text{s/mV}) * v^{1/2}; R^2 = 0.98 \quad (3.4)$$

The electrochemical parameters are calculated on the basis of aforementioned equations and Randle-Sevick equation (Eqs. 2.6 and 2.7). The surface coverage (τ) and effective surface area (A) for the $\text{Ti}_3\text{C}_2\text{T}_x@/\text{ITO}$ electrode is calculated as 0.27 cm^2 and $3.57 \times 10^{-8} \text{ mole/cm}^2$, respectively.

3.3.4 Optimization studies

Several immunosensing parameters have been optimized with the support of DPV technique in order to assess the efficacy of the fabricated immunosensor for EpCAM antigen detection. The pH of the electrolytic solution has a major impact on the electrochemical performance of Immunosensor [10]. Therefore, a change in response current has been evaluated after applying the different pH values between 6 - 8 to the BSA/anti-EpCAM/Ti₃C₂T_x@ITO electrode. The electrolytic solution at pH 6.5 displays the maximum current, which is shown in **Fig. 3.6A**. As a result, this pH is considered an ideal for further research. Another crucial factor influencing the immunosensor's efficacy is the EpCAM antigen's incubation period. As the incubation period increases, the peak current value falls and hits a plateau after 8 min, indicating the completion of reaction as seen in **Fig. 3.6B**.

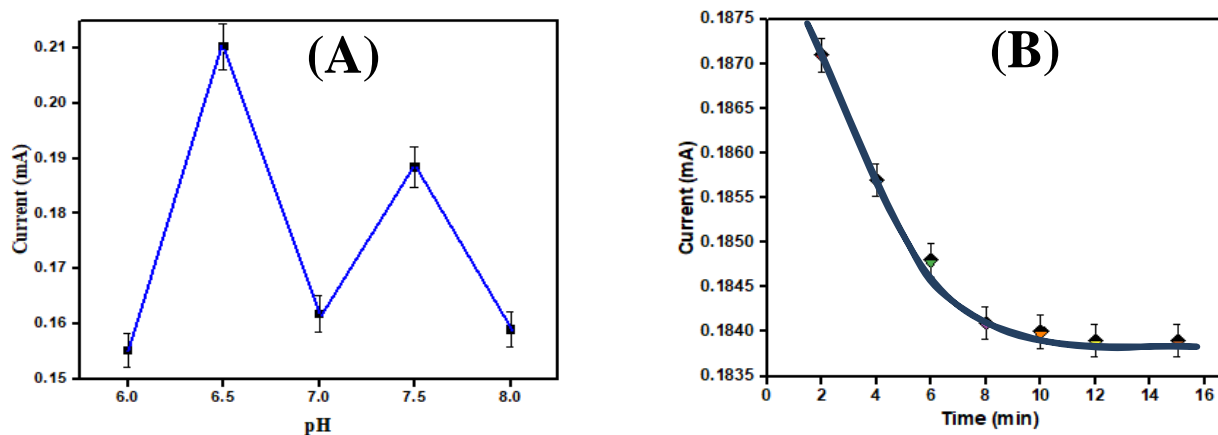


Fig. 3.6 Optimization of (A) pH; and (B) Time of incubation for EpCAM antigen

3.3.5 Electrochemical immunosensing studies

The electrochemical response of BSA/anti-EpCAM/Ti₃C₂T_x@ITO electrode is examined by using DPV technique for the detection of EpCAM antigen. **Fig. 3.7A** displays the bioelectrode's DPV response for different concentrations between 0.1 fg/mL to 100 ng/mL of EpCAM antigen in PBS (6.5 pH) and 5 mM concentration of [Fe(CN)₆]^{3-/4-}. The combination of antigen and antibody on the bioelectrode surface slows down the flow of electrons from the electrolytic solution to the bioelectrode, which is the cause of the declining trend of peak current. The calibration plot of the observed peak current with the log of EpCAM antigen conc. suggested the linearity of biosensor (**Fig. 3.7B**) and follows the Eq. 3.5.

$$\text{Current } (\mu\text{A}) = 190.955 \mu\text{A} - 1.813 \mu\text{A}/(\text{fg/mL}) \times \log C_{\text{EpCAM}}; R^2 = 0.98 \quad (3.5)$$

The sensitivity (Eq. 2.8) of the immunosensor was calculated to be $29.22 \mu\text{A}/(\text{fg/mL} \cdot \text{cm}^2)$ and LOD (Eq. 2.9) was calculated to be 0.1 fg/mL . It has been observed that the proposed BSA/anti-EpCAM/Ti₃C₂T_x@ITO immunosensor proved to be an efficient platform for the detection of very low concentrations of EpCAM antigen.

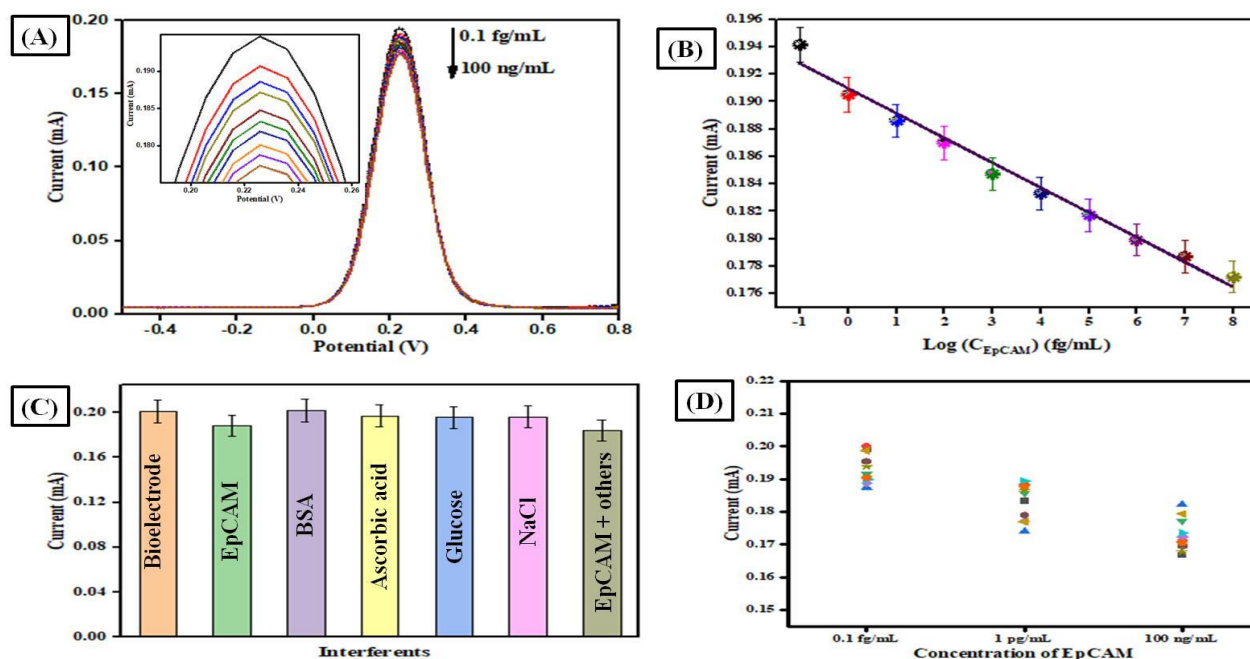


Fig. 3.7 (A) DPV response of BSA/anti-EpCAM/Ti₃C₂T_x@ITO electrode for the detection of EpCAM antigen (0.1 fg/mL to 100 ng/mL, top to bottom) in PBS pH 6.5 containing 5 mM [Fe(CN)₆]^{3-/4-}; (B) Plot depicting the linear relationship between log (C_{EpCAM}) and peak current; (C) Selectivity study of immunosensor in different analytes (100 pg/mL) with respect to EpCAM antigen; and (D) Reproducibility of immunosensor

3.3.6 Interference, reproducibility, repeatability and stability studies

The selectivity of electrochemical immunosensor was evaluated by using the interfering substances such as ascorbic acid, glucose, BSA and NaCl. Even with 100 times higher concentrations of interfering species (1 pg/mL) than EpCAM antigen (0.01 pg/mL), the immunosensor demonstrated a minor change in current with an average RSD of 1.38%. Additionally, a mixture of the aforementioned analytes containing EpCAM antigen was tested to assess the specificity; the results indicate a positive response for the detection of EpCAM, as

shown in **Fig. 3.7C**. It infers that the produced immunosensor is particular and selective for EpCAM antigen detection.

To check the reproducibility of produced immunosensor, DPV response was recorded ten times at each concentration of EpCAM antigen, i.e., 0.1 fg/mL (low), 1 pg/mL (middle), and 100 ng/mL (high), as shown in **Fig. 3.7D**. With respect to 0.1 fg/mL, 1 pg/mL, and 100 ng/mL EpCAM antigen, the RSD values for the BSA/anti-EpCAM/Ti₃C₂T_x@ITO immunosensor are 2.39%, 3.03% and 2.90%, respectively. The produced immunosensor demonstrated a good reproducibility and repeatability, as seen by the low relative standard deviation values.

Finally, the stability of immunosensor is assessed by using 10 fg/mL EpCAM antigen for a period of six weeks (**Fig. 3.8A**). Every week, the DPV response is monitored, and after five weeks, the electrode retains 77% of its initial response, indicating the satisfactory stability.

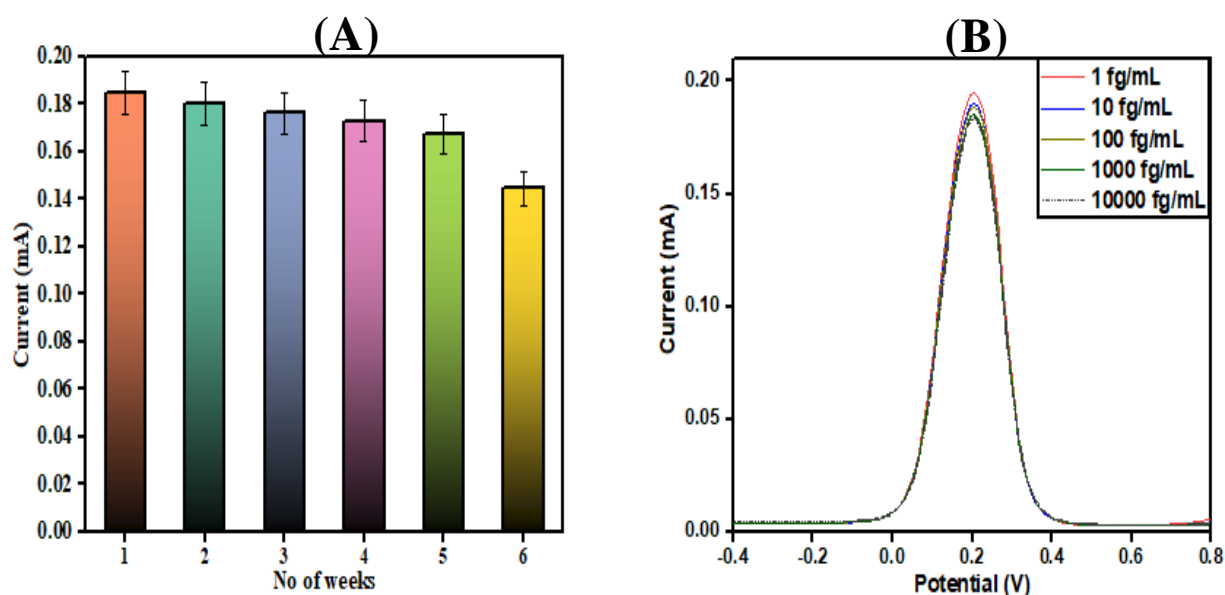


Fig. 3.8 (A) Stability study of BSA/anti-EpCAM/Ti₃C₂T_x@ITO electrode and (B) DPV response for serum sample spiked with EpCAM

3.3.7 Human serum analysis

Artificial human serum is used to investigate the clinical usefulness of the manufactured immunosensor. Different concentration of EpCAM antigen was added to diluted human serum and DPV response was recorded (**Fig. 3.8B**). In **Table 3.1**, we have reported the recoveries

(97.93% to 99.94%) for each analysis of the serum sample. Therefore, the proposed immunosensor has a good potential for EpCAM antigen detection, as evident by the RSD of less than 1.5%.

Table 3.1: Detection of biomarker in spiked serum using BSA/anti-EpCAM/Ti₃C₂T_x@ITO

S.No	Approximate added EpCAM (fg/mL)	Approximate found EpCAM (fg/mL) (SD<2.5%)	Recovery (%) (SD<2%)	RSD (%)
1	1	0.97	97.94	1.469
2	10	9.91	99.16	0.597
3	100	99.15	99.15	0.602
4	1000	999.40	99.94	0.038
5	10000	9989.00	99.89	0.077

3.4 Conclusion

In this chapter, we have successfully fabricated an ultrasensitive electrochemical immunosensor based on Ti₃C₂T_x that can detect EpCAM antigen without the need of any label. This immunosensor exhibits impressive results due to great biocompatibility, excellent dispersion in aqueous phase, high specific area and outstanding electrical conductivity of Ti₃C₂T_x. The electrochemical immunosensor has a good sensitivity of 29.22 $\mu\text{A} \cdot \text{mL} \cdot \text{fg}^{-1} \cdot \text{cm}^{-2}$ for EpCAM antigen detection and a broad linear range (0.1 fg/mL to 100 ng/mL). Additionally, the EpCAM detection in human serum has proved the immunosensor's precision and usefulness.

The results presented in this chapter have been published in “Applied Organometallic Chemistry” 38(8) (2024) e7570.

References:

- [1] L. Chen, X. Shi, N. Yu, X. Zhang, X. Du, J. Lin, Measurement and analysis of thermal conductivity of $Ti_3C_2T_x$ MXene films, *Materials*, 11 (2018) 1701.
- [2] R. Liu, W. Li, High-thermal-stability and high-thermal-conductivity $Ti_3C_2T_x$ MXene/poly (vinyl alcohol)(PVA) composites, *ACS omega*, 3 (2018) 2609-2617.
- [3] D. Zhang, Q. Mi, D. Wang, T. Li, MXene/ Co_3O_4 composite based formaldehyde sensor driven by ZnO/MXene nanowire arrays piezoelectric nanogenerator, *Sensors and Actuators B: Chemical*, 339 (2021) 129923.
- [4] C. Peng, P. Wei, X. Chen, Y. Zhang, F. Zhu, Y. Cao, H. Wang, H. Yu, F. Peng, A hydrothermal etching route to synthesis of 2D MXene (Ti_3C_2 , Nb_2C): Enhanced exfoliation and improved adsorption performance, *Ceramics International*, 44 (2018) 18886-18893.
- [5] G.T. Hermanson, *Bioconjugate techniques*, Academic press, 2013.
- [6] C. Yao, W. Zhang, L. Xu, M. Cheng, Y. Su, J. Xue, J. Liu, S. Hou, A facile synthesis of porous MXene-based freestanding film and its spectacular electroadsorption performance for organic dyes, *Separation and Purification Technology*, 263 (2021) 118365.
- [7] J. Chen, X. Yuan, F. Lyu, Q. Zhong, H. Hu, Q. Pan, Q. Zhang, Integrating MXene nanosheets with cobalt-tipped carbon nanotubes for an efficient oxygen reduction reaction, *Journal of Materials Chemistry A*, 7 (2019) 1281-1286.
- [8] J. Choi, Y.J. Kim, S.Y. Cho, K. Park, H. Kang, S.J. Kim, H.T. Jung, In situ formation of multiple schottky barriers in a Ti_3C_2 MXene film and its application in highly sensitive gas sensors, *Advanced Functional Materials*, 30 (2020) 2003998.
- [9] D.P. Jena, S. Anwar, R. Parida, B. Parida, N.C. Nayak, Structural, thermal and dielectric behavior of two-dimensional layered $Ti_3C_2T_x$ (MXene) filled ethylene–vinyl acetate (EVA) nanocomposites, *Journal of Materials Science: Materials in Electronics*, 32 (2021) 8081-8091.
- [10] O. Jalil, C.M. Pandey, D. Kumar, Highly sensitive electrochemical detection of cancer biomarker based on anti-EpCAM conjugated molybdenum disulfide grafted reduced graphene oxide nanohybrid, *Bioelectrochemistry*, 138 (2021) 107733.

CHAPTER 4

TITANIUM DIOXIDE GRAFTED ON MXENE-BASED IMMUNOSENSOR FOR CANCER BIOMARKER DETECTION

4.1 Introduction

An ultrasensitive immunosensor has been developed using 2D-TiO₂ grown onto the layered 2D-Ti₃C₂T_x sheets by hydrothermal method for label-free EpCAM antigen detection. Here, TiO₂ improves the stability of Ti₃C₂T_x in two ways: (1) by serving as protecting layer to prevent the oxidative deterioration of the inner structure of Ti₃C₂T_x, and (2) by increasing the interlayer spacing in MXene sheets [1, 2]. The details regarding the synthesis of 2D/2D TiO₂/Ti₃C₂T_x hybrid followed by structural, morphological and electrochemical characterization have been discussed in the following sections.

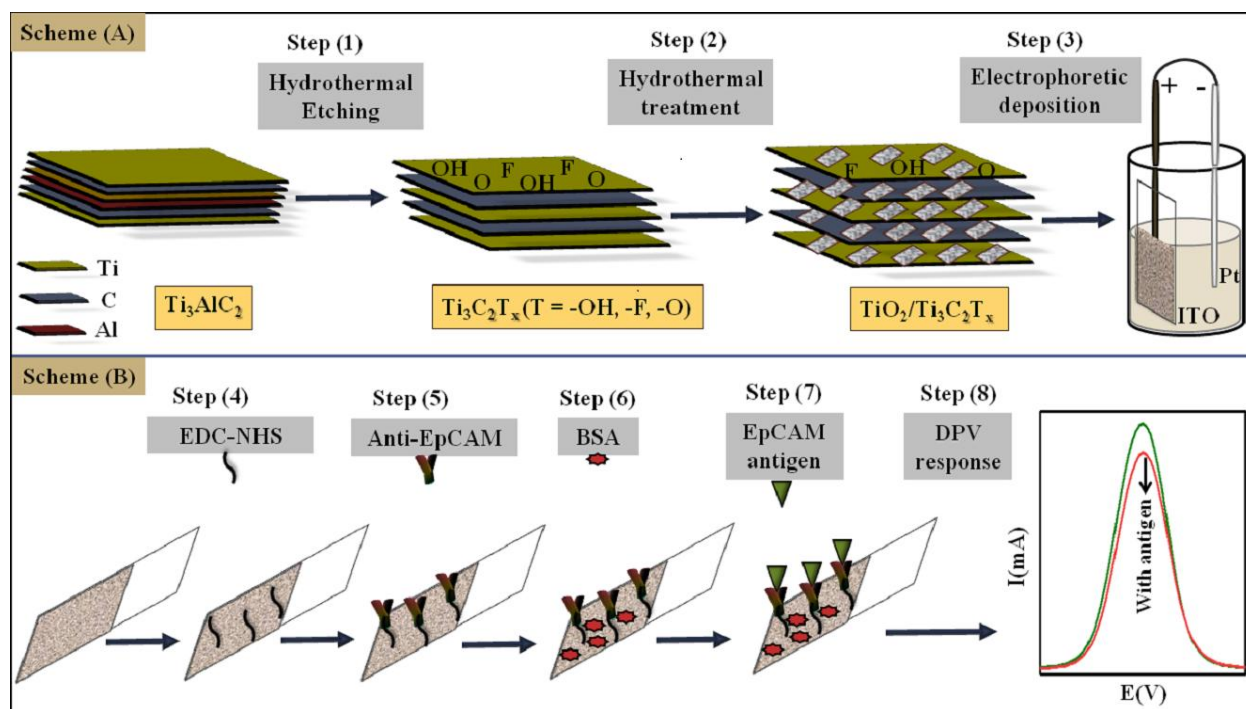


Fig. 4.1: Schematic representation for the fabrication of BSA/anti-EpCAM/TiO₂/Ti₃C₂T_x@ITO immunosensor

4.2 Experimental work

4.2.1 Synthesis of $\text{Ti}_3\text{C}_2\text{T}_x$ & $\text{TiO}_2/\text{Ti}_3\text{C}_2\text{T}_x$

The synthesis method of $\text{Ti}_3\text{C}_2\text{T}_x$ has already been covered in chapter 3. To prepare the $\text{TiO}_2/\text{Ti}_3\text{C}_2\text{T}_x$ hybrid, 70 mg of $\text{Ti}_3\text{C}_2\text{T}_x$ were mixed to 10 mL of 0.1 M HCl under constant stirring. After that, 110 mg of NaBF_4 was added in this mixture and the suspension so obtained was stirred for 1 h. Further, the suspension has been placed in a Teflon-lined autoclave at 180 °C for 10 h. The resulting solution was centrifuged, cleaned with DI water and dried in a vacuum oven at 60 °C [3].

4.2.2 Electrophoretic deposition of $\text{TiO}_2/\text{Ti}_3\text{C}_2\text{T}_x$ hybrid

An ITO-coated glass substrate has been used to deposit $\text{TiO}_2/\text{Ti}_3\text{C}_2\text{T}_x$ hybrid. Pt electrode was placed at 1 cm distance from working electrode for EPD. A colloidal suspension of $\text{TiO}_2/\text{Ti}_3\text{C}_2\text{T}_x$ (80 $\mu\text{g}/\text{mL}$) has been prepared by ultrasonication in DI water prior to deposition. Several potentials have been optimized for smooth deposition. A uniform film of $\text{TiO}_2/\text{Ti}_3\text{C}_2\text{T}_x$ has been prepared at DC potential of 10V applied for 10s.

4.2.3 Fabrication of $\text{TiO}_2/\text{Ti}_3\text{C}_2\text{T}_x$ hybrid based immunosensing platform

In order to design the immunosensor, the above prepared electrode was incubated for one hour with 20 μL EDC:NHS (1:1). Subsequently, immobilization of anti-EpCAM (40 $\mu\text{g}/\text{mL}$) was carried out by drop-casting method followed by incubation for one night at 4 °C.

4.3 Results & discussion

4.3.1 Structural analysis

Fig. 4.2A depicts the XRD pattern of Ti_3AlC_2 , $\text{Ti}_3\text{C}_2\text{T}_x$ and $\text{TiO}_2/\text{Ti}_3\text{C}_2\text{T}_x$. The characteristic peak of aluminium (Al) at $2\theta = 39.1^\circ$ (Ti_3AlC_2 , curve a) was not observed in the XRD pattern of $\text{Ti}_3\text{C}_2\text{T}_x$ and $\text{TiO}_2/\text{Ti}_3\text{C}_2\text{T}_x$, confirming that Al has been completely etched out. The main diffraction peak appeared at $2\theta = 9.6^\circ$ (Ti_3AlC_2 , curve a) has been shifted to 6.4° ($\text{Ti}_3\text{C}_2\text{T}_x$, curve b) and 5.6° ($\text{TiO}_2/\text{Ti}_3\text{C}_2\text{T}_x$, curve c), indicating that the interlayer spacing has further been increased during the synthesis of $\text{TiO}_2/\text{Ti}_3\text{C}_2\text{T}_x$ hybrid. The interlayer spacing was found to be 9.2, 13.8 and 15.8 Å (calculated by $2d \sin \theta = n\lambda$) for Ti_3AlC_2 , $\text{Ti}_3\text{C}_2\text{T}_x$ and $\text{TiO}_2/\text{Ti}_3\text{C}_2\text{T}_x$, respectively. In curve c, the collection of diffraction peaks at 25.4° , 38.1° , 48.1° , 54° , 55.1° , 63° ,

69.1° and 75.2° were observed, representing the anatase form of TiO₂ in the TiO₂/Ti₃C₂T_x hybrid [4].

FTIR spectroscopy technique has been used to examine the chemical structure of the prepared materials (**Fig. 4.2B**). Due to the C-H bond stretching vibrations, the FTIR spectra of Ti₃C₂T_x (curve a) and TiO₂/Ti₃C₂T_x (curve b) show two vibrations at 2981 and 2904 cm⁻¹ [5]. The functional groups present in the Ti₃C₂T_x were confirmed by the characteristic bands that occurred at 1617, 1400 and 1065 cm⁻¹, respectively, and these were attributed to the stretching vibrations of the bonds, namely, C=O, O-H, and C-F. Furthermore, the signals observed within the 400–800 cm⁻¹ range correspond to the stretching vibrations of the Ti–O bond (curve b) [3].

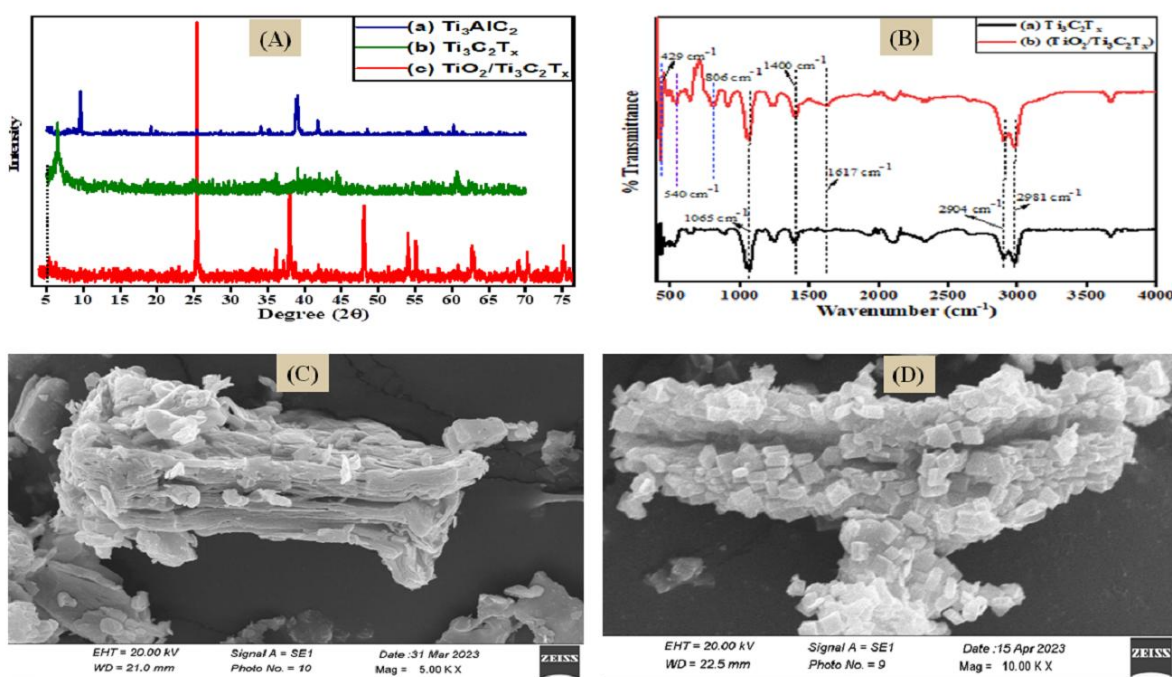


Fig. 4.2 (A) XRD spectra of (a) Ti₃AlC₂, (b) Ti₃C₂T_x (c) TiO₂/Ti₃C₂T_x; (B) FTIR peaks of (a) Ti₃C₂T_x (b)TiO₂/Ti₃C₂T_x; (C) SEM analysis of Ti₃C₂T_x; and (D) SEM analysis of TiO₂/Ti₃C₂T_x

4.3.2 Morphological characterization

The surface morphological behaviour of the produced samples was examined by using the SEM technique. Here, we have observed a 2D laminar structure with a smooth surface in the synthesized Ti₃C₂T_x (**Fig. 4.2C**). However, the SEM image of 2D-TiO₂/Ti₃C₂T_x illustrates a clear, evenly sized and well distributed 2D-sheets of TiO₂ at the edges of Ti₃C₂T_x layers (**Fig.**

4.2D). Further, a fast electron transport through the redox probe was seen to be facilitated owing to the increase in surface area of the hybrid by the biocompatible TiO_2 [6].

4.3.3. Electrochemical characterization

CV analysis was performed to assess the electrochemical performance of various electrodes by using a scan rate of 50 mV/s which is presented in **Fig. 4.3A**. On comparing with $\text{Ti}_3\text{C}_2\text{T}_x$ @ITO electrode (0.462 mA, curve b) and the ITO electrode (0.308 mA, curve a), the $\text{TiO}_2/\text{Ti}_3\text{C}_2\text{T}_x$ @ITO electrode displays the maximum current (0.723 mA) as shown in curve (c). The increased effective surface area following TiO_2 integration may be the cause of the $\text{TiO}_2/\text{Ti}_3\text{C}_2\text{T}_x$ @ITO electrode's improved conductivity. Curve d indicates that the presence of a nonconducting layer of antibody on the surface of the $\text{TiO}_2/\text{Ti}_3\text{C}_2\text{T}_x$ @ITO electrode after immobilization causes a decline in current.

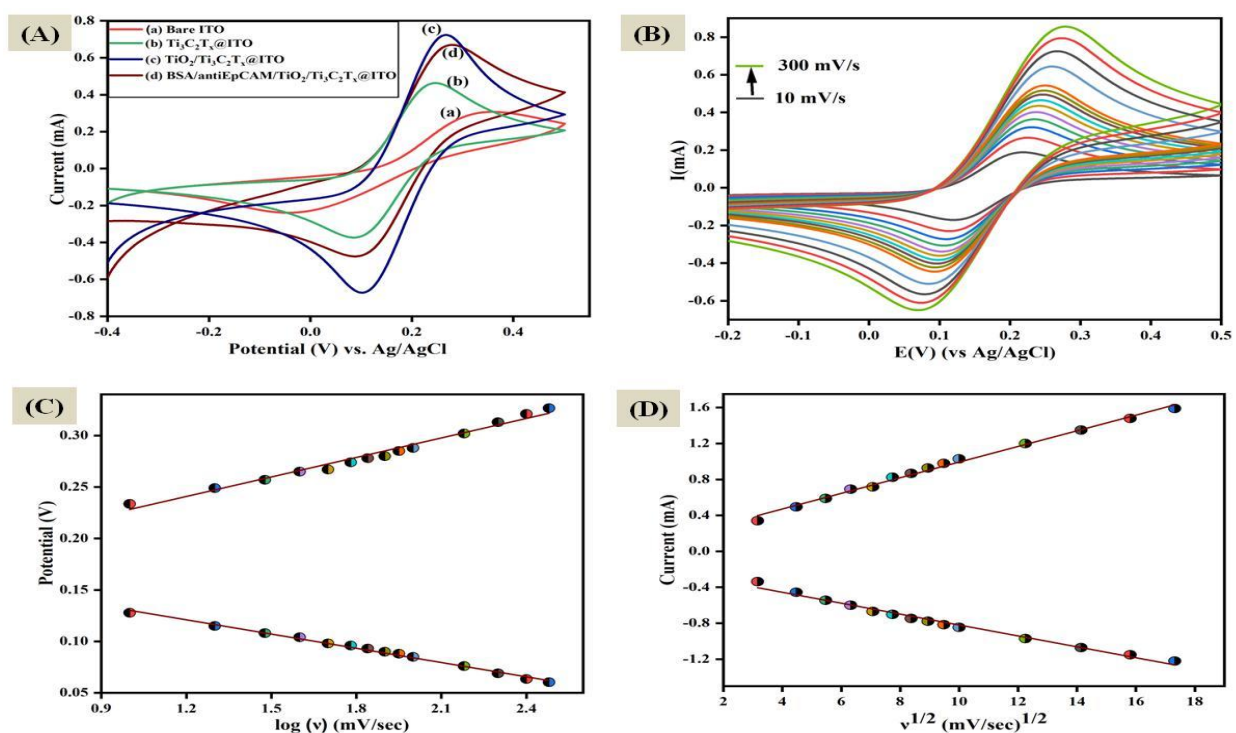


Fig. 4.3 (A) CV analysis of (a) bare ITO, (b) $\text{Ti}_3\text{C}_2\text{T}_x$ @ITO, (c) $\text{TiO}_2/\text{Ti}_3\text{C}_2\text{T}_x$ @ITO and (d) BSA/anti-EpCAM/ $\text{TiO}_2/\text{Ti}_3\text{C}_2\text{T}_x$ @ITO; (B) Scan rate analysis of $\text{TiO}_2/\text{Ti}_3\text{C}_2\text{T}_x$ @ITO; (C) Peak potential against $\log(v)$ for $\text{TiO}_2/\text{Ti}_3\text{C}_2\text{T}_x$ @ITO electrode and (D) anodic and cathodic peak current against $v^{1/2}$ for $\text{TiO}_2/\text{Ti}_3\text{C}_2\text{T}_x$ @ITO in PBS (200 mM, pH =7.4) having $[\text{Fe}(\text{CN})_6]^{3-/4-}$ (5 mM)

The scan rate investigations from 10 - 300 mV/s have also been carried out by using the CV technique for $\text{TiO}_2/\text{Ti}_3\text{C}_2\text{T}_x@/\text{ITO}$ electrode as depicted in **Fig. 4.3B**. A linear pattern was observed as shown in **Fig. 4.3C** when the peak potentials have been plotted against the log (scan rates) by using the Eqs. 4.1 and 4.2.

$$E_{\text{pa}} (\text{V}) [\text{TiO}_2/\text{Ti}_3\text{C}_2\text{T}_x@/\text{ITO}] = 0.1650 (\text{V}) + 0.0632 (\text{V}) * \log v; R^2 = 0.96 \quad (4.1)$$

$$E_{\text{pc}} (\text{V}) [\text{TiO}_2/\text{Ti}_3\text{C}_2\text{T}_x@/\text{ITO}] = 0.1748 (\text{V}) - 0.0456 (\text{V}) * \log v; R^2 = 0.97 \quad (4.2)$$

The slopes of the aforementioned equations and Laviron's equation (Eqs.2.3 to 2.5) were used to compute the value of α and K_s for the $\text{TiO}_2/\text{Ti}_3\text{C}_2\text{T}_x@/\text{ITO}$ electrode. The values of α and K_s were determined to be 0.974 and 2.255 s^{-1} , respectively. Further, it was found that there is a linear relationship between anodic & cathodic peak currents with the square root of the corresponding scan rates as shown in **Fig. 4.3D**. Eqs. 5.3 and 5.4 represent that the electron transmission through the electrodes is a surface-controlled process.

$$I_{\text{pa}} (\mu\text{A}) [\text{TiO}_2/\text{Ti}_3\text{C}_2\text{T}_x@/\text{ITO}] = 123.6 (\mu\text{A}) + 86.98 (\mu\text{A}) (\text{s/mV})^{1/2} * v^{1/2}; R^2 = 0.99 \quad (4.3)$$

$$I_{\text{pc}} (\mu\text{A}) [\text{TiO}_2/\text{Ti}_3\text{C}_2\text{T}_x@/\text{ITO}] = -212.6 (\mu\text{A}) - 60.68 (\mu\text{A}) (\text{s/mV})^{1/2} * v^{1/2}; R^2 = 0.98 \quad (4.4)$$

On the basis of above equations and Randles-Sevick equation (Eqs.2.6 and 2.7), the electrochemical kinetics parameters D , A and τ were calculated to be $43.76 \times 10^{-6} \text{ cm}^2/\text{s}$, 0.31 cm^2 and $3.64 \times 10^{-8} \text{ mole/cm}^2$, respectively.

4.3.4 Optimization studies

DPV technique was used to optimize several biosensing parameters in order to increase the constructed immunosensor's efficiency. The activity of the antibody has been influenced very significantly by the pH of a solution. Once, the BSA/anti-EpCAM/ $\text{TiO}_2/\text{Ti}_3\text{C}_2\text{T}_x@/\text{ITO}$ electrode was subjected to the different pH (6 - 8), the current was reported at each pH. The highest current value was observed at pH 6.5 (**Fig. 4.4A**), and hence it is regarded as ideal pH for biosensing studies. Furthermore, the duration of EpCAM antigen incubation on BSA/anti-EpCAM/ $\text{TiO}_2/\text{Ti}_3\text{C}_2\text{T}_x@/\text{ITO}$ biosensing platform significantly influences the immunosensor's performance. The DPV response was recorded with different incubation time upto 15 min as seen in **Fig. 4.4B**. Here, a decrease in current was also observed with increase in time upto 10 min, after that a saturation stage reaches which is pointing out the completion of reaction.

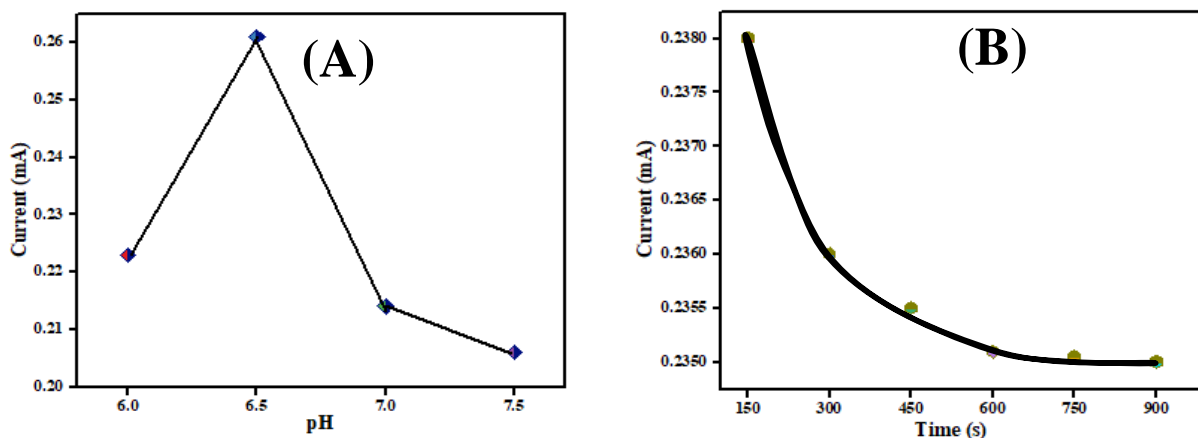


Fig. 4.4: Optimization of (A) pH and (B) Time of incubation for EpCAM antigen.

4.3.5 Electrochemical immunosensing studies

Using the DPV method, the electrochemical response for different concentrations of EpCAM antigen has been examined on a fabricated BSA/anti-EpCAM/TiO₂/Ti₃C₂T_x@ITO biosensing platform. The BSA/anti-EpCAM/TiO₂/Ti₃C₂T_x@ITO immunosensor was subjected to an increasing concentration of EpCAM antigen (1 ag/mL to 10 ng/mL) which results to a decrease in the current response (**Fig. 4.5A**). This decline in peak current is due to the formation of antigen-antibody immune-complex on the immunoelectrode's surface, which further obstructs the flow of electrons from the electrolytic solution to the immunoelectrode [7]. The plot between the inhibition current (ΔI) and the $\log C_{\text{EpCAM}}$ depicts the linearity in the detection as seen in **Fig. 4.5B** by using equation 5.5.

$$\text{Current } (\mu\text{A}) = 124.37 \mu\text{A} + 2.06 \mu\text{A/ag. mL} \times \log C_{\text{EpCAM}}; R^2 = 0.96 \quad (4.5)$$

The sensitivity and detection limit of the immunosensor (Eqs. 2.8 and 2.9) were calculated by using the above regression equation and found to be $6.661 \mu\text{A}/(\text{ag mL}^{-1} \text{ cm}^2)$ & 0.7 ag/mL , respectively. A high sensitivity, low LOD and broad linear range of a fabricated electrochemical immunosensor are due to a synergistic effect of 2D-TiO₂ and 2D-Ti₃C₂T_x.

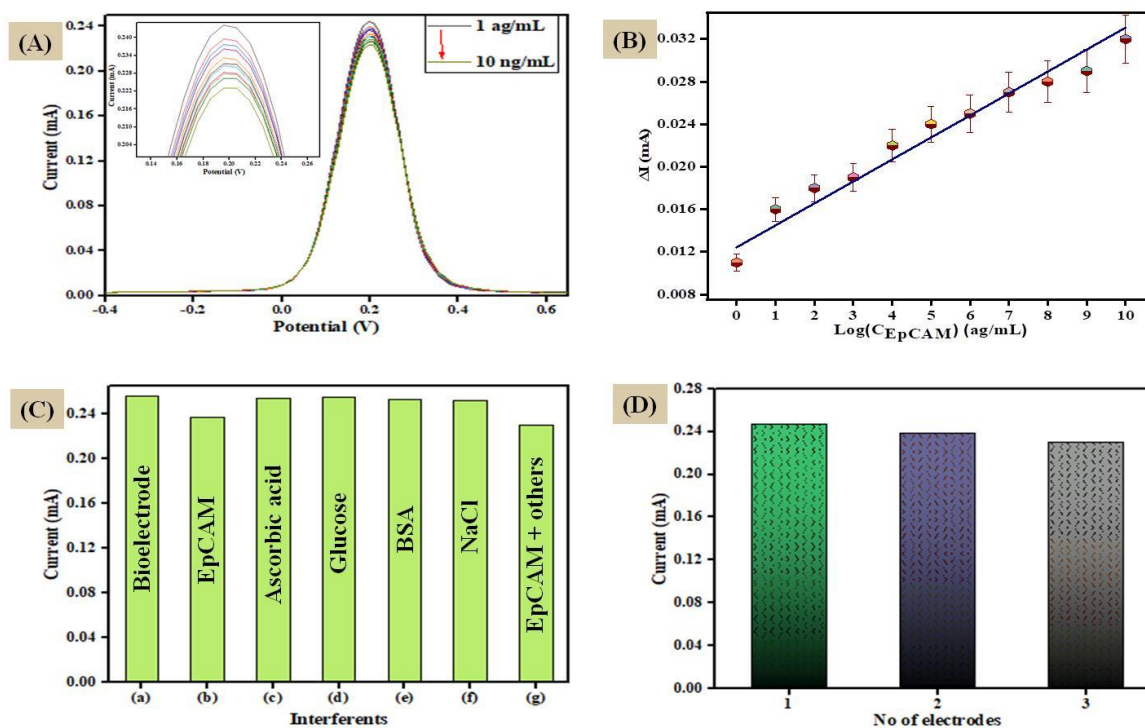


Fig. 4.5 (A) DPV response of BSA/anti-EpCAM/TiO₂/Ti₃C₂T_x@ITO biosensing platform for the detection of EpCAM antigen (from top to bottom, 1 ag/mL to 10 ng/mL) in 6.5 pH PBS containing 5 mM [Fe(CN)₆]^{3-/4-} (inset shows the magnified view of peak currents) (B) Plot depicting a linear relationship of inhibition of peak current with log (C_{EpCAM}) (C) Selectivity study of different analytes (10 fg/mL) w.r.t EpCAM antigen and (D) Reproducibility of immunosensor

4.3.6 Interference, reproducibility and stability studies

The specificity of an electrochemical immunosensor has been investigated in presence of different analytes, such as ascorbic acid, glucose, BSA and NaCl. An equal amount of analytes (10 fg/mL) having 100 times more concentration than EpCAM antigen was incubated with BSA/anti-EpCAM/TiO₂/Ti₃C₂T_x@ITO electrode and DPV response was recorded that indicates almost no change in current (**Fig. 4.5C**). Additionally, a mixture of various analytes along with EpCAM antigen (conc. of 10 fg/mL each) has been used to test the immunosensor's specificity. It was discovered that the current response had decreased, proving the specificity of fabricated immunosensor.

To check the reproducibility, an experiment was conducted by using three different electrodes in 10 ag/mL of EpCAM antigen (**Fig. 4.5D**). The results display an RSD of 3.56%, indicating that the fabricated immunosensor possesses an acceptable reproducibility.

Additionally, the immunosensor's shelf life study was assessed for eight weeks with 10 ag/mL of EpCAM antigen. After six weeks, the peak current dropped by 27%, according to the DPV response, which was measured once a week (**Fig. 4.6A**). After that, the peak current dropped by 33%, indicating that the immunosensor's stability is adequate.

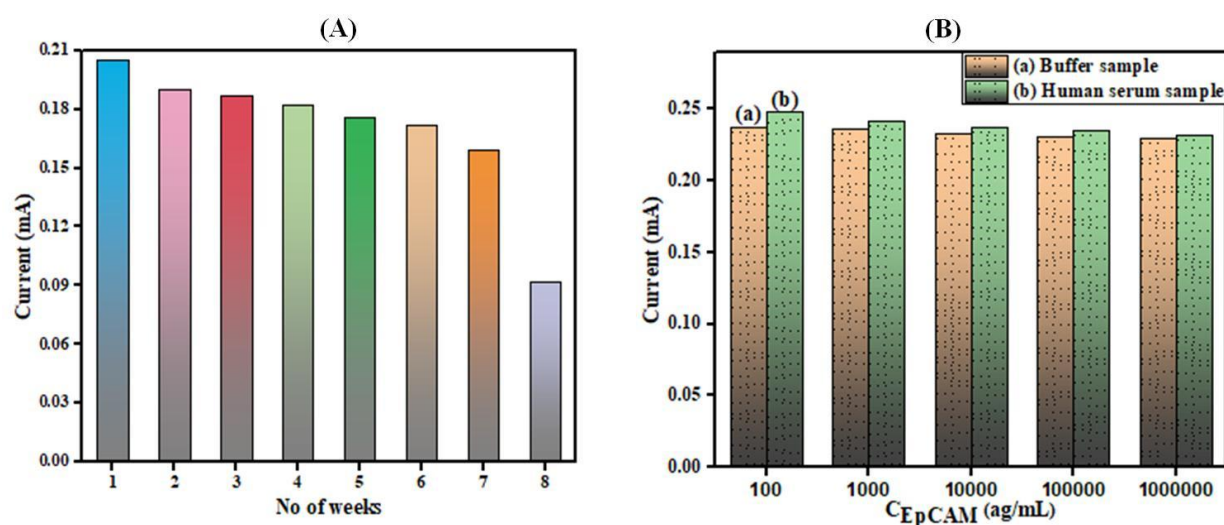


Fig. 4.6 (A) Stability study of immunosensor; and (B) Peak current of immunosensor in (a) buffer and (b) serum sample

4.3.7 Human serum analysis

In order to validate a clinical utility of this developed immunosensor, an artificial human serum sample has been analyzed using the BSA/anti-EpCAM/TiO₂/Ti₃C₂T_x@ITO electrode. Firstly, a serum sample has been diluted ten times using PBS (7.4 pH) before analysis. After that, sample was spiked with varying the EpCAM antigen concentrations from 100 ag/mL to 1 pg/mL and then recorded its DPV response. Interestingly, a spiked serum sample and buffer at the same conc. of EpCAM antigen were found to be in good agreement (**Fig. 4.6B**). **Table 4.1** shows that the recovered percentage of EpCAM antigen ranges from 95.56% to 97.14%. As a result, we can infer that there is great potential for this immunosensor to identify EpCAM antigen.

Table 4.1: Detection of EpCAM in spiked serum sample with BSA/anti-EpCAM/TiO₂/Ti₃C₂T_x@ITO electrode

S.No	Approximate added EpCAM (ag/mL)	Approximate found EpCAM (ag/mL)	Recovery (%)	RSD (%)
1	100	95.56	95.56	3.207
2	1000	975.20	97.52	1.775
3	10000	9831.00	98.31	1.204
4	100000	98298.00	98.30	1.214
5	1000000	991380.00	99.14	0.612

4.4 Conclusion

In this chapter, 2D/2D TiO₂/Ti₃C₂T_x hybrid has been synthesized successfully by one pot hydrothermal method. This hybrid offers a large surface area that is particularly effective for the immobilization of anti-EpCAM due to the synergistic effect of TiO₂ and Ti₃C₂T_x. The electrochemical experiments demonstrate a high sensitivity of 6.661 $\mu\text{A}/(\text{ag mL}^{-1} \text{cm}^2)$ and an extremely low LOD as 0.7 ag/mL for EpCAM antigen detection. Furthermore, this immunosensor exhibits good repeatability, excellent selectivity and stability. Additionally, the immunosensor's clinical applicability was validated using human serum samples. The immunosensor has been found to have a potential for EpCAM antigen detection based on the satisfactory results.

The results presented in this chapter have been published in "Journal of Colloids and Interface Science" 652 (2023) 549-556.

References:

- [1] N. Liu, L. Yu, B. Liu, F. Yu, L. Li, Y. Xiao, J. Yang, J. Ma, Ti_3C_2 -MXene partially derived hierarchical 1D/2D $\text{TiO}_2/\text{Ti}_3\text{C}_2$ heterostructure electrode for high-performance capacitive deionization, *Advanced Science* 10 (2023) 2204041.
- [2] L. Li, G. Jiang, C. An, Z. Xie, Y. Wang, L. Jiao, H. Yuan, Hierarchical $\text{Ti}_3\text{C}_2@ \text{TiO}_2$ MXene hybrids with tunable interlayer distance for highly durable lithium-ion batteries, *Nanoscale* 12 (2020) 10369-10379.
- [3] C. Peng, T. Zhou, P. Wei, X. Yan, Y. Kong, W. Xu, H. Wang, H. Yu, J. Jia, K. Zhang, Steering interfacial charge kinetics: Synergizing cocatalyst roles of $\text{Ti}_3\text{C}_2\text{M}_x$ (MXene) and NCDs for superior photocatalytic performance over TiO_2 , *Applied Surface Science* 599 (2022) 154001.
- [4] Y. Ma, M. Ni, S. Li, Optimization of malachite green removal from water by TiO_2 nanoparticles under UV irradiation, *Nanomaterials* 8 (2018) 428.
- [5] B. Reddy, G.-B. Cho, N. Reddy, H.-J. Ahn, J.-H. Ahn, T. Maiyalagan, K.-K. Cho, Layered-like structure of TiO_2 - Ti_3C_2 Mxene as an efficient sulfur host for room-temperature sodium-sulfur batteries, *Journal of Alloys and Compounds* 883 (2021) 160910.
- [6] W. Lv, J. Zhu, F. Wang, Y. Fang, Facile synthesis and electrochemical performance of TiO_2 nanowires/ Ti_3C_2 composite, *Journal of Materials Science: Materials in Electronics* 29 (2018) 4881-4887.
- [7] O. Jalil, C.M. Pandey, D. Kumar, Electrochemical biosensor for the epithelial cancer biomarker EpCAM based on reduced graphene oxide modified with nanostructured titanium dioxide, *Microchimica Acta* 187 (2020) 1-9.

CHAPTER 5

CuS-DOPED $Ti_3C_2T_x$ -BASED ELECTROCHEMICAL IMMUNOSENSOR FOR EpCAM ANTIGEN DETECTION

5.1 Introduction

Here, a novel CuS-anchored 2D- $Ti_3C_2T_x$ -based electrode has been developed to achieve highly sensitive detection of EpCAM by using anti-EpCAM (**Fig. 5.1**). CuS, when combined with $Ti_3C_2T_x$ works in a synergetic manner to increase the overall stability of hybrid with an improved electroactive surface area supporting the loading of antibody [1]. All the details regarding the synthesis, structural and electrochemical characterization for the fabrication of BSA/anti-EpCAM/CuS/ $Ti_3C_2T_x$ @ITO immunosensor have been discussed in the following sections.

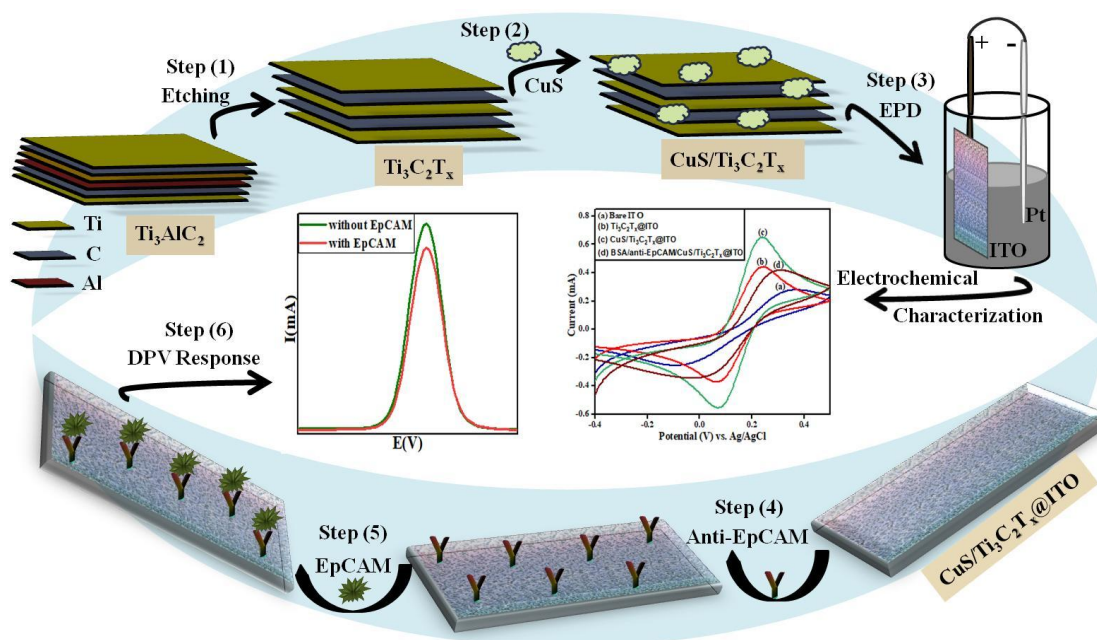


Fig. 5.1: Schematic representation for the fabrication of BSA/anti-EpCAM/CuS/ $Ti_3C_2T_x$ @ITO platform for EpCAM antigen detection

5.2 Experimental section

5.2.1 Synthesis of CuS and CuS/Ti₃C₂T_x

CuS was synthesized by the method as reported earlier with a little modification [2]. 0.8 g of sodium thiosulfate (0.125 M) and copper sulfate (0.5 M) were dissolved in 40 mL and 20 mL DIW, respectively. After 30 min, both solutions were mixed under stirring and transferred to an autoclave and kept for 12 h at 180 °C. The resulting dark-colored suspension was washed with DIW and ethanol under centrifugation, respectively. Subsequently, the precipitate was vacuum-dried at 70 °C to obtain powdered CuS.

CuS/Ti₃C₂T_x hybrid was synthesized by one-pot hydrothermal method. Here, 150 mg of each Ti₃C₂T_x, Na₂S₂O₃ and CuSO₄ were dispersed in 10 mL of DIW separately. Subsequently, mix all the solutions under constant stirring and transfer them to a Teflon-lined autoclave by keeping for 12 h at 180 °C. This mixture has been washed with DIW multiple times under centrifugation and dried in a vacuum oven at 60 °C.

5.2.2 Electrophoretic deposition of CuS/Ti₃C₂T_x hybrid

CuS/Ti₃C₂T_x hybrid was deposited onto the indium-tin-oxide (ITO) coated glass substrate by using a deposition technique like electrophoretic deposition consisting of two electrodes system. Before deposition, a colloidal solution was prepared with CuS/Ti₃C₂T_x hybrid (0.1 mg/mL) in DIW. The electrophoretic deposition was then carried out for 18 s at an ideal DC potential of 10 V. A smooth film appeared on the surface of ITO resulting in the fabrication of CuS/Ti₃C₂T_x@ITO electrode.

5.2.3 Fabrication of biosensing platform

Firstly, the CuS/Ti₃C₂T_x@ITO electrode was incubated with crosslinker EDC: NHS (20 µL) for 30 min. Subsequently, the fabricated electrode was drop-casted with anti-EpCAM (20 µL) and incubated for 8 h at 4 °C. Here, EDC: NHS works in reverse manner and activates the carboxylic groups of the antibody, which further makes the covalent bonds with the functional groups (–OH) of Ti₃C₂T_x. Further, to prevent non-specific reactions, 1% BSA was applied to the immuno-electrodes for 30 min. Finally, the immuno-electrodes were washed with PBS (7.4 pH) three times for further use.

5.3 Results & discussion

5.3.1 Structural analysis

The X-ray diffraction studies of $\text{Ti}_3\text{C}_2\text{T}_x$, CuS and CuS/ $\text{Ti}_3\text{C}_2\text{T}_x$ are represented in **Fig. 5.2A**. The broad diffraction peak at 6.5° in the spectra of $\text{Ti}_3\text{C}_2\text{T}_x$ clearly shows the successful synthesis of $\text{Ti}_3\text{C}_2\text{T}_x$. The XRD curve of CuS shows the peaks at 29.5° , 32° , 48.1° , 53° and 59.5° (JCPDS: 06-0464) [3]. On the other hand, CuS/ $\text{Ti}_3\text{C}_2\text{T}_x$ hybrid matches all the characteristic peaks of CuS at 29.3° , 31.9° and 48° and the main peak of $\text{Ti}_3\text{C}_2\text{T}_x$ shifts from 6.5° to 6.3° indicating an increase in interlayer spacing, which further improves the effective surface area of transducer.

The chemical bonds present in the structure of CuS, $\text{Ti}_3\text{C}_2\text{T}_x$ and CuS/ $\text{Ti}_3\text{C}_2\text{T}_x$ hybrid is demonstrated by FTIR spectroscopy (**Fig. 5.2B**). The dominant band at 598 cm^{-1} in FTIR spectra of CuS is due to the stretching vibrations of Cu–S bond. The additional bands seen at 847 and 1084 cm^{-1} are owing to C–H bending vibrations and C–O stretching vibrations of absorbed alcohol, respectively [4]. The FTIR spectrum of $\text{Ti}_3\text{C}_2\text{T}_x$ displayed C–H bonds stretching vibrations at 2980 and 2908 cm^{-1} . The vibrations at 1393 and 1059 cm^{-1} are attributed to the O–H and C–F bonds stretching vibrations, respectively, which further proved the existence of surface groups (–OH and –F) [5]. The FTIR spectra of the CuS/ $\text{Ti}_3\text{C}_2\text{T}_x$ hybrid thus exhibited all the characteristic peaks of CuS and $\text{Ti}_3\text{C}_2\text{T}_x$.

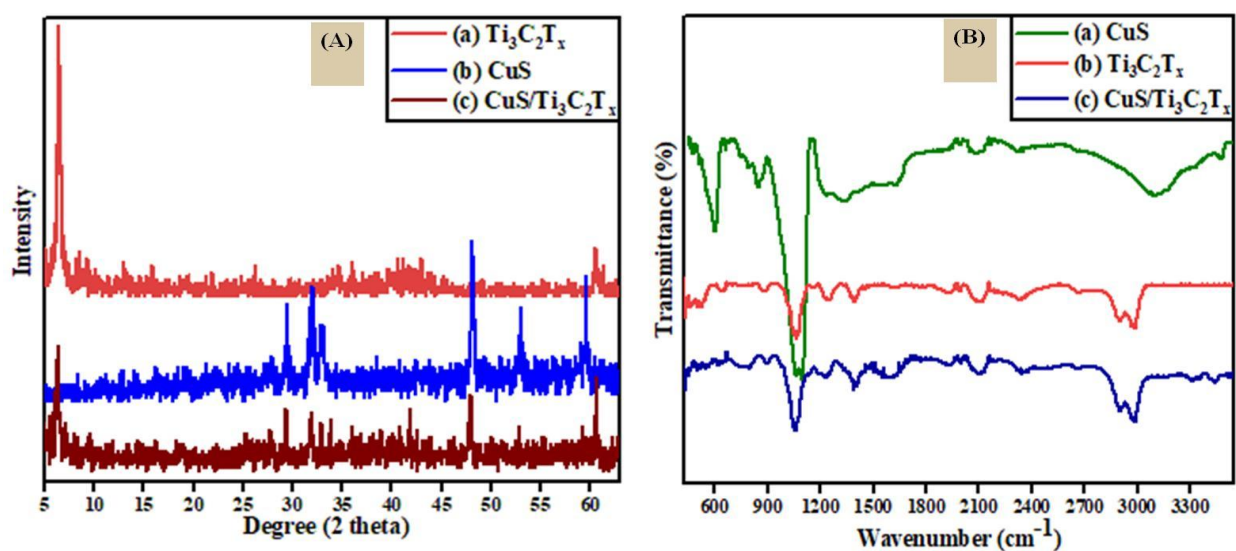


Fig. 5.2: (A) XRD spectra of $\text{Ti}_3\text{C}_2\text{T}_x$ (a), CuS (b) & CuS/ $\text{Ti}_3\text{C}_2\text{T}_x$ (c) (B) FTIR spectra of CuS (a), $\text{Ti}_3\text{C}_2\text{T}_x$ (b), and CuS/ $\text{Ti}_3\text{C}_2\text{T}_x$ (c)

5.3.2 Morphological Characterization

The surface structure of the synthesized $\text{Ti}_3\text{C}_2\text{T}_x$ and $\text{CuS}/\text{Ti}_3\text{C}_2\text{T}_x$ hybrid were analyzed by using a scanning electron microscope. **Fig. 5.3A** represents the 2D-layered accordion-like architecture of $\text{Ti}_3\text{C}_2\text{T}_x$. It is visible that the different layers are separated and parallel to each other. **Fig. 5.3B** revealed that the sphere-like morphology of CuS is anchored onto the surface of $\text{Ti}_3\text{C}_2\text{T}_x$ sheets. The spherical structures of CuS in the magnified view (**Fig. 5.3C**) clearly show a conductive network and space to $\text{CuS}/\text{Ti}_3\text{C}_2\text{T}_x$ hybrid for a better immobilization of antibodies. **Fig. 5.3D** depicts the TEM image of $\text{CuS}/\text{Ti}_3\text{C}_2\text{T}_x$ hybrid, in which CuS particles are distributed onto the 2D- sheet of $\text{Ti}_3\text{C}_2\text{T}_x$. The size of spherically shaped CuS was found to be 22-25 nm (**Fig. 5.3E**).

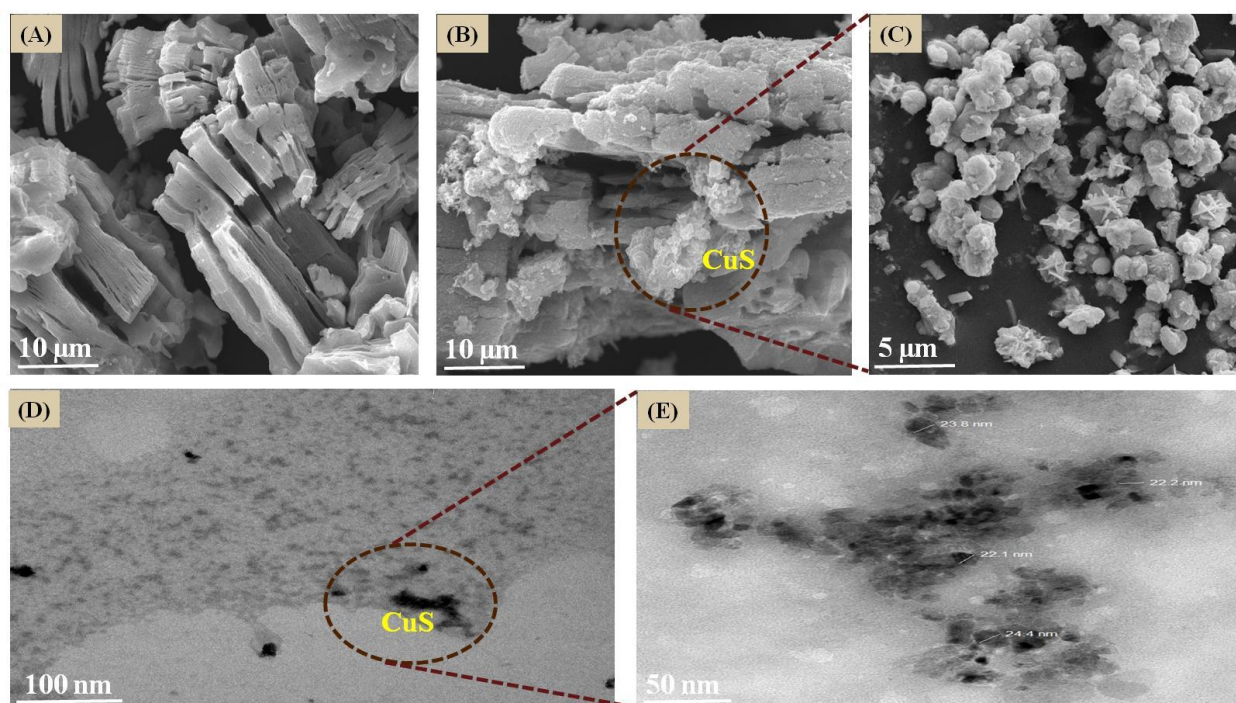


Fig. 5.3: (A) SEM micrograph of $\text{Ti}_3\text{C}_2\text{T}_x$; (B) and (C) SEM image of $\text{CuS}/\text{Ti}_3\text{C}_2\text{T}_x$; (D) and (E) TEM micrograph of $\text{CuS}/\text{Ti}_3\text{C}_2\text{T}_x$

5.3.3 Electrochemical characterization of fabricated electrodes

The different electrodes fabricated such as (a) bare ITO, (b) $\text{Ti}_3\text{C}_2\text{T}_x@$ ITO, (c) $\text{CuS}/\text{Ti}_3\text{C}_2\text{T}_x@$ ITO and (d) BSA/anti-EpCAM/ $\text{CuS}/\text{Ti}_3\text{C}_2\text{T}_x@$ ITO were electrochemically characterized by cyclic voltammetry (CV) analysis (**Fig. 5.4A**) which has been conducted at 50 mV/s [scan rate (v)] in PBS (0.2M) at 7.4 pH containing 5 mM $[\text{Fe}(\text{CN})_6]^{3-/4-}$. It is observed here that the electrochemical current becomes almost 1.5 times after incorporation of CuS , i.e.,

CuS/Ti₃C₂T_x@ITO (0.65 mA) in comparison to Ti₃C₂T_x@ITO (0.442 mA). The electrochemical current decreases to 0.418 mA after immobilization of the antibody resulting to an insulating layer of antigen and antibody on the transducer. Further, the scan rate study (10 - 400 mV/s) of CuS/Ti₃C₂T_x@ITO electrode (**Fig. 5.4B**) demonstrates that a linear trend is observed when we plot peak potentials vs. log v graph, by using Eqs. 5.1 and 5.2 as shown **Fig. 5.4C**.

$$E_{pa} [\text{CuS/Ti}_3\text{C}_2\text{T}_x\text{@ITO}] = 0.138 \text{ (V)} + 0.0623 \text{ (V)} * \log v; R^2 = 0.9703 \quad (5.1)$$

$$E_{pc} [\text{CuS/Ti}_3\text{C}_2\text{T}_x\text{@ITO}] = 0.151 \text{ (V)} - 0.0546 \text{ (V)} * \log v; R^2 = 0.9871 \quad (5.2)$$

The values of electron transfer coefficient (α) and hence apparent charge transfer rate constant (K_s) for CuS/Ti₃C₂T_x@ITO electrode are calculated to be 0.893 and 0.1337 s⁻¹ respectively, by using Laviron's equation (2.3 to 2.5) reported earlier [6].

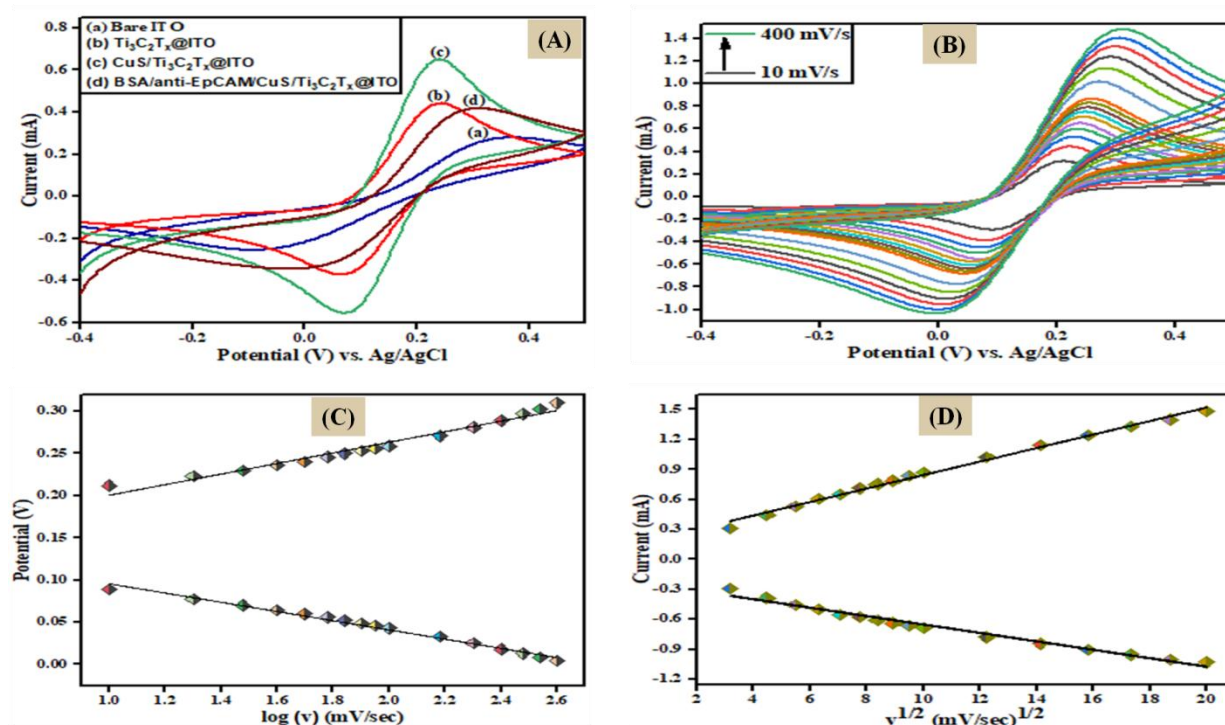


Fig. 5.4: (A) CV plots of bare ITO (a), Ti₃C₂T_x@ITO (b), CuS/Ti₃C₂T_x@ITO (c), and BSA/anti-EpCAM/CuS/Ti₃C₂T_x@ITO (d); (B) Scan rate study (10 – 400 mV/s) of CuS/Ti₃C₂T_x@ITO; (C) Plot of the potential with log of scan rate for CuS/Ti₃C₂T_x@ITO; and (D) Plot between the I_{pa} , I_{pc} and square root of scan rate of CuS/Ti₃C₂T_x@ITO electrode

We can see here a linear relationship between peak currents and the square root of scan rates as depicted in **Fig. 5.4D** by using the Eqs. 5.3 and 5.4, which further demonstrates that electron transfer is a surface-controlled process.

$$I_{pa} [\text{CuS}/\text{Ti}_3\text{C}_2\text{T}_x@\text{ITO}] = 166.5 (\mu\text{A}) + 67.53 (\mu\text{A}) (\text{s/mV})^{1/2} * v^{1/2}; R^2 = 0.9936 \quad (5.3)$$

$$I_{pc} [\text{CuS}/\text{Ti}_3\text{C}_2\text{T}_x@\text{ITO}] = - 233.3 (\mu\text{A}) - 42.16 (\mu\text{A}) (\text{s/mV})^{1/2} * v^{1/2}; R^2 = 0.9801 \quad (5.4)$$

The Randles-Sevick equation is given as $I_p = 2.69 \times 10^5 n^{3/2} ACD^{1/2} v^{1/2}$; where n is no of electrons, C (mole/cm³) is concentration, v (V/s) is scan rate and I_p (A) is the peak current. The slopes of above equations were used to calculate the diffusion coefficient (D), and effective surface area (A). The D and A values for $\text{CuS}/\text{Ti}_3\text{C}_2\text{T}_x@\text{ITO}$ electrode were found to be 51.72×10^{-6} cm²/s & 0.22 cm², respectively. Furthermore, an average surface coverage area (τ) for $\text{CuS}/\text{Ti}_3\text{C}_2\text{T}_x@\text{ITO}$ electrode was calculated to be 6.20×10^{-8} mole/cm², [$I_p = n^2 F^2 A \tau v / 4RT$].

5.3.4 Electrochemical immunosensing study for EpCAM antigen detection

An electrochemical analysis of the $\text{BSA}/\text{anti-EpCAM}/\text{CuS}/\text{Ti}_3\text{C}_2\text{T}_x@\text{ITO}$ electrode was performed by using the DPV technique, over a wide range of EpCAM antigen concentrations (0.01 fg/mL - 100 ng/mL). The DPV responses of fabricated immunoelectrode were recorded by incubating different concentrations of EpCAM antigen, with an incubation time of 10 min. A peak current was found to be decreased as the concentration of EpCAM antigen increased (**Fig. 5.5A**). There is a combination of antigen and antibody on the immunosensing electrode, resulting in the reduction of active sites, which in turn slows down the flow of electrons via the redox probe [7].

Fig. 5.5B shows a calibration curve plotted between the inhibition current (ΔI) and logarithmic scale of EpCAM antigen concentrations. The linearity plot follows the regression equation: [$y = 2.336 x + 16.991$; where $y =$ current, $x =$ logarithm of the concentration of EpCAM and $R^2 = 0.9779$]. By using the slope of the above Eq., the sensitivity and limit of detection were calculated as $461.85 \mu\text{A fg}^{-1} \text{mL cm}^{-2}$ and 0.0057 fg/mL , respectively.

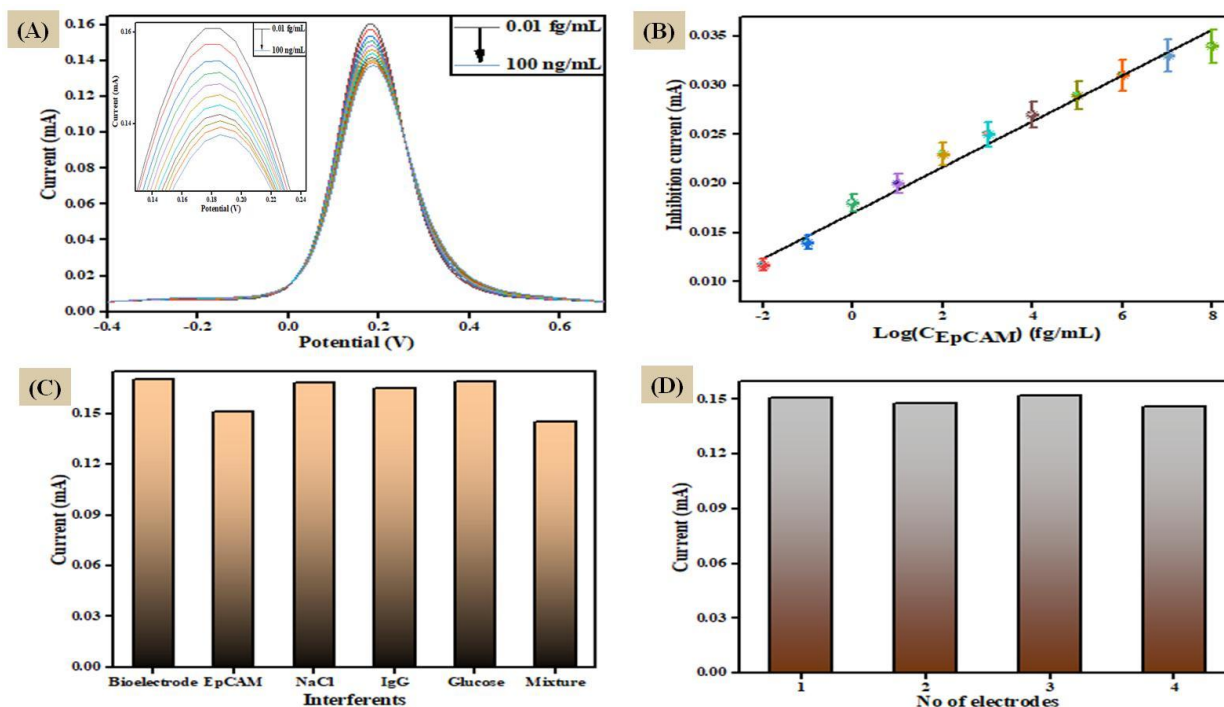


Fig. 5.5: (A) DPV study showing the response of BSA/anti-EpCAM/CuS/Ti₃C₂T_x@ITO electrode with increasing conc. of EpCAM antigen (0.01 fg/mL - 100 ng/mL); (B) Linearity plot between peak current change and log of EpCAM antigen concentration; (C) An interference study of immunosensor with multiple analytes (100 pg/mL); (D) Reproducibility study of immunosensor

5.3.5 Selectivity, reproducibility and shelf life studies

The interference study of BSA/anti-EpCAM/CuS/Ti₃C₂T_x@ITO immunosensor was studied by incubating different interfering species such as sodium chloride (NaCl), immunoglobulin G (IgG) and glucose having a concentration of 100 fg/mL each. The magnitude of peak current did not show much changes with all these species in comparison to EpCAM antigen (10 fg/mL) (**Fig. 5.5C**). Furthermore, the specificity of the fabricated immunosensor was tested with a mixture of all the above analytes in addition to EpCAM antigen. The electrochemical peak current was decreased, which confirms the specificity of the immunosensor.

The reproducibility of this fabricated immunosensor has been examined by DPV technique with four different electrodes prepared in similar conditions by incubating EpCAM antigen (10 fg/mL) (**Fig. 5.5D**). A very low relative standard deviation (RSD) of 2.12% was determined with the constant surface area, thereby proving an excellent reproducibility of this immunosensor.

Finally, the shelf life of this fabricated immunosensor has been tested by using the DPV technique. The analysis was done by incubating EpCAM antigen (10 fg/mL), every 6 days, for up to 42 days. It was observed that the peak current shows a minimal decrease even after 42 days, hence proving the acceptable stability of the immunosensor (**Fig. 5.6A**).

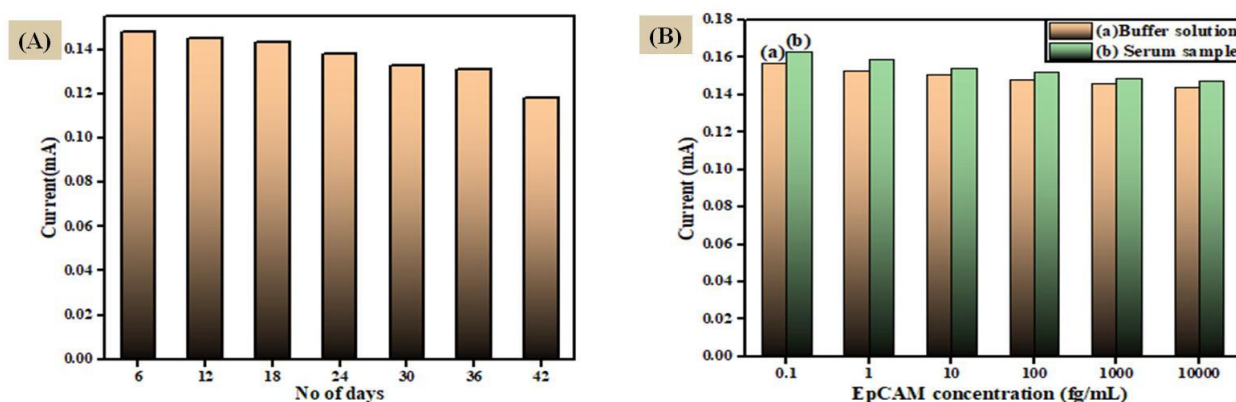


Fig. 5.6: (A) Shelf life study of BSA/anti-EpCAM/CuS/Ti₃C₂T_x@ITO; (B) Comparison of DPV response (a) in buffer sample, and (b) in spiked serum sample (0.1 – 10000 fg/mL)

5.3.6 Human serum analysis

The clinical applicability of the fabricated immunosensor was analyzed with a diluted artificial human serum. The serum was then spiked with various EpCAM antigen concentrations (0.1 fg/mL to 10000 fg/mL) and the electrochemical response was recorded with the BSA/anti-EpCAM/CuS/Ti₃C₂T_x@ITO electrode (**Fig. 5.6B**). In Fig.4D, the bar diagram represents the (a) peak current in buffer solution and (b) peak current in spiked serum samples. The results presented in **Table 5.1** show a good recovery (96.23% to 98.05%) with %RSD less than 3%. Therefore, these results indicate that the immunosensor could be reliable for EpCAM detection.

Table 5.1: Detection of EpCAM in spiked serum sample with BSA/anti-EpCAM/CuS/Ti₃C₂T_x@ITO electrode

S.No	Approximate added EpCAM (fg/mL)	Approximate found EpCAM (fg/mL)	Recovery (%)	RSD (%)
1	0.1	0.09	96.32	2.652
2	1	0.96	96.23	2.720
3	10	9.80	98.05	1.391
4	100	97.37	97.37	1.886
5	1000	979.90	97.99	1.438
6	10000	9664.43	96.64	1.458

5.4 Conclusion

In this chapter, we have developed a CuS/Ti₃C₂T_x hybrid based label-free electrochemical immunosensor for EpCAM antigen detection. This hybrid platform works as an excellent transducer surface due to the synergetic effect. The electrochemical experiments show an incredibly low LOD of 0.0057 fg/mL; for EpCAM antigen, with an ultra-broad detection range of 0.01 fg/mL - 100 ng/mL. Additionally, this fabricated immunosensor delivered an excellent reproducibility, high specificity and selectivity. Furthermore, the serum samples were used to verify the applicability of this immunosensor and found a satisfactory performance.

The results presented in this chapter have been published in “Applied Organometallic Chemistry, 39(2) (2025) e7975.

References:

- [1] Z. Pan, F. Cao, X. Hu, X. Ji, A facile method for synthesizing CuS decorated Ti_3C_2 MXene with enhanced performance for asymmetric supercapacitors, *Journal of Materials Chemistry A* 7 (2019) 8984-8992.
- [2] J. Fang, P. Zhang, H. Chang, X. Wang, Hydrothermal synthesis of nanostructured CuS for broadband efficient optical absorption and high-performance photo-thermal conversion, *Solar Energy Materials and Solar Cells* 185 (2018) 456-463.
- [3] Z. Li, L. Mi, W. Chen, H. Hou, C. Liu, H. Wang, Z. Zheng, C. Shen, Three-dimensional CuS hierarchical architectures as recyclable catalysts for dye decolorization, *CrystEngComm* 14 (2012) 3965-3971.
- [4] S. Riyaz, A. Parveen, A. Azam, Microstructural and optical properties of CuS nanoparticles prepared by sol-gel route, *Perspectives in Science* 8 (2016) 632-635.
- [5] B. Reddy, G.-B. Cho, N. Reddy, H.-J. Ahn, J.-H. Ahn, T. Maiyalagan, K.-K. Cho, Layered-like structure of TiO_2 - Ti_3C_2 Mxene as an efficient sulfur host for room-temperature sodium-sulfur batteries, *Journal of Alloys and Compounds* 883 (2021) 160910.
- [6] S. Chatterjee, H. Singh, D. Hudda, Sweetey, D. Kumar, A Novel Acetylcholinesterase-Based Electrochemical Biosensor Using $\text{g-C}_3\text{N}_4$ @ MoS_2 Nanohybrid for the Detection of Trichlorfon, *Applied Organometallic Chemistry* (2024) e7721.
- [7] W. Hong, S. Lee, E.J. Kim, M. Lee, Y. Cho, A reusable electrochemical immunosensor fabricated using a temperature-responsive polymer for cancer biomarker proteins, *Biosensors and Bioelectronics* 78 (2016) 181-186.

CHAPTER 6

**ELECTROCHEMICAL PAPER BASED IMMUNOSENSOR GRAFTED BY USING
CuS@PEDOT:PSS FOR EpCAM ANTIGEN DETECTION**

6.1 Introduction

This chapter describes the development of a cheap, biodegradable and highly sensitive paper-based immunosensor by using CuS grafted PEDOT:PSS for the detection of EpCAM antigen. The electrochemical paper (EP), DMSO treated CuS@PEDOT:PSS/WP has been fabricated by dip-coating method [1, 2]. The flexible nature of EP allows the effective immobilization of anti-EpCAM. This EP-based Immunosensor, BSA/anti-EpCAM/EP has further been utilized to detect EpCAM antigen. Therefore, it may be a promising cost-effective substitute over other costly conventional techniques for biosensing applications [3, 4].

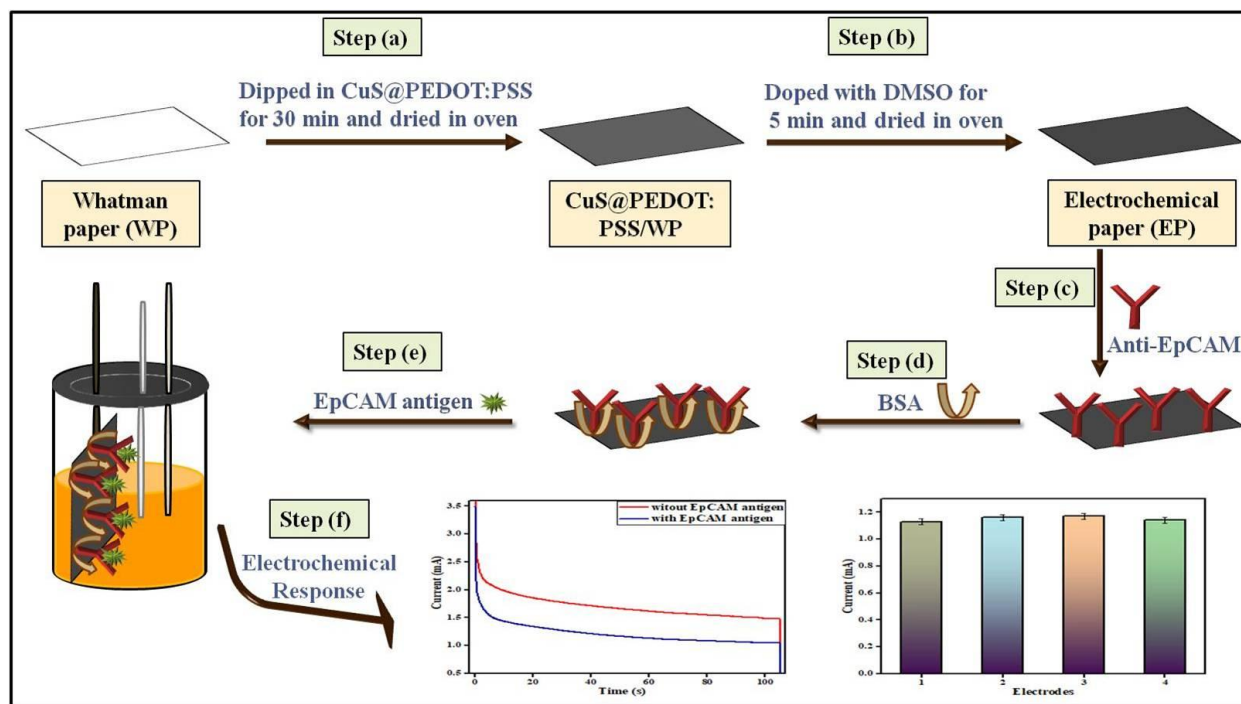


Fig. 6.1: Scheme showing the fabrication and mechanism of EP-based immunosensor

6.2 Experimental Section

6.2.1 Synthesis of CuS

A straightforward hydrothermal technique was used to prepare CuS [5]. Initially, 2.50 g of $\text{CuSO}_4 \cdot 5\text{H}_2\text{O}$ was dissolved in 80 mL of deionized water while constant stirring. In another beaker, 2.48 g of $\text{Na}_2\text{S}_2\text{O}_3 \cdot 5\text{H}_2\text{O}$ was mixed 20 mL of deionized water. To create a colloidal suspension, the prepared solutions were then gradually mixed. Next, this suspension is placed in an autoclave and heated to 180 °C for duration of 12 h. After the mixture has reached room temperature, it is centrifuged and cleaned using a 1:1 ratio of deionized water to ethanol. The final step is to vacuum dry the produced product at 60 °C.

6.2.2 Fabrication of PEDOT:PSS/WP and CuS@PEDOT:PSS/WP electrodes

Conducting paper electrodes were prepared by dip coating method [6]. Firstly, prepare the aqueous suspension of 20% PEDOT:PSS {poly(3,4-ethylenedioxythiophene):poly(styrenesulfonate)} (20 mL) and add 4 mg of CuS to the 10 mL of aforementioned suspension under constant stirring for 2 h in separate beaker. Then, stabilized Whatman paper (WP) was dipped into the above prepared solutions for 30 min and then dried in vacuum oven. This process was repeated three times to obtain the desired flexibility and stability of paper. After that, the CuS@PEDOT:PSS/WP electrode was doped with dimethyl sulfoxide (DMSO) and then vacuum dried. This fabricated paper is referred as electrochemical paper (EP).

6.2.3 Fabrication of Immunosensor

To fabricate Immunosensor, the surface of EP (1x1 cm) electrodes was immobilized with 20 μL of anti-EpCAM (40 $\mu\text{g}/\text{mL}$) by dropcasting method. After that, the Immunosensor has been incubated for 12 hours in a humid chamber. In addition, 1% BSA (20 μL) was applied to the anti-EpCAM/EP electrodes for a duration of 1 h in order to prevent non-specific antigen binding.

6.3 Results and discussion

6.3.1 Morphological characterization

SEM examination was used to determine the surface morphologies of various prepared electrodes and powdered CuS (**Fig. 6.2**). The SEM image of stabilized bare WP presents the fibrous structure of cellulose as shown in **Fig. 6.2A**. Further, the SEM micrograph of

PEDOT:PSS/WP clearly indicates the uniform adsorption of PEDOT:PSS onto the fibres of paper (**Fig. 6.2B**) [7]. An enlarged view of the polymer's smooth adsorption onto the WP is shown in **Fig. 6.2C**. The SEM image of CuS powder shows sphere like morphology along with some tubular structures (**Fig. 6.2D**). Moreover, CuS combined with PEDOT:PSS/WP exhibits the similar morphology, indicating the successful production of CuS@PEDOT:PSS/WP (**Fig. 6.2E**). The magnified image of CuS after incorporation onto the paper is shown in **Fig. 6.2F**.

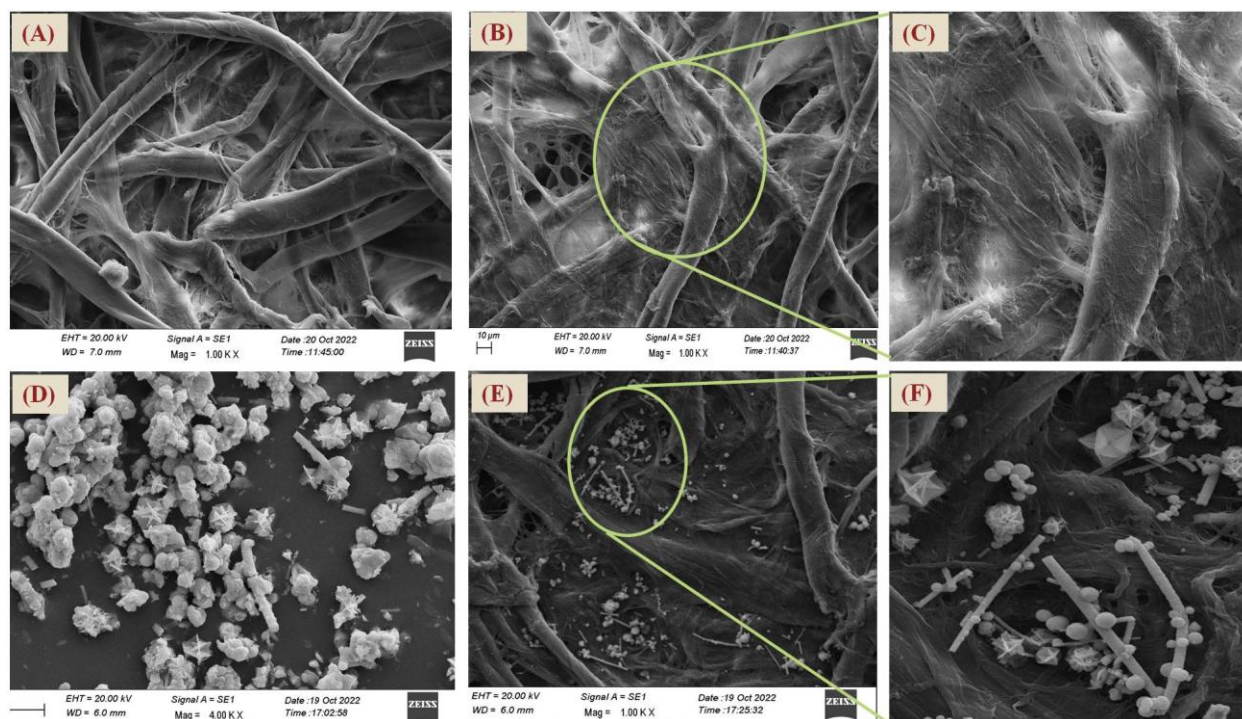


Fig. 6.2: SEM micrographs of (A) WP; (B) PEDOT:PSS/WP; (C) magnified image of PEDOT:PSS adsorption; (D) CuS powder; (E) CuS@PEDOT:PSS/WP and (F) magnified view of CuS structure incorporated into paper

6.3.2 Structural characterization

The XRD patterns for CuS powder and the fabricated electrodes are shown in **Fig. 6.3A**. Curve a represents the XRD spectra of PEDOT:PSS/WP, in which the characteristic peak of PEDOT:PSS is a broad peak that appears at $2\theta = 23^\circ$. Curve b depicts the XRD spectra of CuS@PEDOT:PSS/WP, the two primary peaks of CuS at 29.6° and 48.7° are seen in the diffraction pattern in addition to PEDOT:PSS peak at 23° . And curve c represents the XRD spectra of CuS powder. The peaks located at 27.2° , 27.9° , 29.5° , 32.0° , 32.9° , 48.2° , 52.9° and

59.6° confirms the successful synthesis of CuS [8]. These peaks match the standard CuS data (JCPDS No. 06-0464) well.

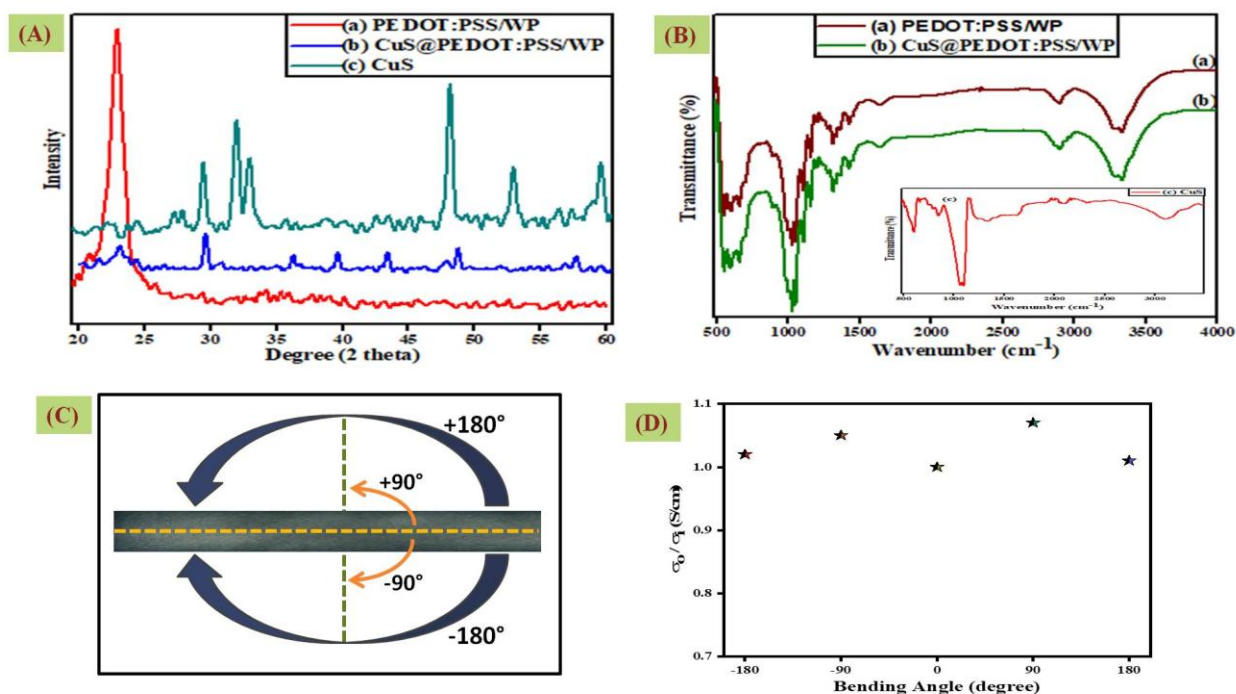


Fig. 6.3 (A) XRD and (B) FTIR spectra of PEDOT:PSS/WP (a), CuS@PEDOT:PSS/WP (b) and CuS powder (c); (C) Diagrammatic view of EP foldings and (D) Plot of relative conductivity vs. angle of bending

FTIR spectroscopy was used to evaluate the surface structures of the different produced electrodes, as illustrated in **Fig. 6.3B**. The symmetric and asymmetric stretching vibrations of the $-\text{SO}_3$ group in the PSS molecule are responsible for the bands seen at 1037 and 1110 cm^{-1} , respectively. The stretching vibrations of the C–S and C–O bonds found in PEDOT are responsible for the peaks that appear around 600 and 1317 cm^{-1} , respectively. The $-\text{OH}$ groups that have been adsorbed on the electrode surface are responsible for the broad absorption peak that appears at 3325 cm^{-1} . Since CuS is present in extremely small amount in the PEDOT:PSS suspension, CuS@PEDOT:PSS/WP (curve b) exhibits nearly identical FTIR spectra. However, CuS powder's FTIR spectrum is displayed. Conversely, the inset (curve c) displays the FTIR spectrum of CuS powder. The presence of a Cu–S bond is shown by the primary absorption peak, which appears at 600 cm^{-1} . The C–O stretching vibration of the ethanol absorbed during the washing process may be the cause of the bands seen at 1056 and 1091 cm^{-1} .

6.3.3 Flexibility study

Conducting paper electrodes were folded in a range of directions from -180° to $+180^\circ$ to determine their degree of flexibility (**Fig. 6.3C**). The downward and upward folding of the electrode is represented by negative and positive angles, respectively. The ratio of observed conductivity (σ_o) and initial conductivity (σ_i), also known as relative conductivity, were displayed against the folding angle (**Fig. 6.3D**). The graph shows the extremely slight conductivity fluctuation of up to 7% suggesting that the paper electrodes are flexible in nature. Moreover, after bending the electrochemical paper hundreds of times, a conductivity experiment is carried out. Conductivity is found to drop by just 13.5%, which could be because of tearing of cellulose fibres.

6.3.4 Electrical conductivity study

The electrical conductivity of the all the fabricated electrodes were calculated by using four point probe method. Additionally, the CuS@PEDOT:PSS/WP electrode was doped with various organic solvents including DMF, DMA, EG and DMSO, to enhance the electrochemical behavior. The conductivity of all modified electrodes have been determined and presented in **Table 6.1**. The electrode treated with DMSO is found to have the maximum conductivity (6.1×10^{-2} S/cm). Following DMSO treatment, there was a significant increase in conductivity, because the PEDOT:PSS structure was reoriented, which further improved the charge carrier mobility [9].

Table 6.1: Electrical Conductivity of all Modified Electrodes

S.No.	Electrodes	Conductivity (S/cm)
1	PEDOT:PSS/WP	2.3×10^{-3}
2	CuS@PEDOT:PSS/WP	8.0×10^{-3}
3	DMF doped CuS@PEDOT:PSS/WP	1.2×10^{-2}
4	DMA doped CuS@PEDOT:PSS/WP	2.6×10^{-2}
5	EG doped CuS@PEDOT:PSS/WP	3.4×10^{-2}
6	DMSO doped CuS@PEDOT:PSS/WP	6.1×10^{-2}

6.3.5 Electrochemical characterization

Using the chronoamperometry approach, all the prepared electrodes are characterized at a potential of 2V at intervals of 0.1 s, electrochemically. An electrochemical method called chronoamperometry measures current change over time in response to potential changes. **Fig. 6.4A** depicts that the CuS@PEDOT:PSS/WP doped with DMSO (EP) electrode shows the highest value of saturation current (2.62 mA). This is because the DMSO treatment eliminates the non-conducting PSS ions, thereby improving the rate at which electrons pass through the redox probe. Lastly, a blockage of the conducting area on the electrode surface occurs after immobilization of anti-EpCAM, which leads to the fall in current (1.57 mA, curve d).

6.3.6 Optimization studies

Several experimental parameters are tuned in order to enhance the performance of the proposed immunosensor. The electrolytic solution's pH has a significant influence on how well the immunosensor works. Thus, the BSA/anti-EpCAM/EP electrode was exposed to varying pH levels, and the chronoamperometric current response was taken (**Fig. 6.4B**). It was observed that in a 7.4 pH solution, the immunosensor exhibits the maximum current, hence found to be ideal for biosensing studies. For the effective detection of EpCAM antigen, the antigen's incubation period is another crucial factor. To check the efficient incubation time, 1 pg/mL of EpCAM antigen was incubated with BSA/anti-EpCAM/EP electrode, and chronoamperometric response was recorded from 2 to 10 min (**Fig. 6.4C**). A plateau is attained after current drop upto 6 min, signifying the end of the reaction.

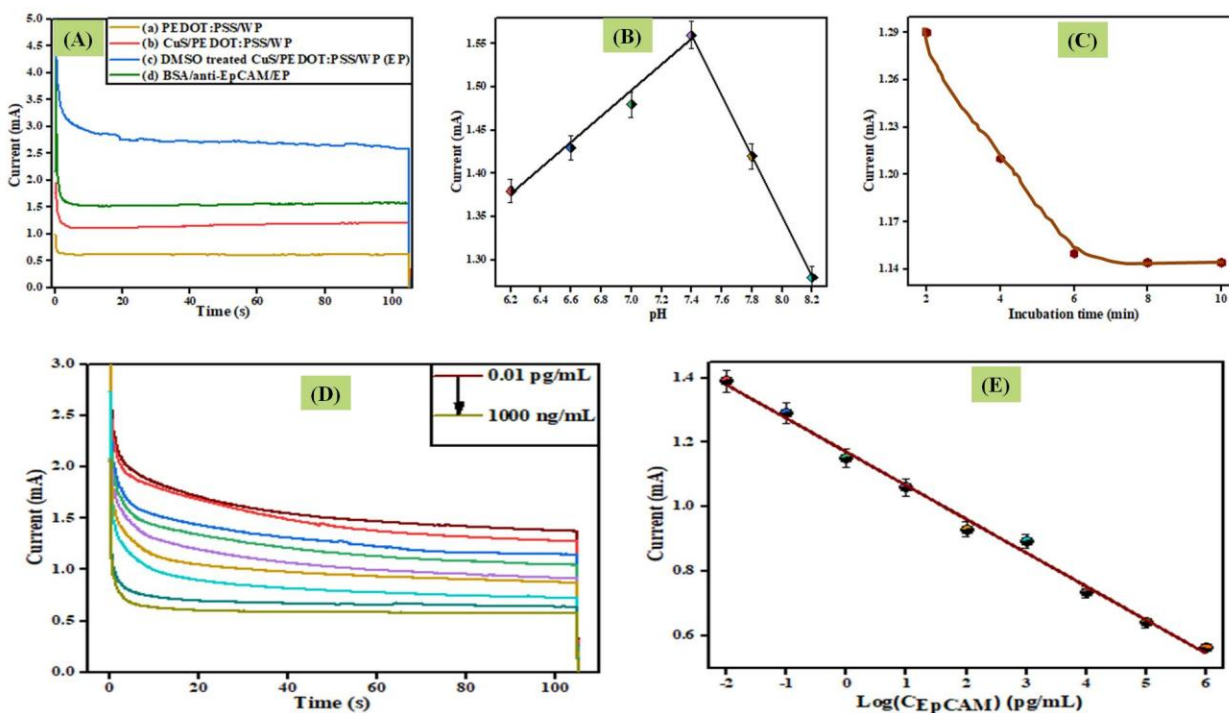


Fig. 6.4 (A) Chronoamperometry curves of (a) PEDOT:PSS/WP, (b) CuS@PEDOT:PSS/WP, (c) EP and (d) BSA/anti-EpCAM/EP; (B) Optimization of effect of pH; (C) Optimization of time of incubation of EpCAM antigen; (D) Electrochemical response study of BSA/anti-EpCAM/EP electrode after incubation of different EpCAM antigen concentrations (0.01 pg/mL to 1000 ng/mL) and (E) Linearity plot of current vs. $\log C_{\text{EpCAM}}$

6.3.7 Electrochemical immunosensing studies

The immunosensing performance was examined as a function of increasing concentration of EpCAM antigen (0.01 pg/mL to 1000 ng/mL) towards BSA/anti-EpCAM/EP electrode (**Fig. 6.4D**). Due to the blockage of the conducting region onto the bioelectrode surface caused by the development of an antigen-antibody immunocomplex, the saturated current decrease with increasing EpCAM antigen concentration. The calibration plot for saturated current vs. \log of EpCAM concentration is shown in **Fig. 6.4E** and follows the following regression equation:

$$\text{Current } (\mu\text{A}) = 1170 \mu\text{A} - 104.31 \mu\text{A}/(\text{pg/mL}) \times \log(C_{\text{EpCAM}}); R^2 = 0.99 \quad (6.1)$$

Using the above equation, the LOD and sensitivity for this biosensor are determined to be 104.31 $\mu\text{A}/(\text{pg/mL})$ and 0.01 pg/mL, respectively.

Conducting paper has several advantages over more expensive glass-based electrodes, the primary one being that it is biodegradable and may be disposed of simply by burning [10]. When

the resulting ash was subjected to the energy dispersive X-ray (EDX) analysis, the primary peaks of carbon and oxygen were appeared as shown in **Fig. 6.5**. In addition, trace amounts of calcium, phosphorus, iron, potassium, and sulfur are found. The low-cost biodegradable platform for point-of-care detection is confirmed by the absence of any harmful elements in the ash.

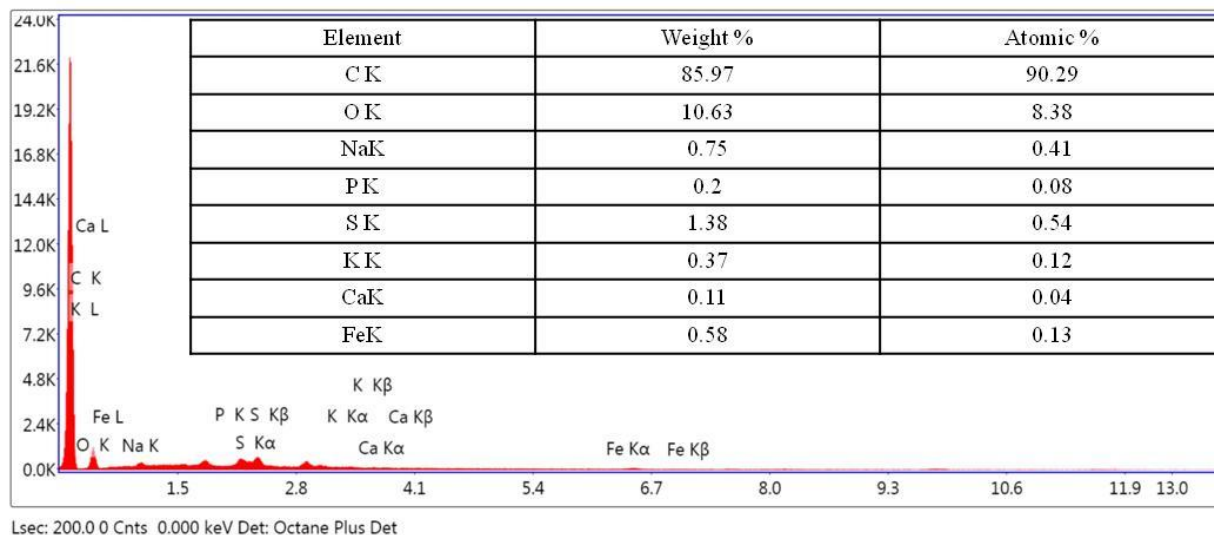


Fig. 6.5 Energy dispersive X-ray (EDX) analysis of ash

6.3.8 Interference, reproducibility and stability studies

The selectivity of fabricated Immunosensor was studied in the presence of different analytes including glucose, NaCl and ascorbic acid (10 pg/mL each) (**Fig. 6.6A**). When comparing the chronoamperometry response to EpCAM antigen (1 pg/mL), there is no significant change in current. Additionally, the immunosensor's specificity is evaluated by measuring the current response when a mixture of interferents containing EpCAM antigen is present. An observed decrease in electrochemical current validates the developed immunosensor's specificity.

Further, to check reproducibility of developed Immunosensor, chronoamperometry response of four distinct BSA/anti-EpCAM/EP electrodes was analyzed as shown in **Fig. 6.6B**. The results indicates that the electrode's saturated current differs a very little with RSD of ~1.59 %.

Lastly, for the purpose of EpCAM antigen detection (1 pg/mL), the immunosensor's storage stability was assessed at regular intervals of 5 days for 30 days (**Fig. 6.6C**). When maintained at 4 °C, it has been observed that the BSA/anti-EpCAM/EP electrode maintains 75% activity even after 30 days.

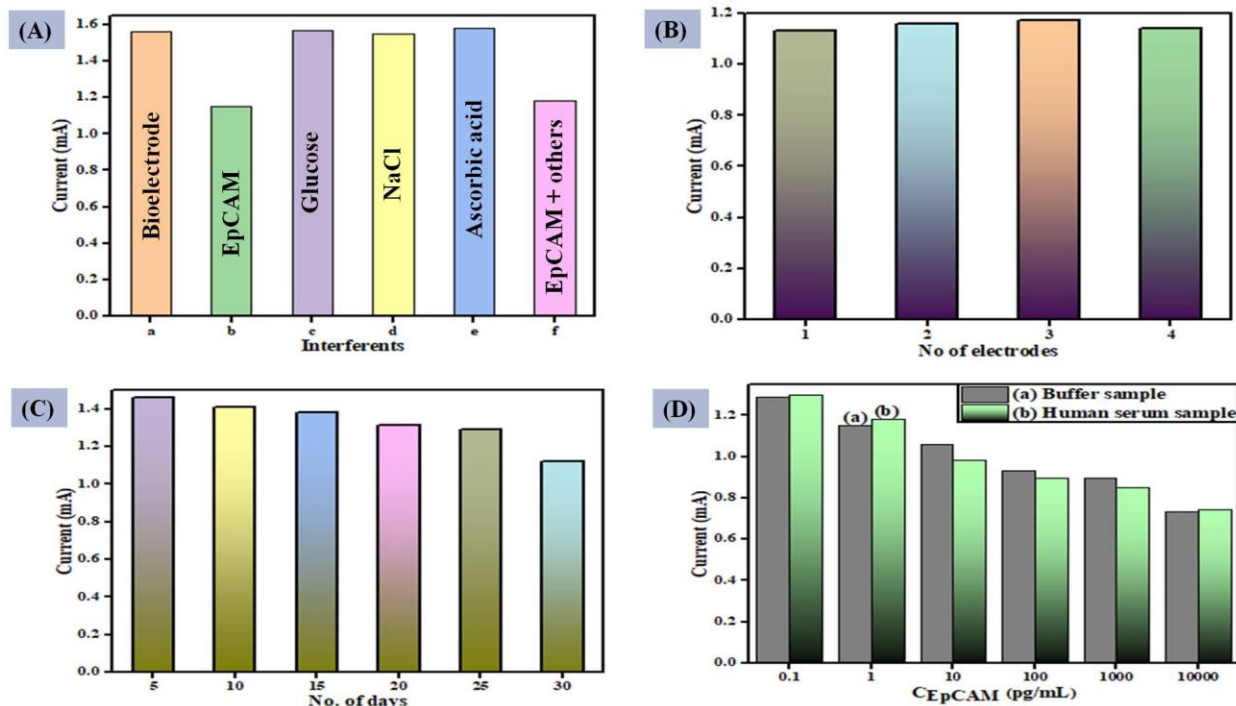


Fig. 6.6 (A) Interference data of BSA/anti-EpCAM/EP electrode in the presence of different analytes (10 pg/mL); (B) Reproducibility data of immunosensor; (C) Stability study of BSA/anti-EpCAM/EP electrode; and (D) Saturated current of immunosensor in buffer (a) and spiked serum sample (b)

6.3.9 Human serum analysis

The precision and applicability of developed immunosensor were analyzed by taking response in the presence of spiked human serum sample. The serum sample was first diluted ten times with 7.4 pH PBS, and then spiked with various EpCAM antigen concentrations (0.1, 1, 10, 100, 1000, and 10,000 pg/mL). The current response has been recorded, and the results showed that the difference between the current of the spiked serum sample and the buffer is very small (**Fig. 6.6D**). **Table 6.2** records the recovery, concentration, and resulting standard deviation of the corresponding data, demonstrating the immunosensor's validation and viability for EpCAM detection in people.

Table 6.2: Detection of biomarker in spiked serum using BSA/anti-EpCAM/EP electrode

S.No	Approximate added EpCAM concentration (pg/mL)	Approximate found EpCAM concentration (pg/mL)	Recovery (%)	RSD (%)
1	0.1	0.09	99.23	0.546
2	1	0.97	97.46	1.821
3	10	10.85	108.50	5.474
4	100	103.97	103.97	2.715
5	1000	1052.81	105.28	3.572
6	10000	9867.00	98.67	0.956

6.4 Conclusion

This chapter presents the fabrication of an electrochemical paper-based immunosensor for the efficient detection of EpCAM antigen. This immunosensor utilizes a sensing platform composed of CuS and PEDOT:PSS-modified conducting paper. Various experimental studies proved that the fabricated platform exhibits excellent electrical conductivity, flexibility and biodegradability. Further, the immunosensing studies of BSA/anti-EpCAM/CuS@PEDOT:PSS electrode confirmed a broad linear range (0.01 pg/mL to 1000 ng/mL) and a high sensitivity {104.31 μ A/(pg/mL)} for EpCAM antigen detection. Additionally, it was investigated that the immunosensor has a 30 days long stability period.

The results presented in this chapter have been published in "Materials Chemistry and Physics" 313 (2023) 128687.

References:

- [1] S. Kumar, M. Umar, A. Saifi, S. Kumar, S. Augustine, S. Srivastava, B.D. Malhotra, Electrochemical paper based cancer biosensor using iron oxide nanoparticles decorated PEDOT: PSS, *Analytica Chimica Acta* 1056 (2019) 135-145.
- [2] S. Kumar, M. Willander, J.G. Sharma, B.D. Malhotra, A solution processed carbon nanotube modified conducting paper sensor for cancer detection, *Journal of Materials Chemistry B* 3 (2015) 9305-9314.
- [3] J. Fang, P. Zhang, H. Chang, X. Wang, Hydrothermal synthesis of nanostructured CuS for broadband efficient optical absorption and high-performance photo-thermal conversion, *Solar Energy Materials and Solar Cells* 185 (2018) 456-463.
- [4] S. Paneru, Sweety, D. Kumar, CuO@PEDOT: PSS-grafted paper-based electrochemical biosensor for paraoxon-ethyl detection, *Journal of Applied Electrochemistry* 53 (2023) 2229-2238.
- [5] S. Kumar, S. Kumar, S. Srivastava, B.K. Yadav, S.H. Lee, J.G. Sharma, D.C. Doval, B.D. Malhotra, Reduced graphene oxide modified smart conducting paper for cancer biosensor, *Biosensors and Bioelectronics* 73 (2015) 114-122.
- [6] K. Singh, A. Ohlan, P. Saini, S. Dhawan, Poly (3, 4-ethylenedioxythiophene) γ -Fe₂O₃ polymer composite—super paramagnetic behavior and variable range hopping 1D conduction mechanism—synthesis and characterization, *Polymers for Advanced Technologies* 19 (2008) 229-236.
- [7] Z. Li, L. Mi, W. Chen, H. Hou, C. Liu, H. Wang, Z. Zheng, C. Shen, Three-dimensional CuS hierarchical architectures as recyclable catalysts for dye decolorization, *CrystEngComm* 14 (2012) 3965-3971.
- [8] L. Pei, J. Wang, X. Tao, S. Wang, Y. Dong, C. Fan, Q.-F. Zhang, Synthesis of CuS and Cu₁.1Fe₁.1S₂ crystals and their electrochemical properties, *Materials Characterization* 62 (2011) 354-359.
- [9] T.-R. Chou, S.-H. Chen, Y.-T. Chiang, Y.-T. Lin, C.-Y. Chao, Highly conductive PEDOT: PSS films by post-treatment with dimethyl sulfoxide for ITO-free liquid crystal display, *Journal of Materials Chemistry C* 3 (2015) 3760-3766.
- [10] S. Kumar, P. Rai, J.G. Sharma, A. Sharma, B.D. Malhotra, PEDOT: PSS/PVA-Nanofibers-Decorated Conducting Paper for Cancer Diagnostics, *Advanced Materials Technologies* 1 (2016) 1600056.

CHAPTER 7

Ag@Ti₃C₂T_x-MODIFIED CONDUCTING PAPER-BASED ELECTROCHEMICAL IMMUNOSENSOR FOR EpCAM DETECTION

7.1 Introduction

In this chapter, a highly bendable Whatman paper-based immunosensor has been developed for the highly sensitive and real time detection of EpCAM antigen. A novel Ag@Ti₃C₂T_x hybrid material is being used with aqueous PEDOT:PSS solution to enhance the numerous electrochemical parameters, viz, conductivity, hydrophilicity, stability etc [1]. The electrode fabrication has been achieved by simple dip-coating method. All the characterizations and biosensing parameters have been examined and reported in the following sections.

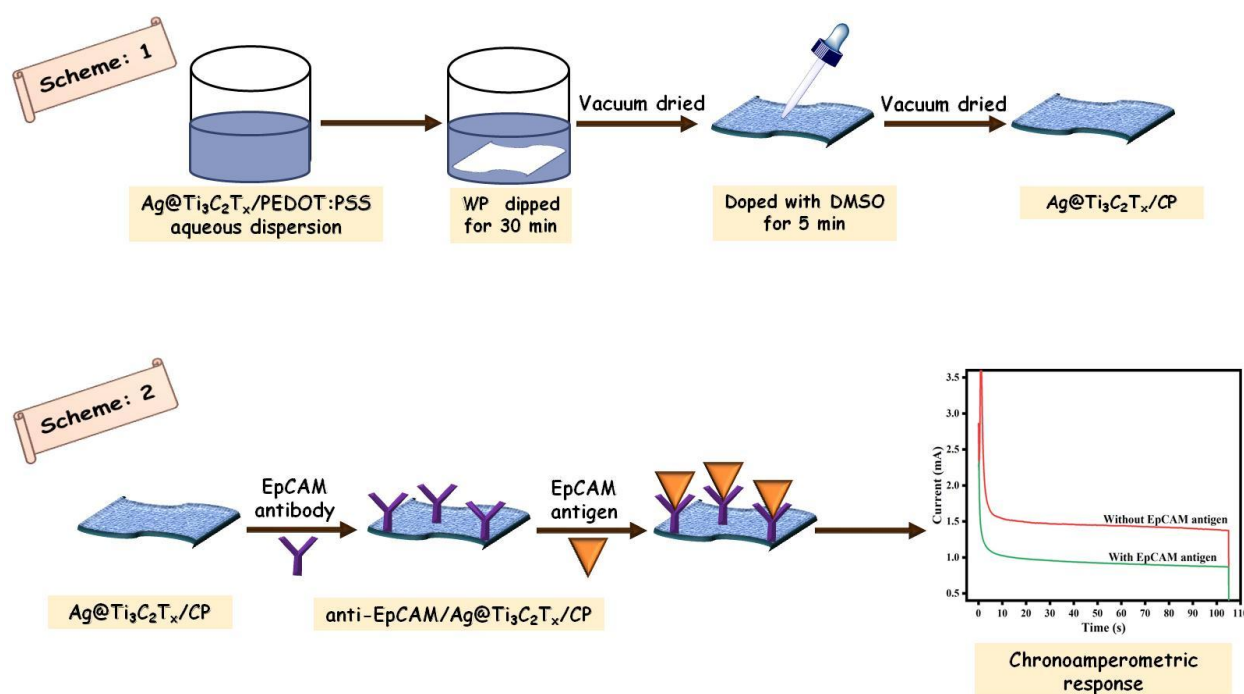


Fig. 7.1: Scheme depicting the fabrication of Ag@Ti₃C₂T_x/CP-based immunosensor

7.2 Experimental section

7.2.1 Synthesis of $Ti_3C_2T_x$ & Ag/ $Ti_3C_2T_x$ hybrid

Though, a synthesis of $Ti_3C_2T_x$ is reported earlier in the chapter 3 of the thesis. Further, Ag particles have been doped onto the $Ti_3C_2T_x$ sheets by one pot method by the direct reduction of $AgNO_3$ salt. This procedure involves the dual action of $Ti_3C_2T_x$ sheets as a self reducing agent as well as a matrix of support for Ag particles. Initially, 100 mg of $Ti_3C_2T_x$ has been dissolved in 20 mL of distilled water under ultrasonication to prepare 5mg/mL stock solution. In another beaker, 33.98 mg of $AgNO_3$ has been dispersed in 20 mL of distilled water under constant stirring. After that the stock solution of $Ti_3C_2T_x$ has been added dropwise to the beaker containing $AgNO_3$ with constant stirring for 60 min. The resulting suspension has been washed with DI water multiple times for the removal of impurities under ultracentrifugation. The obtained solid was dried in vacuum oven to obtain Ag/ $Ti_3C_2T_x$ hybrid [2].

7.2.2 Fabrication of PEDOT:PSS/WP (CP), $Ti_3C_2T_x$ /CP and Ag/ $Ti_3C_2T_x$ /CP electrodes

In order to fabricate the conducting paper electrodes (CP), Whatman paper (WP) made up of cellulose fibres was chosen as a transducer surface because of its biocompatibility and hydrophilicity [3]. Firstly, 20% PEDOT:PSS stock solution has been prepared in DI water. An optimal amount of 5 mg of each $Ti_3C_2T_x$ and Ag/ $Ti_3C_2T_x$ hybrid have been dissolved in 10 mL of stock solution in two separate beakers under constant stirring for 2h. The stabilized WP (1×3 cm) strips have been dipped in all aforementioned solutions separately for 30 min and then vacuum dried. This process has been repeated thrice to obtain better electrical characteristics and mechanical strength. This layer by layer stacking process ensures the formation of uniform and conductive layer of PEDOT:PSS on WP surface. Nevertheless, the PSS dopant increases the durability and processability of the polymer but decreases the electrical conductivity, thereby making high-performance applications inappropriate. To improve conductivity, the modified Ag/ $Ti_3C_2T_x$ /CP electrodes were doped with different concentrations of dimethyl sulfoxide (DMSO) for 5 min. It has been observed that the 50% V/V DMSO doped electrode has the highest electrical conductivity among all.

7.2.3 Biofunctionalization of DMSO treated Ag/ $Ti_3C_2T_x$ /CP electrode

The immobilization of anti-EpCAM has been achieved by physical adsorption. For that process, a 1:1:2 solution containing EDC, NHS and anti-EpCAM (25 μ g/mL) has been prepared in an

Eppendorf tube. Thereafter, DMSO treated Ag/Ti₃C₂T_x/CP electrode was drop-casted with 25 μ L of this active solution, and it was incubated for 6 h at 4 $^{\circ}$ C. Finally, the anti-EpCAM/Ag/Ti₃C₂T_x/CP electrode has been washed with PBS (at pH 7.4) to get rid of unimmobilized antibody that was stuck to the surface of electrode.

7.3 Results & discussion

7.3.1 Morphological characterization

SEM technique is used to determine the surface morphologies of sequential stages of various electrodes prepared in this work which are shown in **Fig. 7.2**. The cellulose fibres of stabilized WP has been uniformly covered by PEDOT:PSS as shown in the SEM image of PEDOT:PSS/WP (CP) (**Fig. 7.2A**) [4]. The SEM image of Ti₃C₂T_x/CP electrode (**Fig. 7.2B**) depicts the incorporation of 2D-Ti₃C₂T_x sheets into the polymer matrix. The SEM analysis of powder Ag/Ti₃C₂T_x (**Fig. 7.2C**) depicts the smooth dispersion of Ag particles onto the layered Ti₃C₂T_x sheets. Similar morphology is being observed when Ag/Ti₃C₂T_x has been incorporated into the CP as shown in **Fig. 7.2D**.

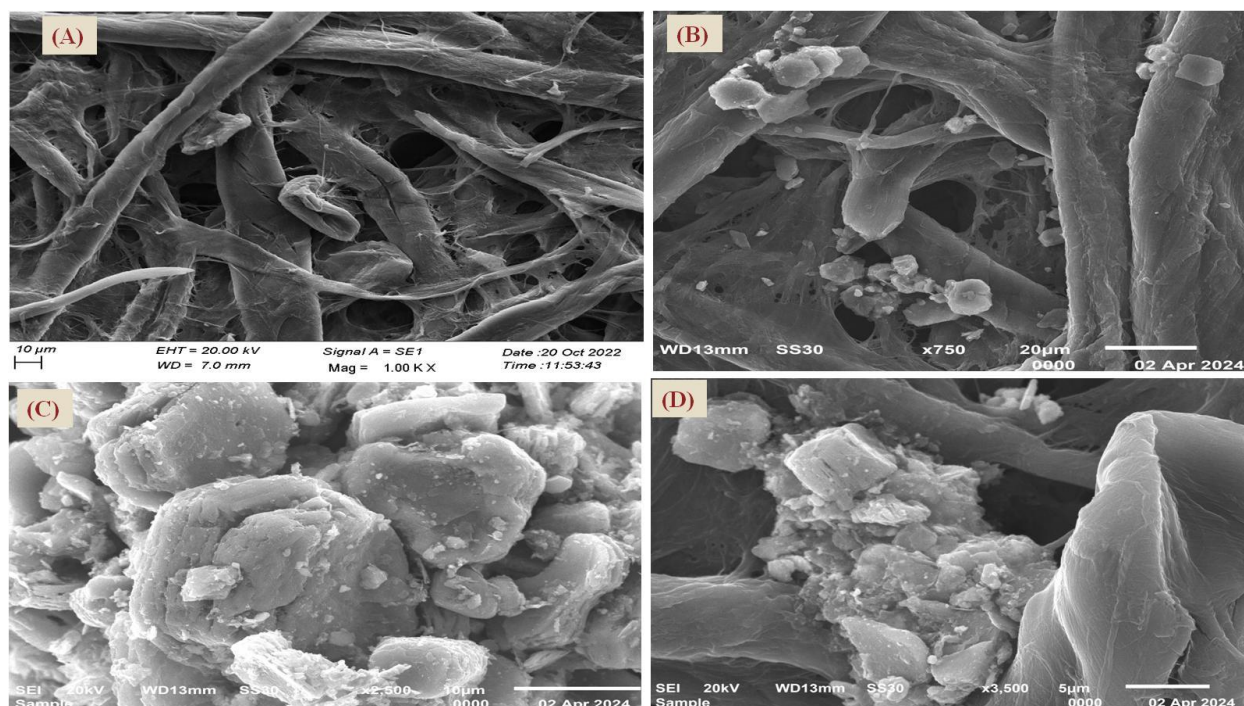


Fig. 7.2: SEM micrographs of (A) PEDOT:PSS/WP (B) Ti₃C₂T_x/CP (C) Ag/Ti₃C₂T_x powder and (D) Ag/Ti₃C₂T_x/CP

7.3.2 Structural characterization

XRD spectroscopy is exploited to analyze the phase purity and crystallinity of MXene derived from MAX phase (**Fig. 7.3A**). It has been observed that the MAX phase disappears completely after hydrothermal etching, as evident by the absence of Al peak at $2\theta = 39.1^\circ$ in curve b and c. The characteristic peak (002) of Ti_3AlC_2 ($2\theta = 9.6^\circ$) has been shifted to a broad peak at 6.4° in $\text{Ti}_3\text{C}_2\text{T}_x$ and $\text{Ag}/\text{Ti}_3\text{C}_2\text{T}_x$ suggesting a drastic loss in the crystallinity. In curve c, the additional peaks of Ag positioned at 38.4° , 44.5° , 64.7° and 77.5° , further confirm the incorporation of Ag particles into the $\text{Ti}_3\text{C}_2\text{T}_x$ sheets [5].

The surface structure and modification of $\text{Ti}_3\text{C}_2\text{T}_x$ and $\text{Ag}/\text{Ti}_3\text{C}_2\text{T}_x$ has been described by FTIR spectroscopy ranging from 400 to 4000 cm^{-1} (**Fig. 7.3B**). The peak observed at 2975 cm^{-1} is due to the stretching vibrations of C–H bond, while the peaks appeared around 1738, 1374, and 1055 cm^{-1} are attributed to the stretching vibrations of C=O, O–H, and C–F bonds [6]. Hence, the presence of –OH and –F groups has been confirmed as surface modifications in $\text{Ti}_3\text{C}_2\text{T}_x$. The additional peaks appeared around 611 and 563 cm^{-1} ascribed to the Ti–O and Ti–C stretching vibrations, respectively. In curve b, the intensity of Ti–O and Ti–C peaks decreases which may be due to the incorporation of Ag particles into the $\text{Ti}_3\text{C}_2\text{T}_x$ sheets. In the FTIR spectra of $\text{Ag}/\text{Ti}_3\text{C}_2\text{T}_x/\text{PEDOT:PSS}/\text{WP}$, the additional peaks appeared at 1044 and 1160 cm^{-1} are owing the presence of – SO_3 group (symmetric and asymmetric stretching vibrations) in PSS molecules.

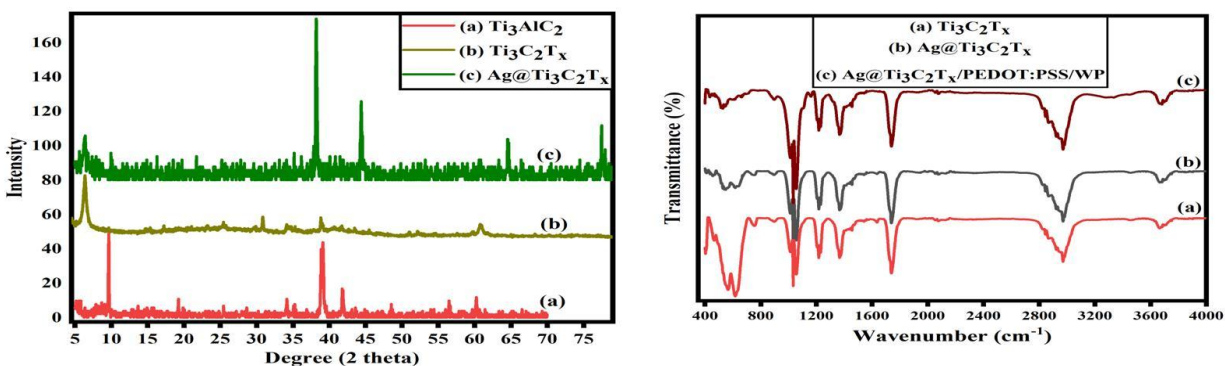


Fig. 7.3 (A) XRD curves of Ti_3AlC_2 (a), $\text{Ti}_3\text{C}_2\text{T}_x$, (b) and $\text{Ag}/\text{Ti}_3\text{C}_2\text{T}_x$ (c); (B) FTIR spectra of $\text{Ti}_3\text{C}_2\text{T}_x$ (a), $\text{Ag}/\text{Ti}_3\text{C}_2\text{T}_x$ (b) and $\text{Ag}/\text{Ti}_3\text{C}_2\text{T}_x/\text{CP}$ (c)

7.3.3 Electrical conductivity and flexibility study

By utilizing a four-probe technique, conductivity measurement tests have been performed to find the conductivity of the different fabricated paper electrodes and the data are reported in **Table 7.1**. Conductivity has been measured to be 2.5×10^{-3} , 7.6×10^{-3} and 10.9×10^{-3} S/cm for PEDOT:PSS/WP (CP), $\text{Ti}_3\text{C}_2\text{T}_x/\text{CP}$ and $\text{Ag}/\text{Ti}_3\text{C}_2\text{T}_x/\text{CP}$ electrodes, respectively. Further considering the effect of organic solvent like DMSO has been studied to improve the electrochemical parameters of $\text{Ag}/\text{Ti}_3\text{C}_2\text{T}_x/\text{CP}$ electrode. It is reported that the DMSO treatment causes the rearrangement in the PEDOT:PSS structure, which further enhances the mobility of charge carriers and resulting in higher conductivity. In addition, DMSO forms a bond with PEDOT and at the same time, PSS is removed with distilled water, resulting in an increase in conductivity [7]. The $\text{Ag}/\text{Ti}_3\text{C}_2\text{T}_x/\text{CP}$ electrode has been optimized with different concentrations of aqueous DMSO such as 25%, 50%, 75% and 100% (V/V). It was found that 50% DMSO treated $\text{Ag}/\text{Ti}_3\text{C}_2\text{T}_x/\text{CP}$ electrode possesses the conductivity (763.5×10^{-3} S/cm) around 70 times higher.

Table 7.1: The electrical conductivity data of different modified electrodes

S. No.	Modified Electrodes	Conductivity (S/cm)
1	PEDOT:PSS/WP (CP)	2.3×10^{-3}
2	$\text{Ti}_3\text{C}_2\text{T}_x/\text{CP}$	7.6×10^{-3}
3	$\text{Ag}@/\text{Ti}_3\text{C}_2\text{T}_x/\text{CP}$	10.9×10^{-3}
4	25% DMSO treated $\text{Ag}@/\text{Ti}_3\text{C}_2\text{T}_x/\text{CP}$	498.2×10^{-3}
5	50% DMSO treated $\text{Ag}@/\text{Ti}_3\text{C}_2\text{T}_x/\text{CP}$	763.5×10^{-3}
6	75% DMSO treated $\text{Ag}@/\text{Ti}_3\text{C}_2\text{T}_x/\text{CP}$	509.1×10^{-3}
7	100% DMSO treated $\text{Ag}@/\text{Ti}_3\text{C}_2\text{T}_x/\text{CP}$	445.5×10^{-3}

Additionally, the flexibility of fabricated electrode has been investigated by folding it at the various angles, ranging from -180° to $+180^\circ$ (-ve and +ve signs show the downward and upward fold) as shown in **Fig. 7.4A**. This electrode was folded at different angles for the first time, but the conductivity did not alter noticeably. A plot of relative conductivity against angle of bending

is shown in **Fig. 7.4B**. A minimal change in conductivity was observed upon folding the electrode at different angles. Furthermore, it is worth important to mention that this low-cost and flexible paper based immunosensor can be easily discarded by incineration [8] and thus disposal is easy. The paper-based sensor can be easily burned in about 10s without producing harmful smoke or toxic gases into the atmosphere.

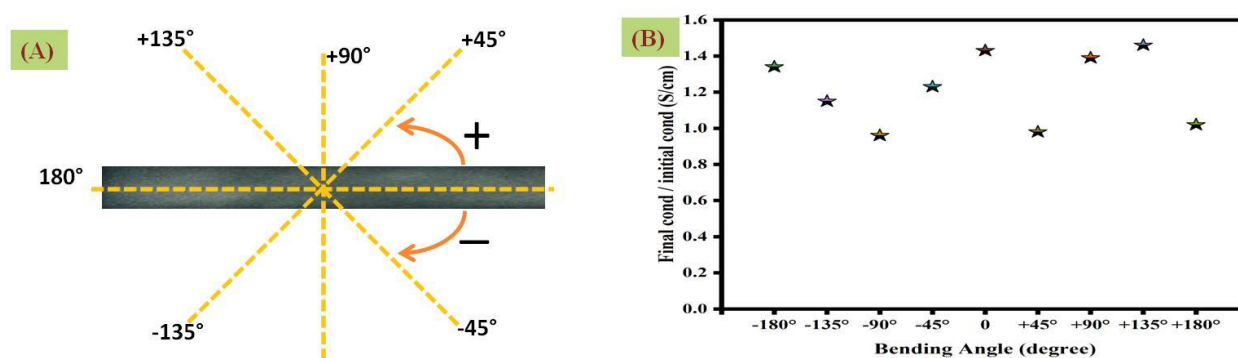


Fig. 7.4: (A) Pictorial view of conducting paper folding at various angles and (B) A plot of the conductivity change (final/initial) against the bending angle

7.3.4 Electrochemical characterization

The electrochemical behaviour analysis of different electrodes has been carried out by using the chronoamperometry technique at an applied potential of 0.2 V with 0.1 s time interval in a 0.2 M PBS (at 6.5 pH) containing 5 mM $[\text{Fe}(\text{CN})_6]^{3-/4-}$. Electrochemical response for all the fabricated electrodes has been recorded under the identical conditions (**Fig. 7.5A**). It was observed that the DMSO treated $\text{Ag}/\text{Ti}_3\text{C}_2\text{T}_x/\text{CP}$ electrode has the highest value of saturation current (2.95×10^{-3} mA) in comparison to $\text{Ag}@/\text{Ti}_3\text{C}_2\text{T}_x/\text{CP}$ (2.09×10^{-3} mA), $\text{Ti}_3\text{C}_2\text{T}_x/\text{CP}$ (1.77×10^{-3} mA) and CP (1.14×10^{-3} mA). The increase in current is due to the incorporation of highly conducting Ag particles that works in a synergistic manner with $\text{Ti}_3\text{C}_2\text{T}_x$. Hence, the $\text{Ag}@/\text{Ti}_3\text{C}_2\text{T}_x/\text{CP}$ electrode is more conducting due to the increase in the effective surface area.

The response time study was performed on the fabricated immunosensor, anti-EpCAM/ $\text{Ag}@/\text{Ti}_3\text{C}_2\text{T}_x/\text{CP}$ to optimize the time required for the completion of anti-EpCAM and EpCAM antigen reaction. For that purpose, anti-EpCAM/ $\text{Ag}@/\text{Ti}_3\text{C}_2\text{T}_x/\text{CP}$ electrode was incubated with EpCAM antigen (50 fg/mL) for 12 min (**Fig. 7.5B**). The saturation current was measured after every 2 min and it was found that the current decreases upto 8 min and then a

stage of saturation was reached. Hence, it was considered as the optimal time for all biosensing studies.

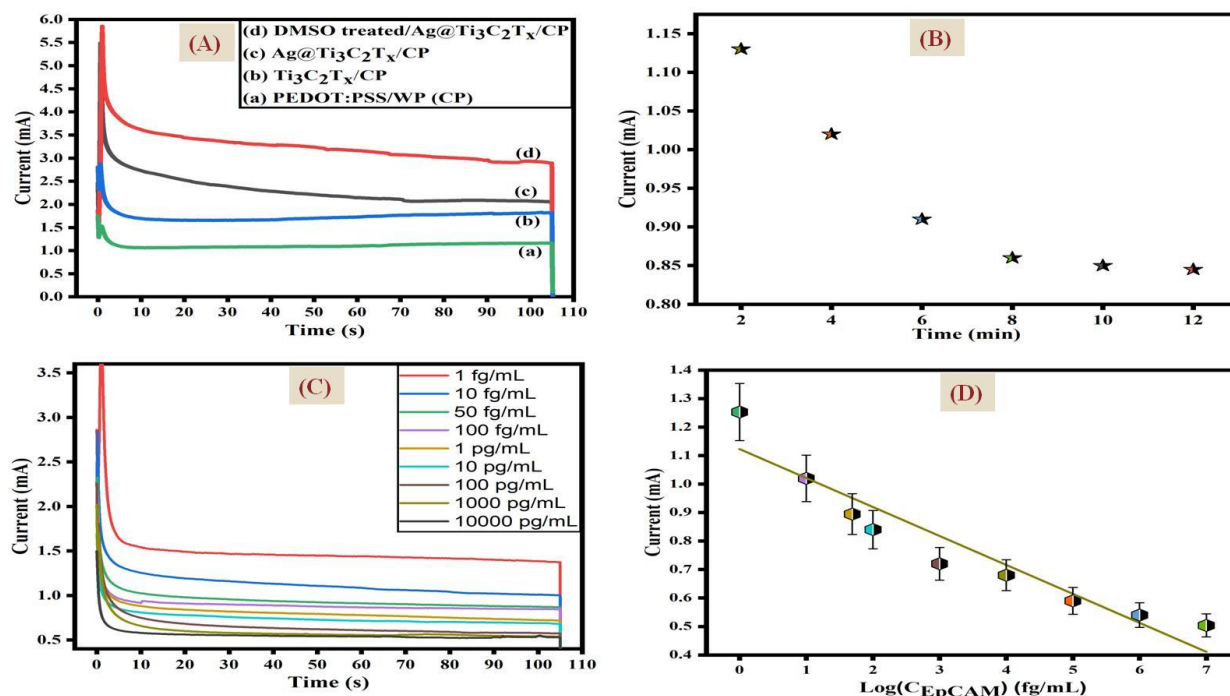


Fig. 7.5: (A) Chronoamperometric plot of CP (a), Ti₃C₂T_x/CP (b), Ag/Ti₃C₂T_x/CP (c), and DMSO treated Ag/Ti₃C₂T_x/CP (d); (B) Optimization for incubation time of EpCAM antigen; (C) Electrochemical response of anti-EpCAM/Ag/Ti₃C₂T_x/CP against different EpCAM antigen concentrations (1 fg/mL – 10000 pg/mL) and (D) Calibration plot of current against log (EpCAM antigen, fg/mL)

7.3.5 Electrochemical response studies

The response study was performed on the fabricated immunosensor, anti-EpCAM/Ag@Ti₃C₂T_x/CP as a function of change in concentration of EpCAM antigen (1 fg/mL – 10000 pg/mL) in 0.2 M PBS solution at 6.5 pH containing 5 mM [Fe(CN)₆]^{3-/4-}. After adding 20 μL of various antigen concentrations, it was found that the current decreases with each addition of EpCAM antigen which is clearly seen in **Fig. 7.5C**. The formation of an immunocomplex on the surface of anti-EpCAM/Ag@Ti₃C₂T_x/CP electrode which results in a decline of rate of electron transfer process, probably due to the blockage of active area on the surface of electrode. The magnitude of current and log of EpCAM antigen concentration shows a linear relationship (**Fig. 7.5D**), as represented by the following regression equation.

$$\text{Current} = -101.66 \mu\text{A} / (\text{fg} \cdot \text{mL}^{-1}) \times \log (C_{\text{EpCAM}}) + 1.12 \text{ mA}; R^2 = 0.88 \quad (7.1)$$

The sensitivity of anti-EpCAM/Ag@Ti₃C₂T_x/CP electrode was estimated from slope analysis and calculated as 44.12 $\mu\text{A} \cdot \text{fg}^{-1} \cdot \text{mL}$ with the detection limit of 0.8 fg/mL.

7.3.6 Real sample studies

The anti-EpCAM/Ag@Ti₃C₂T_x/CP electrode was utilized to examine a serum sample in order to verify the efficacy of fabricated immunosensor. Prior to being spiked with various concentrations of EpCAM antigen (10, 100, 1000, and 10,000 fg/mL), the serum sample was first diluted with PBS (pH = 7.4). The electrochemical data obtained from chronoamperometric response show a good correlation between the saturated current obtained from (a) spiked serum sample and (b) reference buffer sample as given in **Fig. 7.6A** and the data reported in **Table 7.2**. This biosensing platform shows an excellent precision, with an average percentage RSD of less than 2.22%.

Table 7.2: EpCAM detection in serum sample by anti-EpCAM/Ag@Ti₃C₂T_x/CP electrode

S.No.	Approximate added EpCAM (fg/mL)	Approximate found EpCAM (fg/mL)	Recovery (%)	RSD (%)
1	10	9.7	97.17	2.03
2	100	101.8	101.80	1.27
3	1000	991.9	99.19	0.57
4	10000	9691.2	96.91	2.22

7.3.7 Specificity, repeatability and stability studies

Interference test was conducted by using the chronoamperometry approach to investigate the impact of biomolecule like glucose, NaCl, urea and ascorbic acid that are present in the human on the sensing parameters. These results are shown in **Fig. 7.6B**. After adding these interferents (having concentration 50 fg/mL), there was no appreciable change in the electrochemical current in comparison to EpCAM antigen. The anti-EpCAM/Ag@Ti₃C₂T_x/CP electrode, on the other hand, exhibits a notable shift in electrochemical current response with the mixture of all the analytes containing EpCAM antigen. Hence, this immunosensor has been found highly specific and selective for EpCAM antigen detection.

For repeatability study, the chronoamperometry response of the fabricated immunosensor was recorded five times with each concentration of EpCAM antigen, i.e., 10 fg/ml (low), 1 pg/ml (medium), and 1000 pg/ml (high), as depicted in **Fig. 7.6C**. With respect to 10 fg/ml, 1 pg/ml, and 1 ng/ml EpCAM antigen, %RSD values for anti-EpCAM/Ag@Ti₃C₂T_x/CP electrode are reported as 4.95%, 4.01%, and 4.26%, respectively. Low values of relative standard deviations represent that the developed immunosensor exhibits an excellent repeatability and reproducibility.

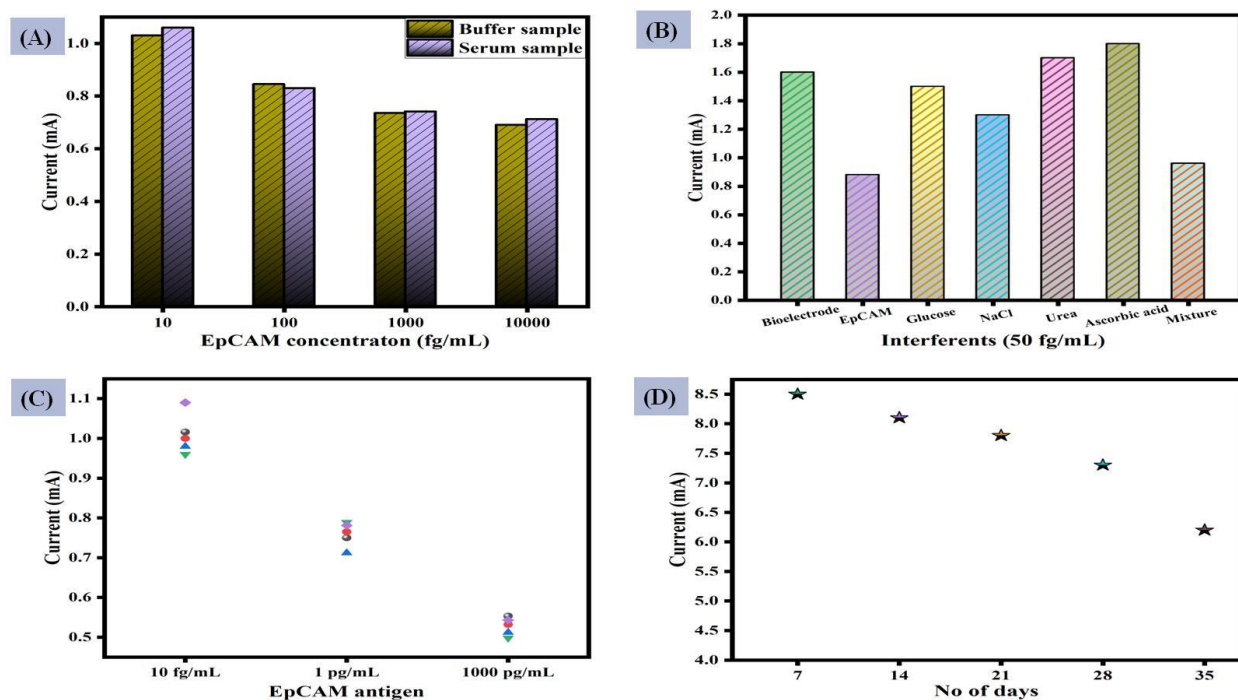


Fig. 7.6: (A) Chronoamperometric saturated current comparison of anti-EpCAM/Ag/Ti₃C₂T_x/CP electrode for EpCAM antigen in buffer and serum sample; (B) Interference study of anti-EpCAM/Ag/Ti₃C₂T_x/CP electrode with various analytes (glucose, NaCl, urea and ascorbic acid); (C) Repeatability study of three different anti-EpCAM/Ag/Ti₃C₂T_x/CP electrodes; (D) Shelf life study of immunosensor

Additionally, the shelf life of the anti-EpCAM/Ag@Ti₃C₂T_x/CP electrode has been assessed up to 35 days at the intervals of 7 days, in the presence of 50 fg/mL EpCAM antigen as depicted in **Fig.7.6D**. These findings show that the immunosensor maintained 84% of the current response up to 28 days. After that the saturated current was declined to 71% of initial value. This stability

is noticeably better than our previous reported immunosensor, BSA/anti-EpCAM/EP, which has a 28-day shelf life.

7.4 Conclusion

This chapter presents the successful invention of an inexpensive, portable, highly stable conducting paper-based immunosensor by using the Ag@Ti₃C₂T_x and PEDOT:PSS. The anti-EpCAM/Ag@Ti₃C₂T_x/CP immunosensor was fabricated by immobilizing anti-EpCAM by drop-cast method. The results of chronoamperometric response study reveal the accurate, rapid and non-invasive detection of EpCAM antigen. This immunosensor displays a good sensing performance with an extremely low LOD (0.8 fg/mL). Furthermore, the extraordinary flexibility and long term stability (35 days) of this immunosensor enables the accurate EpCAM detection with quick response time. The clinical validation of this paper-based sensor was confirmed by detecting the EpCAM antigen with spiked serum samples. Thus, a wide range of applications for biomarker monitoring could benefit greatly from the use of this portable, accurate, and efficient paper-based immunosensor.

References:

- [1] S. Paneru, D. Kumar, Ag-doped-CuO nanoparticles supported polyaniline (PANI) based novel electrochemical sensor for sensitive detection of paraoxon-ethyl in three real samples, *Sensors and Actuators B: Chemical*, 379 (2023) 133270.
- [2] A. Kalkal, S. Kadian, S. Kumar, G. Manik, P. Sen, S. Kumar, G. Packirisamy, Ti_3C_2 -MXene decorated with nanostructured silver as a dual-energy acceptor for the fluorometric neuron specific enolase detection, *Biosensors and Bioelectronics*, 195 (2022) 113620.
- [3] S. Paneru, Sweety, D. Kumar, CuO@PEDOT:PSS-grafted paper-based electrochemical biosensor for paraoxon-ethyl detection, *Journal of Applied Electrochemistry*, 53 (2023) 2229-2238.
- [4] S. Paneru, Sweety, D. Kumar, CeO₂ and PEDOT:PSS modified conducting paper for organophosphate pesticide detection, *Journal of Applied Electrochemistry*, (2024) 1-11.
- [5] K. Fatemeh, M. Mohammad Javad, K. Samaneh, The effect of silver nanoparticles on composite shear bond strength to dentin with different adhesion protocols, *Journal of applied oral science*, 25 (2017) 367-373.
- [6] Sweety, D. Kumar, Electrochemical immunosensor based on titanium dioxide grafted MXene for EpCAM antigen detection, *Journal of Colloid and Interface Science*, 652 (2023) 549-556.
- [7] S. Kumar, M. Umar, A. Saifi, S. Kumar, S. Augustine, S. Srivastava, B.D. Malhotra, Electrochemical paper based cancer biosensor using iron oxide nanoparticles decorated PEDOT:PSS, *Analytica Chimica Acta*, 1056 (2019) 135-145.
- [8] S. Kumar, P. Rai, J.G. Sharma, A. Sharma, B.D. Malhotra, PEDOT: PSS/PVA-Nanofibers-Decorated Conducting Paper for Cancer Diagnostics, *Advanced Materials Technologies*, 1 (2016) 1600056.

CHAPTER 8

CONCLUSION, FUTURE SCOPE AND SOCIAL IMPACT

8.1 Conclusion

The current thesis describes the structural, morphological, and electrochemical properties of $\text{Ti}_3\text{C}_2\text{T}_x$ and its hybrids with TiO_2 , CuS , and Ag particles as well as their prospective applications in biosensors. A number of ultrasensitive electrochemical immunosensing devices have been fabricated for label-free EpCAM antigen (cancer biomarker) detection. In order to improve sensing performance, various attempts have been undertaken to use economical and environment friendly methods for synthesizing different hybrids. For the fabrication of electrochemical immunosensor, the EpCAM antibody corresponding to EpCAM antigen has been used for immobilization onto the electrode surface.

Firstly, BSA/anti-EpCAM/ $\text{Ti}_3\text{C}_2\text{T}_x$ @ITO platform has been fabricated for the electrochemical detection of EpCAM antigen. The layered structure of 2D- $\text{Ti}_3\text{C}_2\text{T}_x$ provides a large specific surface area for better immobilization of antibody. This immunosensor showed a broad linear range (0.1 fg/mL to 100 ng/mL) along with high sensitivity ($29.22 \mu\text{A fg}^{-1} \text{mL cm}^{-2}$) for EpCAM detection. Furthermore, the immunosensor successfully detected EpCAM antigen in spiked human serum samples with a very good recovery rate of 97.9% – 99.9%.

To improve different electrochemical parameters such as biocompatibility, effective surface area and stability of $\text{Ti}_3\text{C}_2\text{T}_x$, TiO_2 has been incorporated into the layers of $\text{Ti}_3\text{C}_2\text{T}_x$. This in-situ grown TiO_2 , increases the stability of $\text{Ti}_3\text{C}_2\text{T}_x$ by improving the interlayer spacing in its sheets and serving as a protective layer to prevent the oxidative deterioration of the inner structure of $\text{Ti}_3\text{C}_2\text{T}_x$. The electrochemical immunosensor has been fabricated by immobilizing anti-EpCAM onto the $\text{TiO}_2/\text{Ti}_3\text{C}_2\text{T}_x$ @ITO electrode. The outstanding analytical performance of the immunosensor is owing to the increase in specific surface area and electrical conductivity of 2D/2D $\text{TiO}_2/\text{Ti}_3\text{C}_2\text{T}_x$ hybrid. The BSA/anti-EpCAM/ $\text{TiO}_2/\text{Ti}_3\text{C}_2\text{T}_x$ @ITO electrode provided a broad 1 ag/mL to 10 ng/mL range and extremely low LOD, 0.7 ag/mL for EpCAM detection. Furthermore, the produced immunosensor exhibits good selectivity, repeatability, and long-term stability (56 days).

In the next chapter, stable $\text{CuS}/\text{Ti}_3\text{C}_2\text{T}_x$ hybrid has been synthesized via one-pot hydrothermal technique. The increase in electron transfer rate for $\text{CuS}/\text{Ti}_3\text{C}_2\text{T}_x$ hybrid due to the synergetic

effect of CuS and $\text{Ti}_3\text{C}_2\text{T}_x$, as compared to $\text{Ti}_3\text{C}_2\text{T}_x$ makes it a promising candidate for the immobilization of antibody. The fabricated immunosensor, BSA/anti-EpCAM/CuS/ $\text{Ti}_3\text{C}_2\text{T}_x$ @ITO offers a good linearity in 0.01 fg/mL to 100 ng/mL range with an excellent LOD, 0.0057 fg/mL. The validity of this sensor with spiked serum samples proved its clinical applicability in humans.

Further, the CuS and Ag/ $\text{Ti}_3\text{C}_2\text{T}_x$ particles have been dispersed into PEDOT:PSS aqueous solution separately and subsequently used to fabricate paper-based electrochemical sensors for EpCAM detection. The conducting paper electrodes have been fabricated with the aforementioned suspensions by simple dip-coating technique. The modified paper electrodes have further been treated with dimethyl sulfoxide to enhance the electrical conductivity and stability of paper. The CuS/PEDOT:PSS and Ag/ $\text{Ti}_3\text{C}_2\text{T}_x$ /PEDOT:PSS based immunosensors have been found to detect EpCAM antigen with acceptable detection limit of 0.01 pg/mL and 0.8 fg/mL, respectively. The electrochemical findings confirm that the immunosensors exhibit good stability, repeatability, and selectivity.

Thus, a wide range of applications for biomarker monitoring could benefit greatly from the use of portable, accurate, and efficient paper-based immunosensor.

8.2 Future scope

- Even though EpCAM antigen has been successfully detected in human serum samples, additional research should be done, because no single cancer biomarker satisfies every need for an ideal cancer biomarker. In order to support appropriate and timely clinical decision-making, a multiple markers detection technique combining both new and established cancer biomarkers must be developed.
- The advanced synthesis and surface modification strategies are required for Mxene-based nanocomposites for the development of electrochemical biosensors for low concentration cancer biomarker detection.
- It may be possible to develop sophisticated microfluidic devices that can detect extremely low quantities of biomolecules.
- Additionally, the flexible and eco-friendly disposable paper sensor may be explored for the fabrication of eco-friendly low-cost point-of-care device to detect different infectious diseases.

- In future, the health and government sectors can invest in these systems and taking an essential step towards commercialization of these platforms.

8.3 Social Impact

- Remote health monitoring with biosensors helps to minimize hospitalizations and disruptions.
- Early diagnosis and monitoring of pathological conditions, particularly cancer disease, may greatly improve prognosis and survival rates by analyzing molecular biomarkers using biosensor platforms.
- Diagnostics using portable and in situ sensing equipment at the patient's bedside can significantly lower the death rate and enhance clinical results.

PUBLICATIONS

1. **Sweety**, Devendra Kumar, "Development of $Ti_3C_2T_x$ -based novel immunosensor for cancer biomarker detection", *Applied Organometallic Chemistry*, 38(8) (2024) e7570.
2. **Sweety**, Devendra Kumar, "Electrochemical immunosensor based on titanium dioxide grafted MXene for EpCAM antigen detection", *Journal of Colloid and Interface Science*, 652 (2023) 549-556.
3. **Sweety**, Saroj Paneru, Devendra Kumar, "CuS modified PEDOT:PSS grafted paper-based electrochemical immunosensor for EpCAM biomarker detection", *Materials Chemistry and Physics*, 313 (2023) 128687.
4. **Sweety**, Saroj Paneru, Devendra Kumar, "A copper sulfide doped 2D-MXene-based ultrasensitive label-free electrochemical immunosensor for EpCAM antigen detection", *Applied Organometallic Chemistry*, 39(2) (2025) e7975.
5. Saroj Paneru, **Sweety**, Devendra Kumar, "CuO@PEDOT:PSS-grafted paper-based electrochemical biosensor for paraoxon-ethyl detection", *Journal of Applied Electrochemistry*, 53 (2023) 2229-2238.
6. Saroj Paneru, **Sweety**, Devendra Kumar, "CeO₂ and PEDOT:PSS modified conducting paper for organophosphate pesticide detection", *Journal of Applied Electrochemistry*, 54 (2024) 1875-1885.
7. Poornima Bohra, Priya, **Sweety**, Divya Hudda, Devendra Kumar, "CuS@rGO grafted PEDOT:PSS paper based electrochemical biosensor for fenitrothion detection", *Applied Organometallic Chemistry*, 39(2) (2025) e70002.
8. Srijita Chatterjee, Harshita Singh, Divya Hudda, **Sweety**, Devendra Kumar, "A novel acetylcholinesterase-based electrochemical biosensor using g-C₃N₄@MoS₂ nanohybrid for the detection of trichlorfon", *Applied Organometallic Chemistry*, 38(12) (2024) e7721.

9. **Sweety**, Divya Hudda, Devendra Kumar, "Ultrasensitive electrochemical detection of EpCAM antigen based on anti-EpCAM conjugated with highly flexible Ag@Ti₃C₂T_x modified conducting paper platform". (Communicated)
10. **Sweety**, Divya Hudda, Devendra Kumar, Green one pot synthesized CeO₂@MXene coupled with molecularly imprinted polymer for selective analysis of EpCAM as a cancer biomarker. (Communicated)
11. Saroj Paneru, **Sweety**, Devendra Kumar, "CeO₂ nanocrystal-enhanced polyaniline biosensor for organophosphate detection: A step towards sustainable agriculture", (Communicated)
12. Yashaswini, **Sweety**, Divya Hudda, Devendra Kumar, "Non-enzymatic CeO₂ grafted Ti₃C₂T_x-based electrochemical sensor for fenitrothion detection". (Communicated)
13. **Sweety**, Devendra Kumar, "Mini Review: MXene-based electrochemical biosensors for cancer biomarker detection". (Manuscript under preparation)
14. Divya Hudda, **Sweety**, Devendra Kumar, "Highly sensitive and selective molecularly imprinted electrochemical sensor based on Ag@TiO₂/MXene for levofloxacin determination". (Manuscript under preparation)
15. Nishul Khanna, Diksha Bhatla, Divya Hudda, **Sweety**, Devendra Kumar, "MXene decorated graphitic carbon nitride based acetylcholinesterase biosensor for the detection of trichlorfon".(Manuscript under preparation)

CONFERENCES

- (1) Oral Presentation at International Conference on “Surface Chemistry SUCH-2022” held on 11th and 12th February, 2022 organized by Department of Chemistry, Annamalai University, Annamalai Nagar, Tamil Nadu, India.
- (2) Presented a poster at International virtual Conference on “Nanotechnology: Opportunities & Challenges (ICNOC–2022)” held on 28-30 November, 2022 organized by Department of Applied Sciences & Humanities, Jamia Millia Islamia, Delhi, India.
- (3) Presented a poster at 7th International Conference on “Nanoscience and Nanotechnology (ICONN-2023)” held on 27-29 March, 2023 organized by Department of Physics and Nanotechnology, SRM IST, Tamil Nadu, India.
- (4) Oral Presentation at International Conference on “Chemical & Allied Science and their Applications” held on 20 January, 2023 organized by Department of Applied Chemistry, Delhi Technological University, Delhi, India.
- (5) Presented a poster at International Conference on “Catalysis for Clean Energy Technologies and Sustainable Development” held on 5th and 6th April, 2024 organized by Punjab University, Chandigarh, India.
- (6) Attended an International Conference on “Advanced Materials and Characterization” held on 24-26 April, 2021 organized by Mattest Research Academy, Chennai, Tamil Nadu, India.
- (7) Attended a one day virtual workshop on “Accelerators/Incubation- Opportunities for Students & Faculties- Early Stage Entrepreneurs” held on 19th June, 2021 at Department of Applied Chemistry, Delhi Technological University, Delhi, India.
- (8) Attended a Five days “Information Literacy Workshop on E-Resources: A Gateway for Research” held on 5-9 September, 2022 organized by Delhi Technological University, Delhi, India.

- (9) Attended “The Annual Information Literacy Workshop on e-Resources: A Gateway for Research” held on 25-29 September, 2023 organized by Delhi Technological University, Delhi, India.

Development of $\text{Ti}_3\text{C}_2\text{T}_x$ -based novel immunosensor for cancer biomarker detection

Sweety  | Devendra Kumar 

Department of Applied Chemistry, Delhi Technological University, Delhi, 110042, India

Correspondence

Devendra Kumar, Department of Applied Chemistry, Delhi Technological University, Delhi 110042, India.
Email: dkumar@dce.ac.in

Funding information

Council Scientific and Industrial Research (CSIR), Government of India, New Delhi, Grant/Award Number: 08/133 [0051]/2020-EMR-I

In this study, an ultrasensitive label-free electrochemical immunosensor based on $\text{Ti}_3\text{C}_2\text{T}_x$ (Mxene) with a 2D-layered morphology has been proposed for the detection of EpCAM antigen. A hydrothermal method is employed for the synthesis of $\text{Ti}_3\text{C}_2\text{T}_x$ by using a less toxic exfoliating reagent, NaBF_4 . The bioelectrode, BSA/anti-EpCAM/ $\text{Ti}_3\text{C}_2\text{T}_x$ @ITO, has been fabricated by electrophoretic deposition of $\text{Ti}_3\text{C}_2\text{T}_x$ onto the ITO electrode, followed by an immobilization of EpCAM antibody. Electrochemical response studies reveal that the immunosensor shows a high sensitivity of $29.22 \mu\text{A fg}^{-1} \text{ ml cm}^{-2}$ and a wide linear range from 0.1 fg/ml to 100 ng/ml, for EpCAM antigen detection. Further, the good stability of this fabricated immunosensor is an additional advantage for EpCAM antigen detection in serum samples.

KEYWORDS

electrophoretic deposition, epithelial cell adhesion molecules, immunosensor, $\text{Ti}_3\text{C}_2\text{T}_x$

1 | INTRODUCTION

In recent years, cancer has become the second leading reason of death worldwide. Early and sensitive detection of tumor markers is a great strategy for the diagnosis and prognosis of cancer patients.^{1,2} Epithelial cell adhesion molecule (EpCAM) is a cell-to-cell adhesion homophilic glycoprotein antigen expressed on circulating tumor cells (CTCs).³ An average concentration range of CTCs is identified as 1–100 CTCs per 10^7 white blood cells in 1 ml of blood.⁴ EpCAM antigen contributes a significant role in the diagnosis and screening of various types of carcinomas arising from the head, neck, prostate, breast, stomach, colon, rectum, pancreas, biliary tract, and hepatic origin.⁵ Mostly, immunoassay techniques are frequently used for the diagnosis of biomarkers, which are based on the specific biorecognition of antigens by antibodies.⁶ Several techniques, like chemiluminescence immunoassay,⁷ enzyme-linked immunosorption assay,⁸ radioimmunoassay,⁹ and sandwich-type immunosensor¹⁰ have been used for the detection of tumor biomarkers. Although, these techniques give trustworthy results but have some serious limitations,

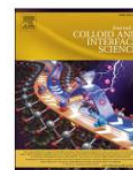
such as requiring highly trained manpower, time-consuming, complex, and expensive.

Recently, biosensors have been considered the most accurate, fast, and sensitive analytical method for biomarker detection.¹¹ They identify cancer biomarkers by employing biorecognition elements like antibodies, DNA, RNA, etc., which transform biological signals into observable electrical signals.¹² Though numerous varieties of biosensors have been published for the identification of biomarkers.¹³ Nonetheless, electrochemical biosensors have been widely used due to their ease of operation, high sensitivity, low cost, and fast response.^{14–17} Electrochemical sensors that monitor the interaction of antigens and antibodies are referred to as electrochemical immunosensor. Certain biosensors have been developed in the last couple of years for the detection of epithelial cancer biomarkers.^{18–20} Recently, Ying Ma et al. described an aptamer-modified quasi-ZIF-67@Au@methylene blue hybrid for highly sensitive detection of EpCAM.²¹ Lina Zhu et al. proposed an electrochemical aptasensor based on CdSe/ZnS QDs for the successful detection of EpCAM.²² In our previous work, we developed a



Contents lists available at ScienceDirect

Journal of Colloid And Interface Science

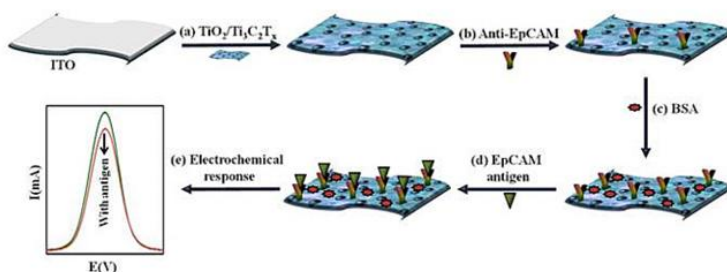
journal homepage: www.elsevier.com/locate/jcis

Electrochemical immunosensor based on titanium dioxide grafted MXene for EpCAM antigen detection

Sweety, Devendra Kumar*

Department of Applied Chemistry, Delhi Technological University, Delhi 110042, India

GRAPHICAL ABSTRACT



ARTICLE INFO

Keywords:

Titanium dioxide
MXene
Electrochemical immunosensor
Cancer biomarker
EpCAM
DPV technique

ABSTRACT

This study proposes the fabrication of a highly sensitive electrochemical immunosensor for label-free detection of EpCAM antigen. MXenes, novel 2D materials have become popular owing to their unique electrochemical properties. Unlike conventional immunosensors, which are unable to detect the carcinoma at primary stage and also time consuming, the use of highly conducting MXene provides a label-free and highly sensitive immunosensor. Herein, we develop a unique immunosensor, which is based on the in-situ growth of 2D-TiO₂ onto the novel 2D-Ti₃C₂T_x sheets by hydrothermal treatment. The 2D/2D TiO₂/Ti₃C₂T_x hybrid provides a platform having a large effective surface area, and more number of electrochemically active sites to enhance the electron transfer rate through the redox probe. The designed sensing platform, BSA/anti-EpCAM/TiO₂/Ti₃C₂T_x@ITO shows a broad linear range (1 ag/mL to 10 ng/mL) with high sensitivity (6.661 $\mu\text{A ag}^{-1} \text{mL cm}^{-2}$), and low detection limit (0.7 ag/mL) for EpCAM antigen detection under optimized conditions. The proposed immunosensor possesses good reproducibility, long-term stability, and outstanding selectivity and specificity. Moreover, the clinical applicability of the novel immunosensor is tested in spiked human serum showing good recovery.

1. Introduction

Cancer biomarkers are a type of biochemical substance generated by

human tumor tissues. These biomarkers determine the existence, growth and stage of tumors, and have clinical significance in the early monitoring of these tumors [1]. Epithelial cell adhesion molecule (EpCAM), a cancer

* Corresponding author.

E-mail addresses: 29.sweetyjain@gmail.com (Sweety), dkumar@dce.ac.in (D. Kumar).

<https://doi.org/10.1016/j.jcis.2023.08.099>



Received 27 June 2023; Received in revised form 9 August 2023; Accepted 16 August 2023

Available online 16 August 2023

0021-9797/© 2023 Elsevier Inc. All rights reserved.

RESEARCH ARTICLE

A Copper Sulfide Doped 2D-MXene-Based Ultrasensitive Label-Free Electrochemical Immunosensor for EpCAM Antigen Detection

Sweety  | Saroj Paneru | Devendra Kumar 

Department of Applied Chemistry, Delhi Technological University, Delhi, India

Correspondence: Devendra Kumar (dkumar@dce.ac.in)

Received: 12 July 2024 | Revised: 28 October 2024 | Accepted: 24 December 2024

Funding: The authors received no specific funding for this work.

Keywords: CuS | electrochemical immunosensor | EpCAM antigen | MXene

ABSTRACT

Herein, a novel CuS-anchored 2D-Ti₃C₂T_x composite material was synthesized by a one-pot hydrothermal method. This CuS/Ti₃C₂T_x hybrid was used to prepare a novel label-free electrochemical immunosensor for EpCAM antigen detection. The immunosensor has been fabricated by electrophoretic deposition of CuS/Ti₃C₂T_x hybrid onto the ITO electrode followed by the immobilization of anti-EpCAM. The electrochemical biosensing studies of this fabricated immunosensor, BSA/anti-EpCAM/CuS/Ti₃C₂T_x@ITO demonstrated a wide linear range (0.01 fg/mL to 100 ng/mL) and low LOD (0.0057 fg/mL), together with high sensitivity (461.85 μA fg⁻¹ mL cm⁻²) for EpCAM antigen detection. The clinical validation of the proposed immunosensor was conducted with serum samples. Moreover, the immunosensor was found to be reproducible, specific, selective, and stable over a long period of 42 days.

1 | Introduction

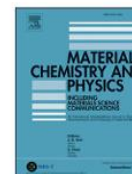
MXenes and their composites are very advantageous materials owing to their excellent thermal and electrical conductivity, biocompatibility, low toxicity, high hydrophilicity, large surface area, and interlayer spacing in their sheets [1]. Additionally, these materials possess good ion and electron transport behavior because of tailorable hydroxyl, fluoride, and oxygen containing functional groups on their surfaces [2]. MXene is a 2D inorganic material, generally expressed as carbide/nitride/carbonitride of early transition metals in the periodic table. The name, MXene, is derived from its precursor, MAX phase (M_{n+1}AX_n), where M = Sc, Ti, Zr, Hf, V, Nb, Ta, Cr, Mo, W; A = group IIIA or IVA element; X = C and/or N; and n = 1, 2, 3 [3]. It is remarkably different from other 2D materials such as transition metal dichalcogenide, graphene, and graphitic carbon nitride; in respect of the bonding between different layers. These 2D materials have weak van der Waals force of attraction between their layers,

whereas MXenes are bounded together by strong metallic bonds via 'A' layers in the MAX phase [4]. MXenes having the general formula, M_{n+1}X_nT_x, are obtained by the selective etching of "A" layers from the MAX phase, where T_x represents the surface functional groups like -O, -OH, -F [5]. These hydrophilic moieties present on the surface provide superior water dispersibility to the MXenes [6]. These functional groups can be easily tailored by different surface functionalization methods like hydrothermal method [7], in situ polymerization [8], and heat and milling treatment [9]. MXenes are now considered to have unique properties and potential for their applications in different fields such as catalysis [10], energy storage [11], biomedicine [12], and sensing [13]. Furthermore, the MXenes have found applications in the environmental remediation because it is not only made up of non-toxic elements like Ti, C, and/or N, but their degradation byproducts (CO₂ and N₂) are also environment-friendly [14]. Nowadays, 2D-layered MXene-based electrodes have gained popularity as research hotspots in different fields. MXenes have



Contents lists available at ScienceDirect

Materials Chemistry and Physics

journal homepage: www.elsevier.com/locate/matchemphys

CuS modified PEDOT:PSS grafted paper-based electrochemical immunosensor for EpCAM biomarker detection

Sweety, Saroj Paneru, Devendra Kumar*

Department of Applied Chemistry, Delhi Technological University, Delhi, 110042, India

HIGHLIGHTS

- An electrochemical paper-based immunosensor has been designed using CuS and PEDOT:PSS.
- This low cost and flexible platform may be a promising candidate over other costly conventional electrodes.
- It exhibits high sensitivity of $104.31 \mu\text{A pg}^{-1} \text{mL}$ in broad range of 0.01 pg/mL to 1000 ng/mL , for EpCAM detection.
- The clinical applicability and validity has been checked with human serum sample.

ARTICLE INFO

Keywords:

CuS
 PEDOT:PSS
 Electrochemical immunosensor
 EpCAM
 Electrochemical paper

ABSTRACT

A novel CuS grafted PEDOT:PSS conducting paper-based electrochemical immunosensor has been successfully fabricated for the detection of EpCAM antigen. Electrical conductivity is further improved by doping the CuS@PEDOT:PSS/WP electrode with different organic solvents such as N,N-dimethyl formamide (DMF), N,N-dimethyl acetamide (DMA), ethylene glycol (EG) and dimethyl sulfoxide (DMSO). It is observed that DMSO doped conducting paper shows the highest conductivity ($6.1 \times 10^{-2} \text{ S/cm}$) among all these solvents. This low cost, biodegradable electrochemical paper-based immunosensor (BSA/anti-EpCAM/EP) possesses a broad linear range from 0.01 pg/mL to 1000 ng/mL for EpCAM antigen detection. The immunosensor is found to have high sensitivity of $104.31 \mu\text{A pg}^{-1} \text{mL}$. This conducting paper based immunosensor is further used to detect EpCAM antigen in human serum samples, thereby confirming a cost effective clinical tool over other costly conventional techniques.

1. Introduction

Cancer is one of the leading causes of mortality worldwide with 19.3 million reported cases and 10 million deaths in 2020. It is expected that cancer cases may reach to 28.4 million in 2040 globally, a 47 % rise from 2020 [1]. There are various factors such as environmental factors, viruses, genetic factors, immune deficiency, UV radiation and food habits which results into cancer [2]. Traditional methods for cancer diagnosis include several kinds of histopathological techniques, imaging modalities, ultrasonography, magnetic resonance imaging etc., and tumor marker analysis [3]. All these methods have their own limitations such as inability to detect carcinoma at initial stage, very expensive, time consuming and unable to differentiate between benign and malignant tumor. Also, these techniques should be performed at regular intervals for effective diagnosis, screening and treatment of disease which is very

painful for a patient [4].

Cancer biomarkers are the characteristics that can measure the existence and growth of tumors in human body [5]. Lately, liquid biopsy are used to detect various biomarkers namely cell-free DNA, circulating tumor DNA, circulating tumor cells and cancer-related soluble proteins [6]. Among them, circulating tumor cells (CTCs) are assumed to be potential candidate for early detection of metastasis [7]. CTCs are the tumor cells shed by the primary tumor into the blood stream [8]. Epithelial cell adhesion molecule (EpCAM) has been identified as a predictive CTCs biomarker expressed in most cancer cells [9]. It is a cell surface transmembrane glycoprotein that is overexpressed in epithelial cancers derived from lung, breast, colorectal, prostate, head, neck and hepatic origin [10]. Hence, the EpCAM is a potential candidate for both detection and monitoring of cancerous cells [11]. Owing to very low concentration of secreted EpCAM from CTCs, previously established

* Corresponding author.

E-mail addresses: 29.sweetyjain@gmail.com (Sweety), saroj4843@gmail.com (S. Paneru), dkumar@dce.ac.in (D. Kumar).

<https://doi.org/10.1016/j.matchemphys.2023.128687>

Received 25 August 2023; Received in revised form 3 November 2023; Accepted 15 November 2023

Available online 16 November 2023

0254-0584/© 2023 Elsevier B.V. All rights reserved.



DELHI TECHNOLOGICAL UNIVERSITY

(Formerly Delhi College of Engineering)

Shahbad Daultapur, Bawana Road, Delhi- 110042

PLAGIARISM VERIFICATION

Title of the Thesis “**Electrochemical Immunosensor for cancer biomarker detection**”

Total Pages **106**

Name of the Scholar **Sweety**

Supervisor **Prof. D. Kumar**

Department **Applied Chemistry**

This is to report that the above thesis was scanned for similarity detection. Process and outcome is given below:

Software used: **Turnitin**, Similarity Index: **7%**, Total Word Count: **28169**

Date: **11-11-2024**

Candidate's Signature

Signature of Supervisor

CURRICULUM VITAE



Sweety

Senior Research Fellow
Department of Applied Chemistry
Delhi Technological University
New Delhi – 110042

Nationality: Indian
D.O.B: 29 May, 1992
Contact: +917015822492
Email: 29.sweetyjain@gmail.com

CSIR- JRF with AIR-55 in December, 2017

Academic Qualifications

M.Sc - Chemistry (69.01%), Maharshi Dayanand University, Rohtak, 2014
B.Sc - PCM (73.99%), Kurukshetra University, Kurukshetra, 2012
12th - All subjects (81.20%), Haryana Board of School Education, 2009
10th - All subjects (73.99%), Haryana Board of School Education, 2007

Title of Research: *Electrochemical immunosensor for cancer biomarker detection*

Research Highlights

- Synthesis and characterization of novel 2D-material (MXene) and its composite with different metal, metal oxides and sulfides
- Electrochemical characterization by using CV, Chronoamperometry and EIS techniques
- Electrochemical biosensing studies of immunosensor for cancer biomarker detection
- Selectivity, reproducibility and clinical applicability studies of fabricated sensors

Instrumental Skills

X-ray Diffractometer, Fourier Transform Infrared Spectrometer, Potentiostat/Galvanostat: Cyclic Voltammetry, Chronoamperometry, Differential Pulse Voltammetry, Electrochemical Impedance Spectroscopy.

Awards and Achievements

1. Got Research Excellence Award presented excellence in research to publish a paper "Electrochemical immunosensor based on titanium dioxide grafted MXene for EpCAM antigen detection" by Delhi Technological University on September 5, 2024.
2. Got Research Excellence Award presented excellence in research to publish a paper "CuO@PEDOT:PSS-grafted paper-based electrochemical biosensor for paraoxon-ethyl detection" by Delhi Technological University on September 5, 2024.